JAERI-M
90-106

REFLOOD BEHAVIOR AT LOW INITIAL CLAD TEMPERATURE IN SLAB CORE TEST FACILITY CORE-II

July 1990

Hajime AKIMOTO, Kazuharu OKABE*, Makoto SOBAJIMA, Yutaka ABE
Takamichi IWAMURA, Akira OHNUKI, Tsutomu OKUBO
Hiromichi ADACHI** and Yoshio MURAO

日本原子力研究所
Japan Atomic Energy Research Institute

JAERI-Mレポートは，日本原子力研究所が不定期に公刊している研究報告書です。
入手の問合わせは，日本原子力研究所技術情報部情報資料課（〒319－11茨城県那珂郡東海村）あて，お申しこしください。なお，このほかに財団法人原子力弘済会資料センター（〒319-11茨城県那珂郡東海村日本原子力研究所内）で複写による実費頒布をおこなっております。

JAERI-M reports are issued irregularly.
Inquiries about availability of the reports should be addressed to Information Division, Department of Technical Information, Japan Atomic Energy Research Institute, Tokai-mura, Naka-gun, Ibaraki-ken 319-11, Japan.

編集兼発行　日本原子力研究所
印　　刷　日立高速印刷株式会社

Reflood Behavior at Low Initial Clad Temperature in Slab Core Test Facility Core-II

Hajime AKIMOTO, Kazuharu OKABE*, Makoto SOBAJIMA+, Yutaka ABE
Takamichi IWAMURA, Akira OHNUKI, Tsutomu OKUBO
Hiromichi ADACHI** and Yoshio MURAO

Department of Reactor Engineering
Tokai Research Establishment
Japan Atomic Energy Research Institute
Tokai-mura, Naka-gun, Ibaraki-ken

(Received June 11, 1990)

In order to study the reflood behavior with low initial clad temperature, a reflood test was performed using the Slab Core Test Facility (SCTF) with initial clad temperature of 573 K. The initial clad temperature of the test(573 K) was determined based on the best-estimate calculated result(550 K) with TRAC code for a PWR. The test conditions of the test are identical with those of SCTF base case test S2-SH1(initial clad temperature 1073 K) except the initial clad temperature. Through the comparison of results from these two tests, the following conclusions were obtained.

(1) The low initial clad temperature resulted in the low differential pressures through the primary loops due to smaller steam generation in the core.

(2) The low initial clad temperature caused the accumulated mass in the core to be increased and the accumulated mass in the downcomer to be decreased in the period of the lower plenum injection with accumulator

---

This work was performed under contract with the Atomic Energy Bureau of Science and Technology of Japan.

+ Department of Fuel Safety Research

* Mitsubishi Atomic Power Industry

** Yamagata University

(before 50s). In the later period of the cold leg injection with LPCI (after 100s), the water accumulation rates in the core and the downcomer were almost the same between both tests.

(3) The low initial clad temperature resulted in the increase of the core inlet mass flow rate in the lower plenum injection period. However, the core inlet mass flow rate was almost the same regardless of the initial clad temperature in the later period of the cold leg injection period because the core inlet mass flow rate is limited mainly by the ECC water injection rate into the cold leg in the SCTF.

(4) The low initial clad temperature resulted in the low turnaround temperature, high temperature rise and fast bottom quench front propagation.

(5) In the region apart from the quench front, low initial clad temperature resulted in the lower heat transfer. In the region near the quench front, almost the same heat transfer coefficient was observed between both tests.

(6) No flow oscillation with a long period was observed in the SCTF test with low initial clad temperature of 573 K, while it was remarkable in the Cylindrical Core Test Facility (CCTF) test which was performed with the same initial clad temperature. It is considered that no flow oscillation is induced in the SCTF because the SCTF has no active steam generator while the CCTF has active steam generators.

Keywords : Reactor Safety, PWR, Reflood, SCTF, Heat Transfer, Two Phase Flow

平板第２次炉心試験における低被覆管初期温度時の再冠水挙動

日本原子力研究所東海研究所原子炉工学部
秋本　肇・岡部　一治*・傍島　真+
阿部　豊・岩村　公道・大貫　晃
大久保　努・安達　公道**・村尾　良夫

（1990年6月11日受理）

低被覆管初期温度時の再冠水挙動を調べるために，被覆管初期温度を573Kに設定して，平板炉心試験（SCTF）を用いて試験（試験名S2－09）を実施した。同試験での被覆管初期温度（573K）は，最適評価コードTRACによる実炉最適予測計算結果（550K）を参照して定めた。被覆管初期温度を除いた試験条件は，SCTF基準試験S2－SHI（被覆管初期温度1073K）と同一に設定した。両試験結果を比較検討し，以下の事柄がわかった。

(1) 低被覆管初期温度により，炉心内の蒸気発生量は小さくなるため，一次系ループ差圧は小さくなった。

(2) 下部プレナム注水期間（再冠水開始後50秒以前）において，低被覆管温度のために，炉心内蓄水量は増加しダウンカマ内蓄水量は減少した。コールドレグ注水期間の後半（100秒以降）では，両試験でダウンカマ及び炉心での蓄水速度はほぼ等しかった。

(3) 低被覆管初期温度により，下部プレナム注水期間での炉心入口流量は増加した。しかしながらコールドレグ注水期間の後半での炉心入口流量は被覆管初期温度によらずほぼ等しかった。これはコールレグ注水期間では，炉心入口流量が主にコールドレグへのECC注入量により制限されたためである。

(4) 低被覆管初期温度により，ターンアラウンド温度は低く，温度上昇量は高く，クエンチ速度は大きくなった。

(5) クエンチ点から離れた領域では，低被覆管初期温度により熱伝達率は低くなった。クエンチ点の近くでは両試験でほぼ等しい熱伝達率が観察された。

(6) 被覆管初期温度を573KとしたSCTFによる試験では，同一の初期温度で実施された円筒炉心試験（CCTF）による試験でみられた様な長周期の流動振動は観察されなかった。この相異は，SCTFでは，CCTFと異なり発熱源となり得る蒸気発生器が模擬されていないことに起因すると考えられる。

本報告書は，電源開発促進対策特別会計法に基づき，科学技術庁からの受託によって行った研究の成果である。
東海研究所：〒319-11　茨城県那珂郡東海村白方字白根2-4
+　燃料安全工学部
*　三菱原子力工業
**　山形大学

Contents

目　　次

Nomenclature

A ; cross sectional area (m^2),

C_{pl} ; specific heat of water (J/(kgK)),

g ; acceleration of gravity (m/s^2),

h_{fg} ; latent heat for condensation of steam (J/kg),

K ; flow resistance coefficient,

M ; accumulated mass (kg),

m ; mass flow rate (kg/s),

m_{BCL} ; mass flow rate through the broken cold leg of pressure vessel side (kg/s),

m_c ; total condensation rate in cold legs and downcomer (kg/s),

m_{ECC} ; ECC water injection rate into intact cold leg (kg/s),

m_{ICL} ; mass flow rate through the intact cold leg (kg/s),

T_{ECC} ; ECC water temperature (K),

T_{sat} ; saturation temperature (K),

U_g ; superficial steam velocity ($=m_g/\rho_g A$) (m/s),

ΔP ; differential pressure (Pa),

ρ_g ; steam density at upper plenum (kg/m^3).

List of Tables

List of Figures

1. Introduction

A reflood test program using large scale test facilities is being conducted at Japan Atomic Energy Research Institute (JAERI)[1]. The facilities are the Cylindrical Core Test Facility (CCTF) and the Slab Core Test Facility (SCTF). This report describes the test results from the SCTF Test S2-09 (Run 614).

In previous reflood tests with CCTF and SCTF, most of the tests were performed with relatively high initial clad temperature (nominally 1073 K) because those tests were based on the results from a licensing calculation of a PWR. Recently, a best estimate calculation was performed with TRAC (Transient Reactor Analysis Code) at Los Alamos National Laboratory for a double ended, cold leg break loss-of-coolant accident (LOCA) of a typical Westinghouse PWR[2]. In the calculation, the peak clad temperature was about 550 K at reflood initiation under most probable conditions. The best-estimate calculation suggests the possibility that the initial clad temperature assumed in the licensing calculation is unrealistically high compared to that in a PWR-LOCA. The calculation also suggestes that the data base with low initial clad temperature is important to understand the reflood phenomena as well as that with high initial clad temperature.

Test S2-09 (Run 614) was conducted to investigate the thermal hydraulic behavior during the reflood phase in the case of low initial clad temperature. In Test S2-09 (Run 614), the peak clad temperature at reflood initiation was set at 573 K instead of 1073 K for the base case test Test S2-SH1 (Run 604) in SCTF Core-II test series in order to simulate the calculated results for a PWR LOCA with TRAC code. The other test conditions of Test S2-09 (Run 614) were the same as those of the base case test in order to study the effect of the initial clad temperature.

Presented in Appendix A are a brief description of SCTF Core-II and calculation methods of mass balance, steam generation rate and additional horizontal differential pressures. Some selected data obtained in Test S2-09 are presented in Appendix B.

2. Test Description

2.1 Test Facility

Figure 1 shows schematic diagram of the SCTF[3),(4)]. The primary coolant loops consist of a hot leg equivalent to the actual hot legs, a steam-water separator corresponding to the steam generator, an intact cold leg equivalent to the three intact cold legs, a broken cold leg of the pressure vessel side and a broken cold leg of the steam-water separator side. These two broken cold legs are connected to two containment tanks of which pressure is controlled by exhausting steam to the atmosphere.

The flow area scaling ratio of the primary loops is 1/21 to a 1,100 MWe PWR. The flow areas of the hot leg, the intact cold leg and the broken cold leg are 0.0826, 0.0697 and, 0.0179 m^2, respectively. In the SCTF, the vertical dimensions of the hot leg and cold legs are designed to be the same as those of a PWR in order to properly simulate the flow behavior affected by the gravity force; such as the water carry-over through the hot leg. The flow resistance coefficients through the primary loops are adjusted by orifice plates in the primary loops. In the tests described in this report, orifice diameters are 86.4, 179.9 and 173.3 mm for the broken cold leg of the steam-water separator side, the intact cold and the pump simulator of the intact loop, respectively. No orifice plate is inserted in the broken cold leg of the pressure vessel side.

The emergency core cooling system (ECCS) of the SCTF consists of an accumulator (Acc) and a low pressure coolant injection (LPCI) systems. Figure 2 shows the vertical cross section of the pressure vessel which includes a simulated core, an upper plenum, a lower plenum, a core baffle and a downcomer. The simulated core consists of eight bundles arranged in a row, simulating the radial slab extracted from a PWR core with full height, full radius and one bundle width. In Fig. 2, Bundle 1 corresponds to the central bundle and Bundle 8 to the peripheral bundle in the actual PWR core, respectively. Each bundle consists of 234 heater rods and 22 non-heated rods arranged in 16×16 array. The pitch, the outer diameter and the heated length of heater rods are 14.3 mm, 10.7 mm and 3.66 m, respectively. These dimensions are identical with those for a 15×15 fuel rod assembly in a Westinghouse type PWR. Each heater rod has a 17 step chopped cosine axial power profile with a peaking factor of 1.40. The core and the upper plenum

are enveloped by honeycomb thermal insulators to minimize the wall thermal effect.

More detailed information of the SCTF is summarized in Appendix A.

2.2 Test Conditions

Figure 3 shows comparisons of measured ECC (Emergency Core Cooling) water injection rate and water temperature at the lower plenum and the intact cold leg between Tests S2-SH1[5] and S2-09. The location of the water injection is switched from the lower plenum to the intact cold leg at 55 s in both tests. Figure 4 shows comparison of total power supplied to the heater rods in the core. The core power is maintained constant for 40 s after the reflood initiation and then it is decayed following the decay curve type of ((ANS + Actinide) × 1.02 (40 s after scram)). Figure 5 shows comparison of the pressure in the containment tank I between both tests. The pressure in Test S2-09 is slightly lower (by about 0.01 MPa) than that in Test S2-SH1 during the test. Figure 6 shows comparison of clad surface temperatures between Tests S2-SH1 and S2-09 at the reflood initiation. The maximum clad temperatures are 591 and 1076 K in Tests S2-09 and S2-SH1, respectively. The initial stored energy based on the saturation temperature for the system pressure is about 6.8 times in Test S2-SH1 compared to that in Test S2-09.

Table 1 summarizes major test conditions of Tests S2-SH1 and S2-09. Except the initial clad temperature, the test conditions are almost the same in these two tests. In this report, Test S2-SH1 will be called "high temperature test". Test S2-09 will be called "low temperature test".

3. Results and Discussion

3.1 Effect of Initial Clad Temperature on Flow Behavior through Primary Loops

Figure 7 shows comparisons of differential pressure along the primary loops between high and low temperature tests. In both tests, the differential pressure through each section of the primary loop increases with time in the lower plenum injection period ($0<t<55$s). After 100 s, the differential pressures through the intact and broken cold legs decrease with time in both tests. The differential pressures from low temperature test is lower than those from high temperature test in both lower-plenum and cold-leg injection periods.

Figure 8 shows comparisons of mass flow rate through each section of the primary loops (the intact cold leg, the broken cold leg of steam-water separator side, the broken cold leg of pressure vessel side and the exhaust line from the containment tank II to the atmosphere) between high and low temperature tests. Table 2 summarizes the calculated flow resistance coefficient at 100 and 300 s. In high temperature test, the flowmeter at the intact cold leg was failed to measure the mass flow rate due to zero shift of the sensor. For the mass flow rate through the intact cold leg in high temperature test, an estimation was made with the following relations;

$$m_{ICL} = m_{BCL} + m_C \tag{1}$$

$$m_C = \begin{cases} 0 & \text{(in lower plenum injection period)} \\ \dfrac{C_{pl}(T_{sat} - T_{ECC})\, m_{ECC}}{h_{fg}} & \text{(in cold leg injection period)} \end{cases} \tag{2}$$

In the relation mentioned above, the following assumptions were included.

(1) No condensation or evaporation occurs in the lower plenum injection period.

(2) In the cold leg injection period, complete mixing of steam with injected water is established in the intact cold leg and then thermal equilibrium is attained in the region.

The discrepancy of the mass flow rate through the intact cold leg between the measured and estimated results was $\pm$ 0.5 kg/s at most in low temperature test. It was $\pm$ 0.2 kg/s after 100 s in low temperature test. It is considered that the estimated mass flow rate is reasonable except in the short period following

the switch of the ECC water injection location from the lower plenum to the intact cold leg.

The mass flow rates through each section of the primary loops show the maximum rates at about the time when the ECC water injection location is switched from the lower plenum to the intact cold leg in both tests. The mass flow rate in low temperature test is lower than that in high temperature test through each section of the primary loops.

The calculated flow resistance coefficients are about the same between both tests. The result shows that the lower differential pressure through the primary loops in low temperature test are attributed mainly to the lower mass flow rate through the primary loops compared to high temperature test.

The steam through primary loops is generated in the core due to the heat transfer between heater rods and fluid. The initial stored energy is about 6.8 times in high temperature test compared to that in low temperature test at reflood initiation. It is supposed that the steam generation rate is different between high and low temperature tests. Figure 9 shows the cmoparisons of the steam generation rate in each bundle of the core. The generation rate was calculated based on the energy balance relation in the core (see Appendix A). Figure 10 shows the comparison of the total steam generation rate in eight bundles between the measured and calculated results. The estimation method based on the core energy balance is considered to be reasonable because the error of the calculated steam generation rate is estimated to be $\pm$ 15%. Figure 9 shows that the steam generation rate is lower in low temperature test than that in high temperature test. This result confirms that the lower mass flow rates through the primary loops in low temperature test is due to lower steam generation rate in the core compared to that in high temperature test.

In Fig. 9, the equivalent steam generation rate to the supplied power is also shown. Because the supplied power is almost the same between both tests, the equivalent steam generation rate is also almost the same between both tests. The discrepancy between the equivalent steam generation rate to the supplied power and the steam generation rate by the energy balance calculation indicates the net contribution of the released energy from the heater rods beside the supplied power to the steam generation. Figure 9 confirms that the net contribution of the release of the stored energy from the heater rods is smaller in low temperature test than that in high temperature test. For example, at 200 s, the steam generation rates by the core energy balance

calculation are higher by 36 % and 27 % than those from the supplied power in high and low temperature tests respectively. Even though the initial stored energy is 6.8 times in the high temperature tests compared to that of low temperature test at reflood initiation, the contribution of the stored energy is only 1.5 times that in low temperature test at 200 s. It is caused by faster quench front propagation in low temperature test as will be discussed later.

For the flow behavior through the primary loops, the low initial clad temperature resulted in the low differential pressure and mass flow rates through the primary loops due to the small steam generation rate in the core.

3.2 Effect of Initial Clad Temperature on Flow Behavior in pressure Vessel

Figure 11 shows the differential pressures through the core and the downcomer. The differential pressure through the core in low temperature test is higher than that in high temperature test, while the differential pressure through the downcomer of low temperature test is lower than that of high temperature test. In the SCTF, the bottom of the broken cold leg is located at the elevation of 4.777 m from the bottom of the core heated part. If the downcomer is filled with the saturated water at 0.2 MPa to the level of the broken cold leg, static water head through downcomer is calculated to be 44.2 kPa. The measured differential pressure is about 32 kPa at most. Because the downcomer wall is not superheated in the SCTF tests. It is expected that the downcomer is filled with solid water to some level. In case that the differential pressure is 32 kPa, the free surface of the solid water is located at 1.32 m below the bottom of the broken cold leg. It is considered that the water overflow through the broken cold leg is small in the SCTF tests.

If the friction loss and the acceleration loss is negligible, the differential pressure can be related to the accumulated mass by the equation, given by

$$M = \frac{A\,\Delta P}{g} \quad . \tag{3}$$

Table 3 shows the time-averaged water accumulation rate estimated with Eq. (3). In the lower plenum injection period, the water accumulation rate in the core of low temperature test is 1.42 times the rate of high temperature

test. The rate in the downcomer of low temperature test is 0.82 times the rate of high temperature test. In the lower plenum injection period, more water accumulated in the core for the lower initial clad temperature test. On the contrary, in the later period of the cold leg injection, the water accumulation rates in the core and the downcomer are almost the same between both the tests.

Figure 12 shows comparisons of the core inlet mass flow rate and the core inlet mass flow between high and low temperature tests. The core inlet mass flow rate shown in Fig. 12 was calculated based on the mass balance relation in the pressure vessel (see Appendix A). The core inlet mass flow is the time-integrated one of the mass flow rate evaluated based on the mass balance relation. The core inlet mass flow indicates the total mass through the core inlet after the reflood initiation.

Table 4 summarizes the time-averaged core inlet mass flow rate. In the lower plenum injection period (before 50 s), the time-averaged core inlet mass flow rates are 10.69 and 12.85 kg/s in high and low temperature tests, respectively. The ECC water injection rate in the lower plenum is about 20.0 kg/s in both tests. Roughly speaking, about a half of the injected water flows into the core and another half of the injected water flows into the downcomer in the lower plenum injection period. In the lower injection period, the time-averaged core inlet mass flow rate in low temperature test is higher by 2.16 kg/s than that in high temperature test.

As shown in Table 3, the water accumulation rate in the core is 2.9 kg/s higher in low temperature test than that of high temperature test in the lower plenum injection period. Although the core inlet mass flow rate increased by low initial clad temperature, the mass flow rate through the core outlet decreased in the period by low initial clad temperature due to increase of the water accumulation rate in the core.

After the switch of the ECC water injection location from the lower plenum to the cold leg, the core inlet mass flow rate is decreased as shown in Fig. 12. The reduction occurs more quickly in low temperature test than in high temperature test. In the period between 50 and 100 s, the time-averaged core inlet mass flow rete in low temperature test is lower than that in high temperature test. Figure 11 shows that the differential pressure through the downcomer is reduced in high temperature test right after the switch of the ECC water injection location. It seems that some amount of

accumulated water in downcomer was supplied to the core right after switching.

After 100 s, the core inlet mass flow rate is almost the same between both the tests as shown in Fig. 12. The time-averaged core inlet mass flow rates between 100 and 300 s are 4.98 and 5.22 kg/s in high and low temperature tests, respectively. The core inlet mass flow rate is almost identical with the ECC water injection rate into the cold leg (that is, 5.1 kg/s). The core inlet mass flow rate is limited mainly by the ECC water injection rate into the cold leg in the SCTF. Even though the SCTF tests were performed under the gravity feed condition, the core inlet mass flow rate is not controlled by the feedback effect of the generated steam in the core in the later period of the cold leg injection. It is important to adjust the ECC injection rate carefully in order to simulate the flow conditions of actual PWRs properly.

The ECC injection rates of the SCTF Tests S2-SH1 and S2-09 were adjusted in order to establish the same core inlet mass flow rate as in the CCTF base case test, that was conducted with a high initial clad temperature of 1073 K. One can expect that the core inlet mass flow rate in the Test S2-SH1 is reasonable for the simulation of flow conditions in actual PWRs with a high initial clad temperature. In the SCTF Test S2-09, the same ECC injection rate as the SCTF S2-SH1 was applied although the initial clad temperature was different between two tests. It should be noted that there is a possibility that the core inlet mass flow rate is strongly affected by the initial clad temperature due to the system feedback effect in actual PWRs. Although the SCTF Test S2-09 was performed under the gravity feedback condition, the test should be treated as a parametric test for the initial clad temperature without system feedback effect as in the so-called forced feed test.

Figure 13 shows the comparisons of the axial core differential pressures along Bundle 4 of the core. In the period right after the reflood initiation (before 20 s), the lower initial clad temperature resulted in the lower core differential pressure in the region above 0.700 m from the bottom of the core heated part. It is supposed that the fluid swell is less significant in low temperature test because of less steam generation in the period right after the reflood initiation. In the later period of the tests, the core differential pressure of each section increases as the quench front propagates the section in both tests. Because the quench front propagates faster in low temperature test than in high temperature test, the differential pressure of each section is higher in low temperature test than that in high temperature

test. After the whole part of the section is quenched, the differential pressure through the section is nearly the same between both the tests. The low initial clad temperature causes the water accumulation rate in the core to be increased because of the fast propagation of the quench front.

3.3 Effect of Initial Clad Temperature on Core Cooling Behavior

Figure 14 shows comparisons of the clad surface temperature between high and low temperature tests at the elevations of 1.735 and 2.330 m from the bottom of the core heated part in Bundles 4 and 8, respectively. The lower initial clad temperature resulted in the lower turnaround temperature and the faster quench at the elevations of 1.735 and 2.330 m. The turnaround temperature in low temperature test is lower at other elevations than that in high temperature test, as shown in Fig. 15. Figure 16 indicates the temperature rises along the Bundle 4. The temperature rise is defined as the difference of the temperatures between the turnaround and the reflood initiation. The lower initial clad temperature resulted in the higher temperature rise except the top part of core (above 2.76 m). Figure 17 shows the comparisons of the quench times and temperatures between high and low temperature tests in Bundles 4 and 8. The lower initial clad temperature resulted in the faster quench propagation, especially in the lower part of the core.

Figure 18 shows heat transfer coefficients at the elevations of 1.735, 1.905 and 2.330 m from the bottom of the core heated part in Bundles 4 and 8. The heat transfer coefficients in low temperature test are higher than those in high temperature test at every elevation. The lower initial clad temperature resulted in the higher core heat transfer coefficient. In high temperature test, the heat transfer coefficient in Bundle 4 is higher than that in Bundle 8 except the point right before the quench occurs at each elevation. Similar relation can be observed between the heat transfer coefficients of Bundles 4 and 8 at the elevation of 2.330 m in low temperature test. At the elevations of 1.735 and 1.905 m in low temperature test, the dependency of the heat transfer coefficients on the bundle location looks similar to that in low temperature test, although it is not so clear as that at the elevation of 2.330 m.

Figure 19 shows the heat transfer coefficients at the elevation of 1.905 m in terms of the distance from the quench front. When the ECC water

injection location was switched from the lower plenum to the cold leg, the quench front located at 0.63, 0.59, 0.61 and 0.65 m from the bottom of the core heated part in Bundles 2, 4, 6 and 8 in high temperature test, respectively. Those located at 1.26, 1.16, 1.23 and 1.30 m in Bundles 2, 4, 6 and 8 in low temperature test, respectively. In the region apart from the quench front, the heat transfer coefficient from high temperature test is higher than that from the low temperature test. It is supposed that the higher heat transfer coefficient in higher temperature test is caused by the increase of the water carry-over. In the region near the quench front (less than 30-40 cm from the quench fronth), almost the same heat transfer coefficient is observed between both tests.

3.4 Comparison with CCTF Results

In order to study the thermal hydraulic behavior with low initial clad temperature, a test was conducted using the CCTF[6]. The SCTF and CCTF results are compared to get better understanding of the SCTF results. Figure 20 shows the core inlet mass flow rate from the SCTF and CCTF tests which were performed with the initial clad surface temperature of 573 K. In the SCTF test (low temperature test: Test S2-09), no significant oscillation can be observed, while oscillation with a long period is remarkable in the CCTF tests. In the reference (6), the flow oscillation in the CCTF test is attributed to the system coupling effect among the water accumulation in the upper plenum, the water carry-over from the upper plenum to the steam generator and the steam generation at the steam generator. In the mechanism of the flow oscillation described in the reference, the steam generation due to the evaporation of the carried water at the steam generator is one of the key causes of the flow oscillation because it can push the water in the upper plenum beck to the core due to the increased loop differential pressure. Because no active steam generator is installed in the SCTF, such a feedback effect from the steam generation at the steam generator can not exist in the SCTF. It is considered that no flow oscillation is observed in the SCTF Test S2-09 because the SCTF has no active steam generator.

Figure 21 shows the temperature rise at the central part of the core. In the SCTF tests, the temperature rise of the low temperature test is higher than that of the high temperature test. On the other hand, in the CCTF tests,

the temperature rise is lower in the test with initial clad temperature of 573 K than those in the tests with higher initial clad temperature. The dependency of the temperature rise on the initial clad temperature in the SCTF test is the same as those in the previous tests performed under the forced feed test such as the FLECHT test. As previously mentioned, the core inlet mass flow rate is controlled mainly by the ECC injection rate in the SCTF gravity tests. Therefore, the core inlet mass flow rate was weakly affected by the initial clad temperature in the SCTF gravity feed test as well as the so-called forced feed test. In the CCTF tests, the low initial clad temperature resulted in the increase of the core inlet mass flow rate and caused the temperature rise to be decreased in the test with a low initial clad temperature of 573 K. In actual PWRs, such a system effect as in the CCTF test can be expected. It is considered that the temperature rise in actual PWRs with low initial clad temperature of 573 K should be smaller than that in the SCTF test because of the increased core inlet mass flow rate arising from the system effect.

4. Conclusions

In order to study the reflood behavior with low initial clad temperature, a reflood test was performed using the Slab Core Test Facility (SCTF) with initial clad temperature of 573 K. Through the comparison with results from the test with initial clad temperature of 1073 K, the following conclusions were obtained.

(1) The low initial clad temperature resulted in the low differential pressures through the primary loops due to smaller steam generation in the core.

(2) The low initial clad temperature caused the accumulated mass in the core to be increased and the accumulated mass in the downcomer to be decreased in the period of the lower plenum injection with accumulator (before 50s). In the later period of the cold leg injection with LPCI (after 100s), the water accumulation rates in the core and the downcomer were almost the same between both tests.

(3) The low initial clad temperature resulted in the increase of the core inlet mass flow rate in the lower plenum injection period. However, the core inlet mass flow rate was almost the same regardless of the initial clad temperature in the later period of the cold leg injection period because the core inlet mass flow rate is limited mainly by the ECC water injection rate into the cold leg in the SCTF.

(4) The low initial clad temperature resulted in the low turnaround temperature, high temperature rise and fast bottom quench front propagation.

(5) In the region apart from the quench front, low initial clad temperature resulted in the lower heat transfer. In the region near the quench front, almost the same heat transfer coefficient was observed between both tests.

(6) No flow oscillation with a long period was observed in the SCTF test with low initial clad temperature of 573 K, while it was remarkable in the CCTF test which was performed with the same initial clad temperature. It is considered that no flow oscillation is induced in the SCTF because the SCTF has no active steam generator while the CCTF has active steam generators.

Acknowledgment

The authors are much indebted to Drs. M. Shiba and Y. Kaneko for their guidance and encouragement for this program. The authors wish to express their thanks to Messrs. T. Iguchi, J. Sugimoto and T. Hojo for their helpful discussions.

They also would like to express their thanks to the 2D/3D project members of the U. S. A and F. R. G. for their valuable discussions.

References

(1) Hirano, K., Murao, Y., : J. At. Energy Soc. Japan, (in Japanese), 22 (10, 681 (1980).
(2) Fujita, R. K., et al. : LA-2D/3D-TN-83-4, (1983).
(3) Adachi, H., et al. : JAERI-M 83-080, (1983).
(4) Sobajima, M., et al. : Design of Slab Core Test Facility (SCTF) in Large Scale Reflood Test Program, Part II : Core-II, to be published as a JAERI-M report.
(5) Iwamura, T., et al. : JAERI-M 85-106. (1985).
(6) Okabe, K., et al. : Quick-look Report on CCTF Core-II Reflood Test C2-12 (Run 71)-Best Estimate Reflood Experiment-, to be published as a JAERI-M report.

Acknowledgment

The authors are much indebted to Drs. M. Shiba and Y. Kaneko for their guidance and encouragement for this program. The authors wish to express their thanks to Messrs. T. Iguchi, J. Sugimoto and T. Hojo for their helpful discussions.

They also would like to express their thanks to the 2D/3D project members of the U. S. A and F. R. G. for their valuable discussions.

References

(1) Hirano, K., Murao, Y., : J. At. Energy Soc. Japan, (in Japanese), 22 (10, 681 (1980).
(2) Fujita, R. K., et al. : LA-2D/3D-TN-83-4, (1983).
(3) Adachi, H., et al. : JAERI-M 83-080, (1983).
(4) Sobajima, M., et al. : Design of Slab Core Test Facility (SCTF) in Large Scale Reflood Test Program, Part II : Core-II, to be published as a JAERI-M report.
(5) Iwamura, T., et al. : JAERI-M 85-106. (1985).
(6) Okabe, K., et al. : Quick-look Report on CCTF Core-II Reflood Test C2-12 (Run 71)-Best Estimate Reflood Experiment-, to be published as a JAERI-M report.

Table 1 List of major test conditions

Item \ Test name	High temperature (Test S2-SH1)	Low temperature (Test S2-09)
Initial maximum clad temperature (K)	1076	591
System pressure (MPa)	0.20	0.20
Initial average core power (kW/m)	1.041	1.033
Radial power profile (*1)	1.001:1.063:1.013:0.923	1.005:1.059:1.017:0.919
Decay curve type	(*2)	(*2)
Injection rate into lower plenum (kg/s)	20.0	19.3
Duration time of injection into lower plenum (s)	52.0	55.5
Injection rate into cold leg (kg/s)	5.3	5.4
ECC water temperature (K)	351	351

(*1) $P_{12} : P_{34} : P_{56} : P_{78}$

$P_{ij} = (P_i + P_j)/2$ where P_i : radial peaking factor of i-th bundle

(*2) (ANS + Actinide) x 1.02 (40 s after scram)

Table 2 Comparison of loop flow resistance coefficient between high and low temperature tests

(a) Intact cold leg

Time / Test name	100	300
High temperature test	40	44
Low temperature test	45	45

(b) Broken cold leg of S/W separator side

Time / Test name	100	300
High temperature test	23	22
Low temperature test	22	25

(c) Broken cold leg of PV side

Time / Test name	100	300
High temperature test	5.3	5.0
Low temperature test	4.9	3.9

Table 3 Water accumulation rates into core and downcomer

(1) In lower plenum injection period (0 s < t < 55 s)

Test name / Location	High temperature test	Low temperature test
Core	6.9	9.8
Downcomer	6.8	5.6

(2) In cold leg injection period (100 s < t < 300 s)

Test name / Location	High temperature test	Low temperature test
Core	0.85	0.85
Downcomer	0.19	0.20

Table 4 Comparison of time-averaged core inlet mass flow rate between high and low temperature tests

Test name / Period (s)	High temperature test	Low temperature test
0 - 50	10.69	12.85
50 - 100	7.95	6.43
100 - 300	4.98	5.22

Note

Lower plenum injection

Injection rate (kg/s): 20.0

Injection period (s) : 0 - 55

Cold leg injection

Injection rate (kg/s): 5.1

Injection period (s) : after 55

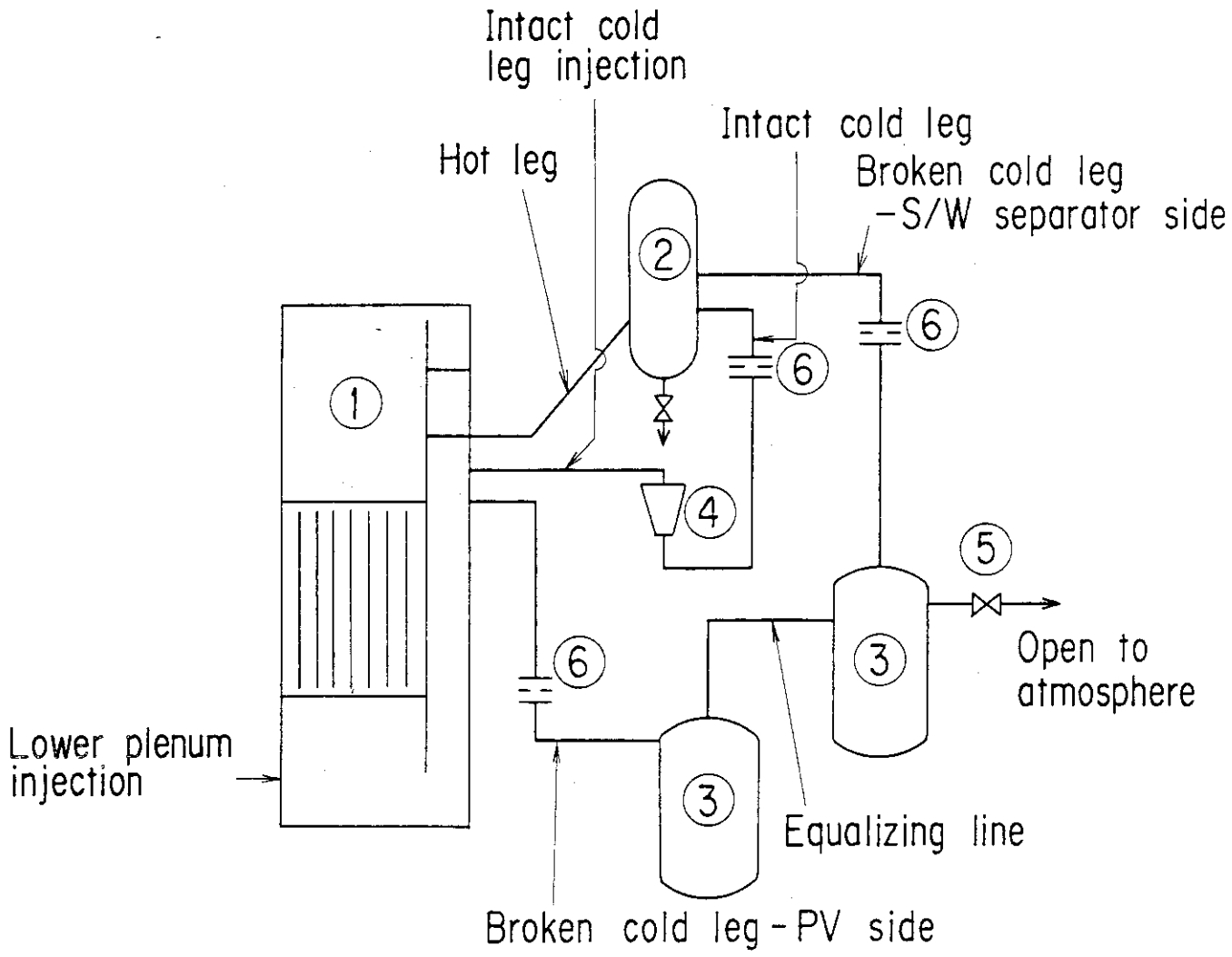

Fig. 1 Schematics of Slab Core Test Facility (SCTF)

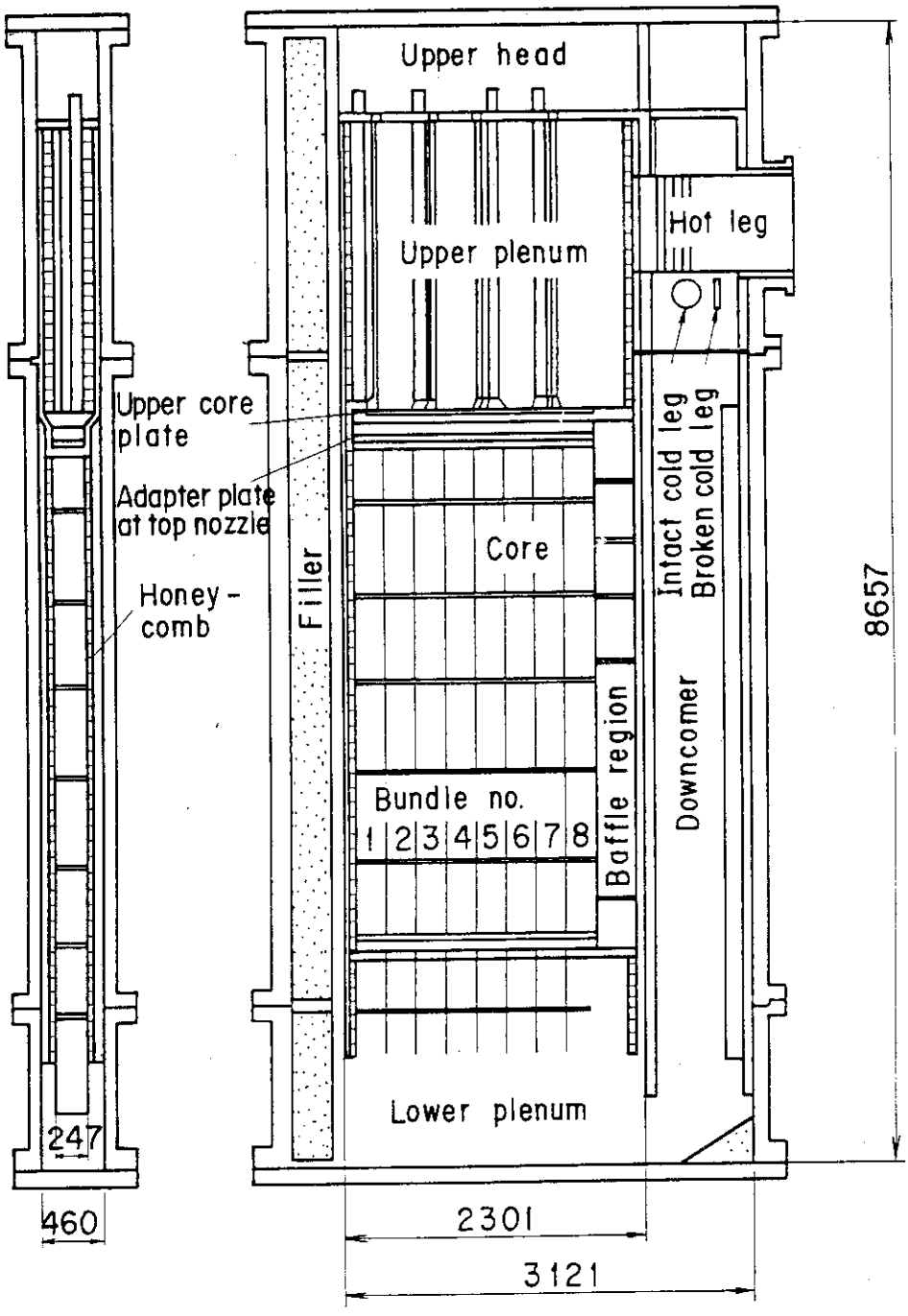

Fig. 2 Vertical cross section of SCTF pressure vessel

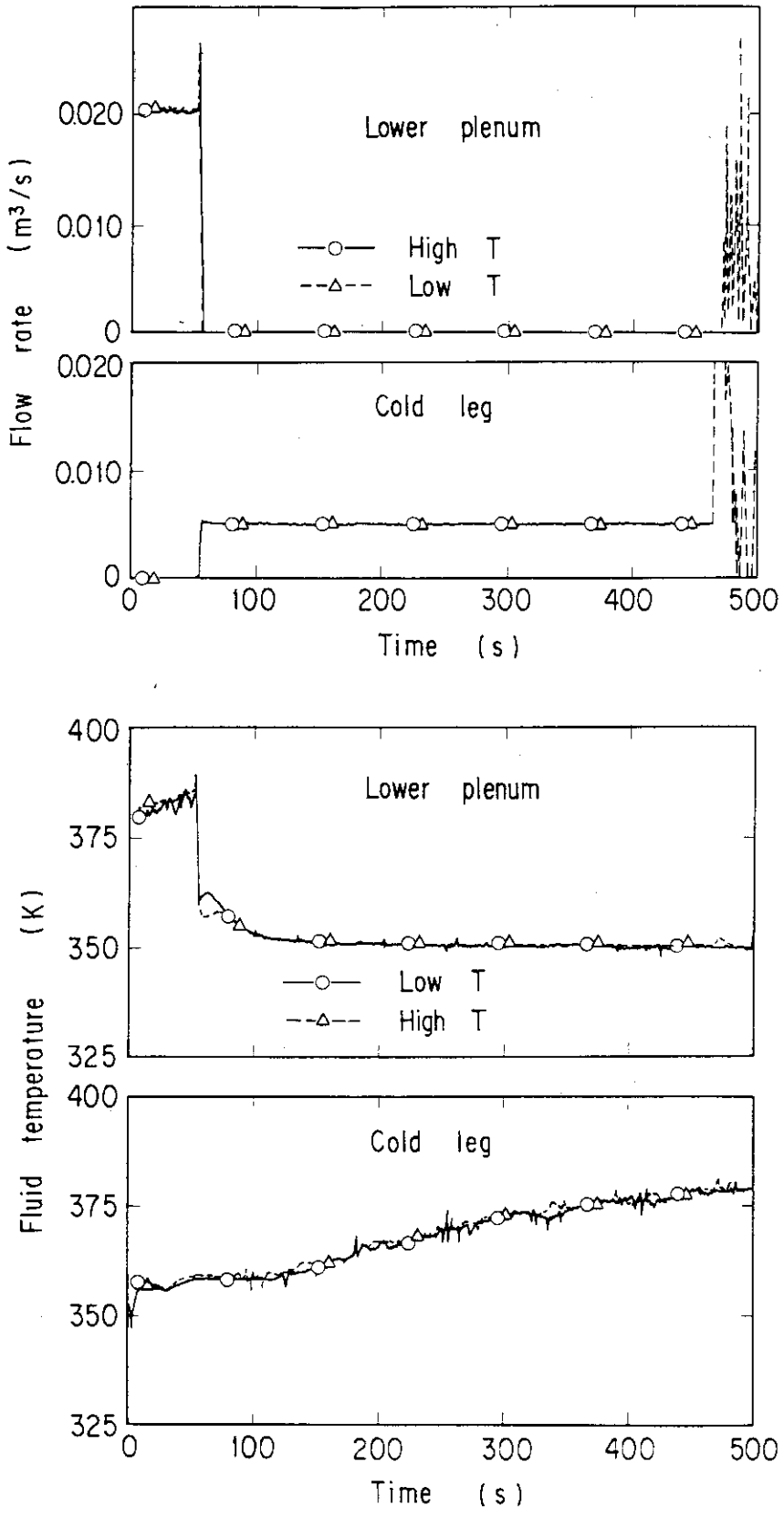

Fig. 3 ECC water injection rate and fluid temperature at ECC injection port

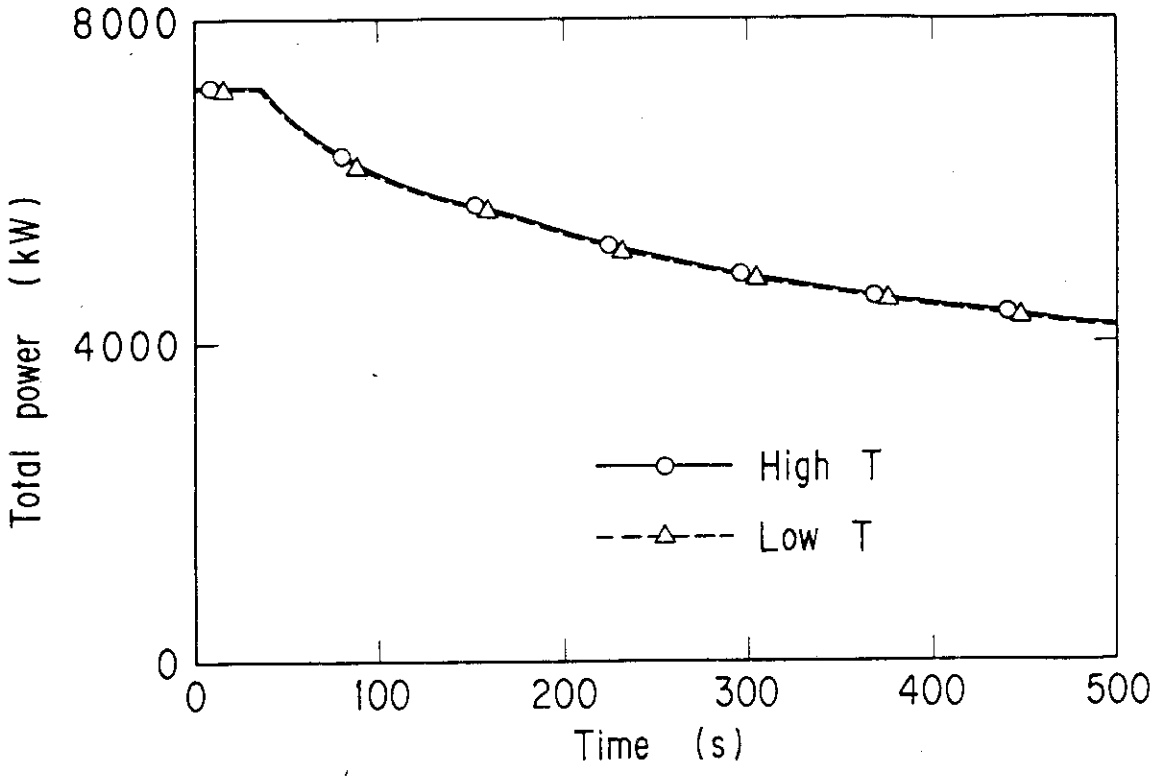

Fig. 4 Total power supplied to core

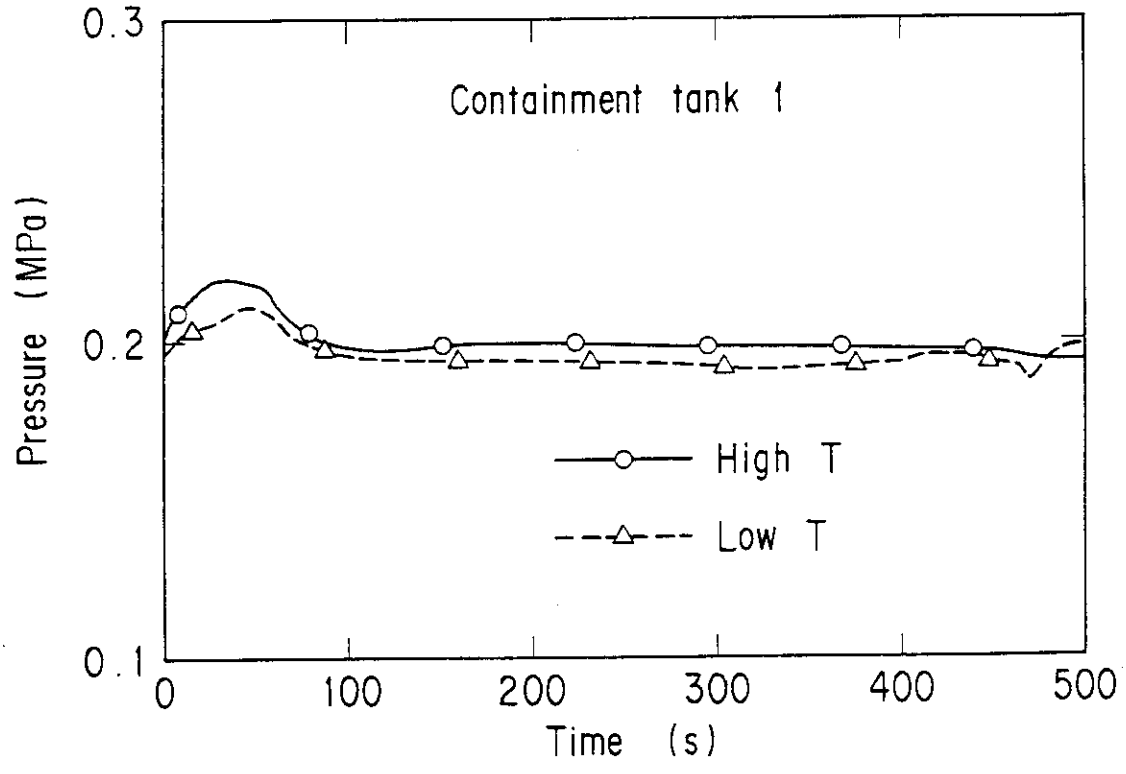

Fig. 5 Containment pressure

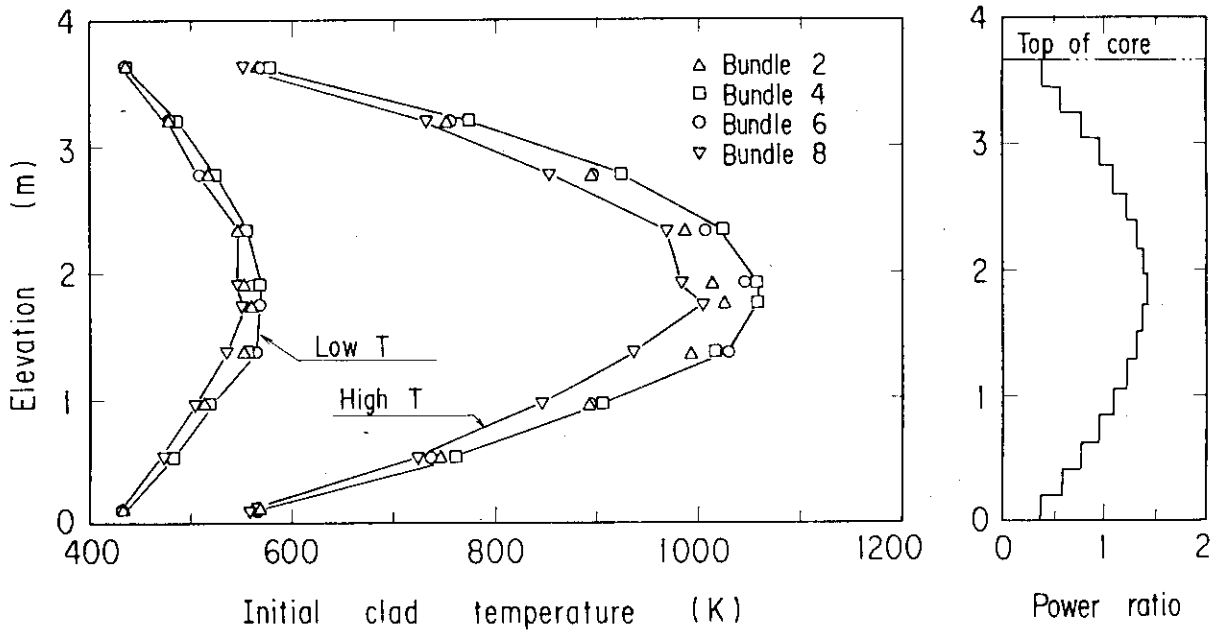

Fig. 6 Initial clad temperature

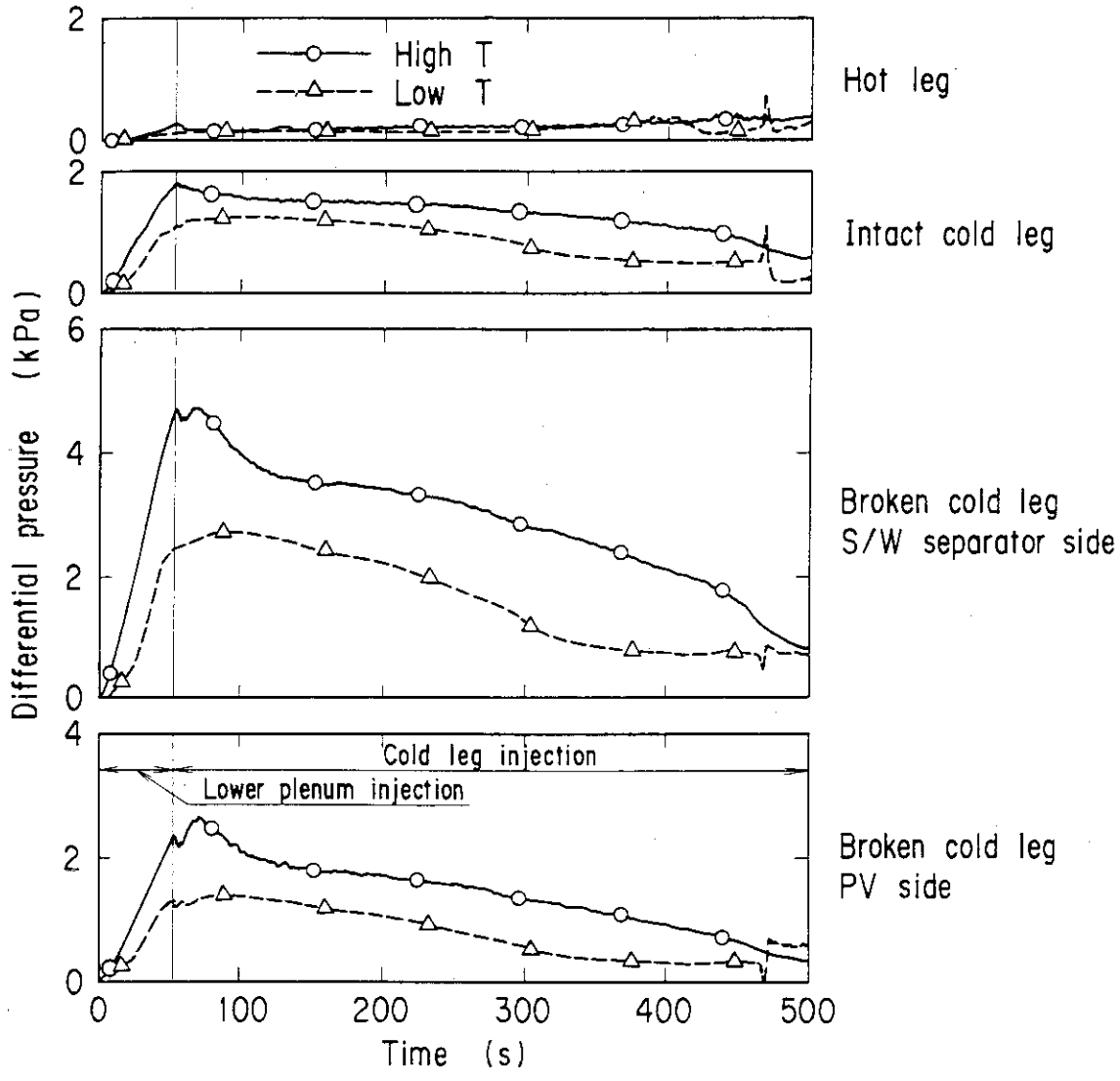

Fig. 7 Differential pressure through each section of primary loops

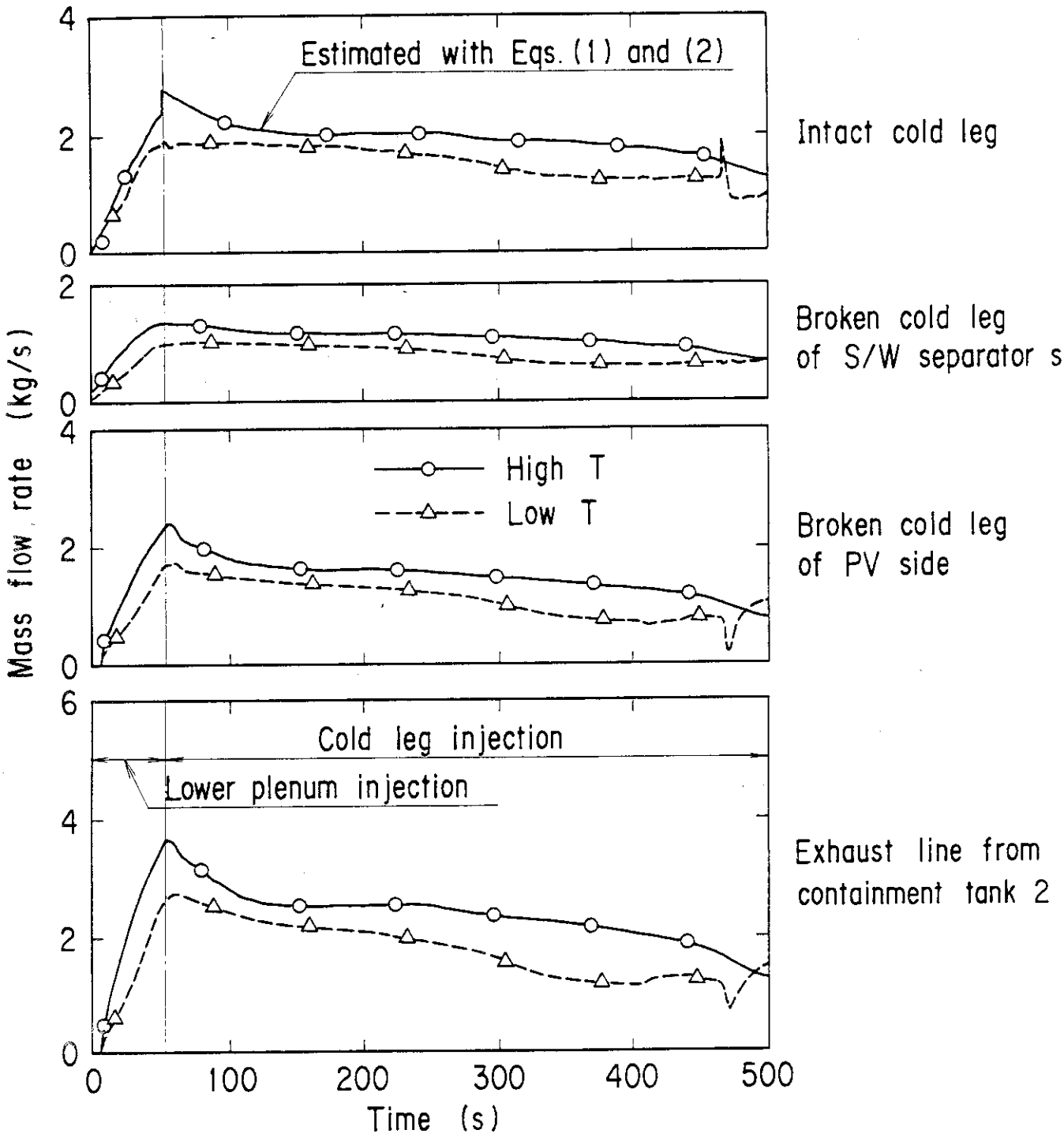

Fig. 8 Mass flow rate through each section of primary loops

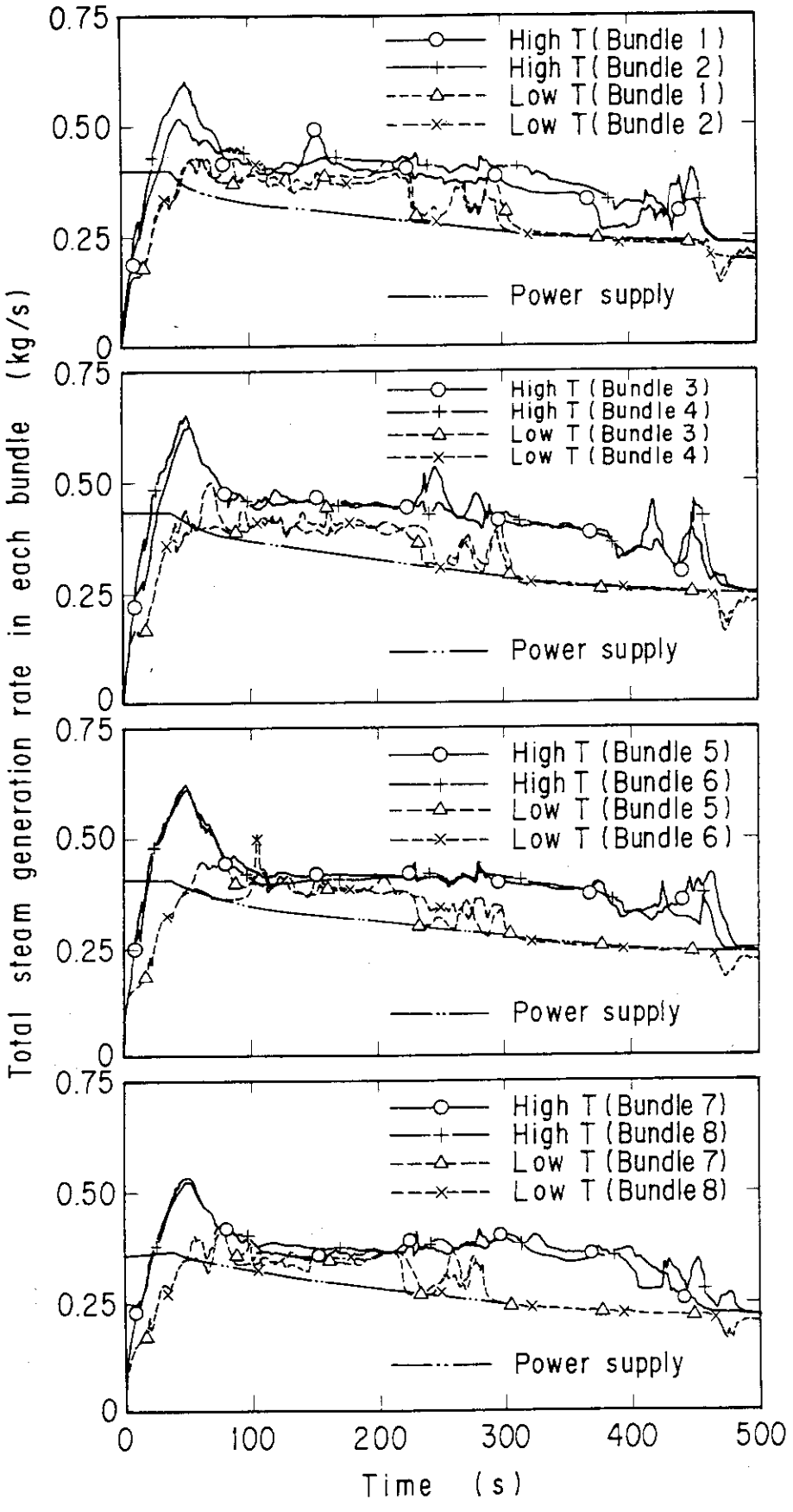

Fig. 9 Steam generation rate in each bundle in core

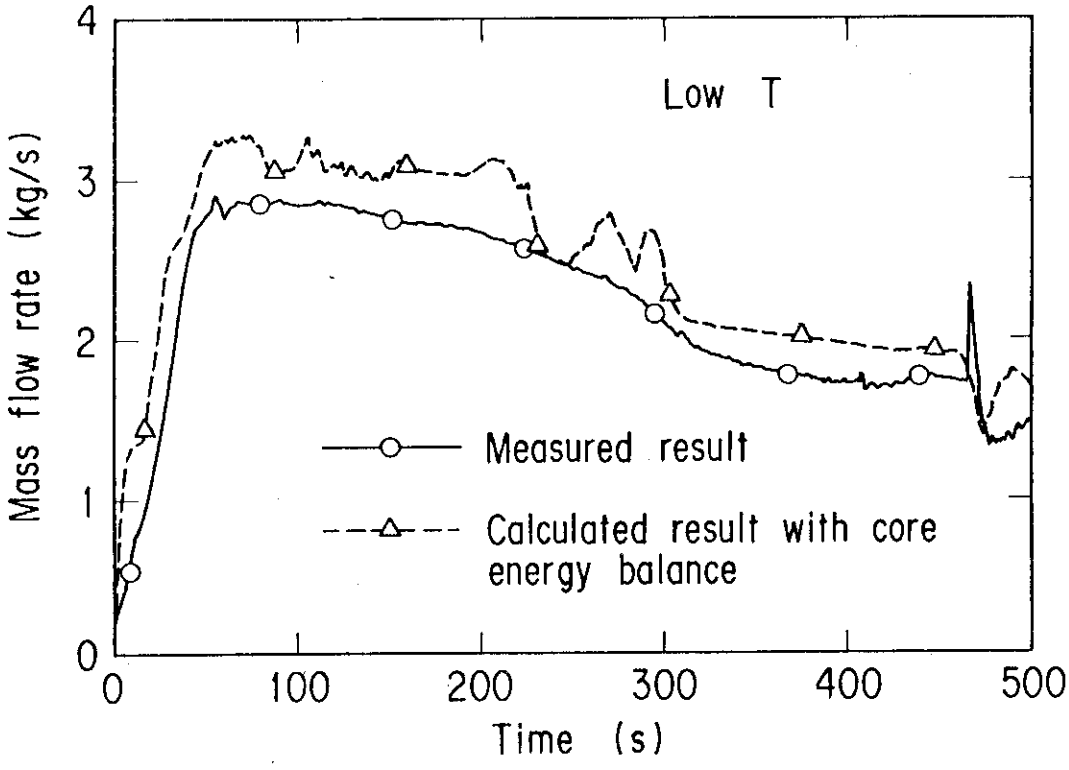

Fig. 10 Comparison of steam mass flow rate at core outlet between measured and calculated results

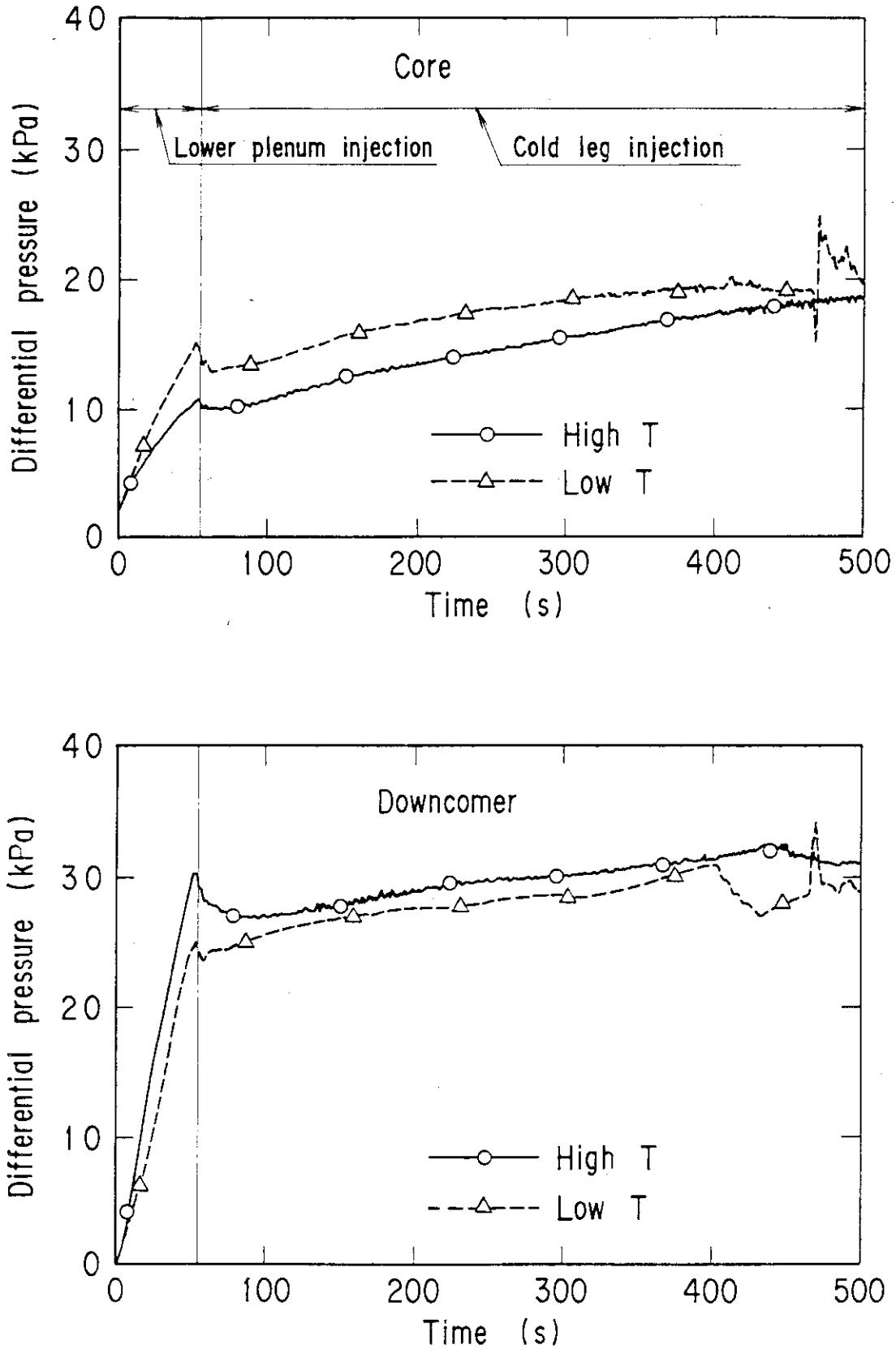

Fig. 11 Differential pressure through core and downcomer

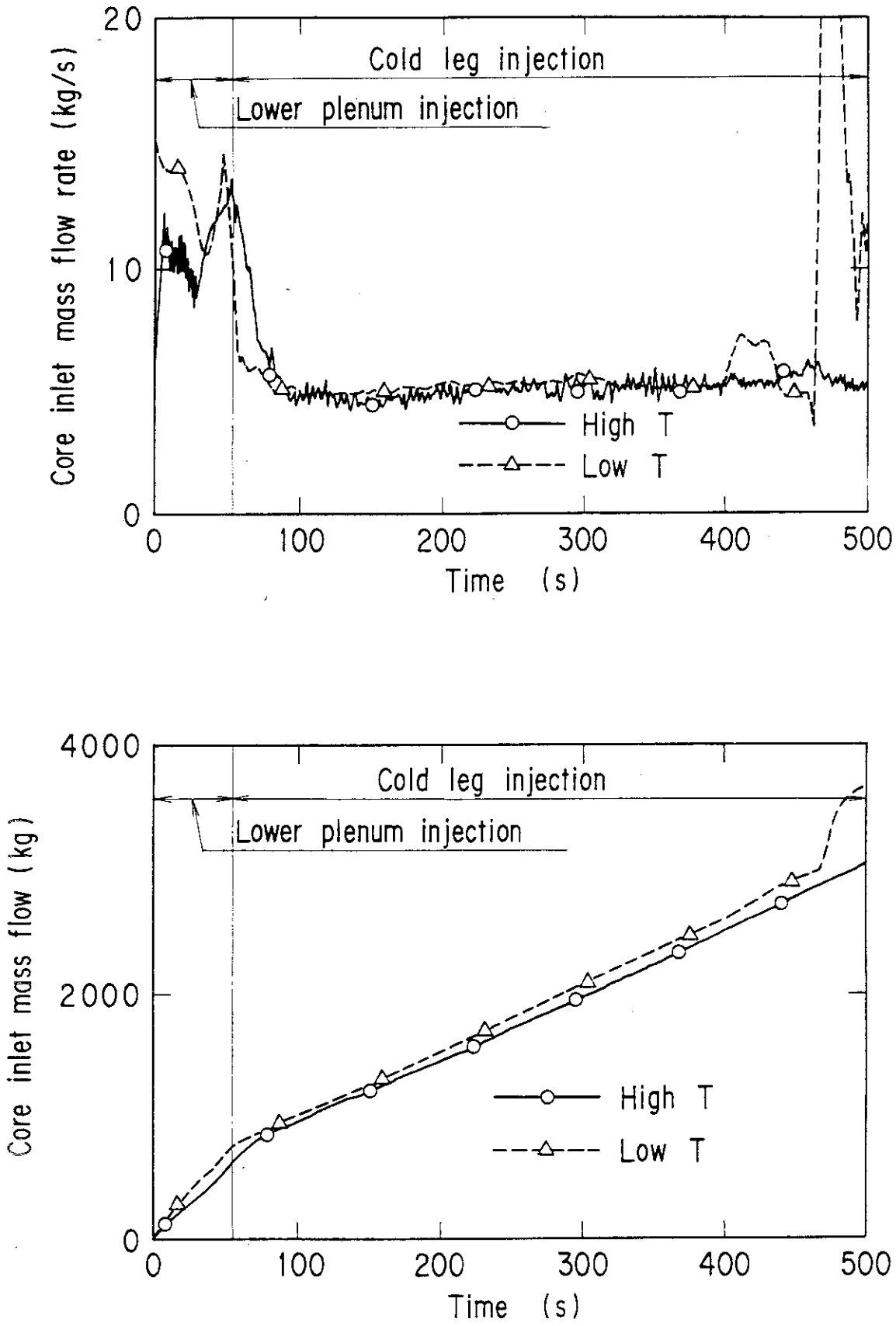

Fig. 12 Core inlet mass flow rate and core inlet mass flow

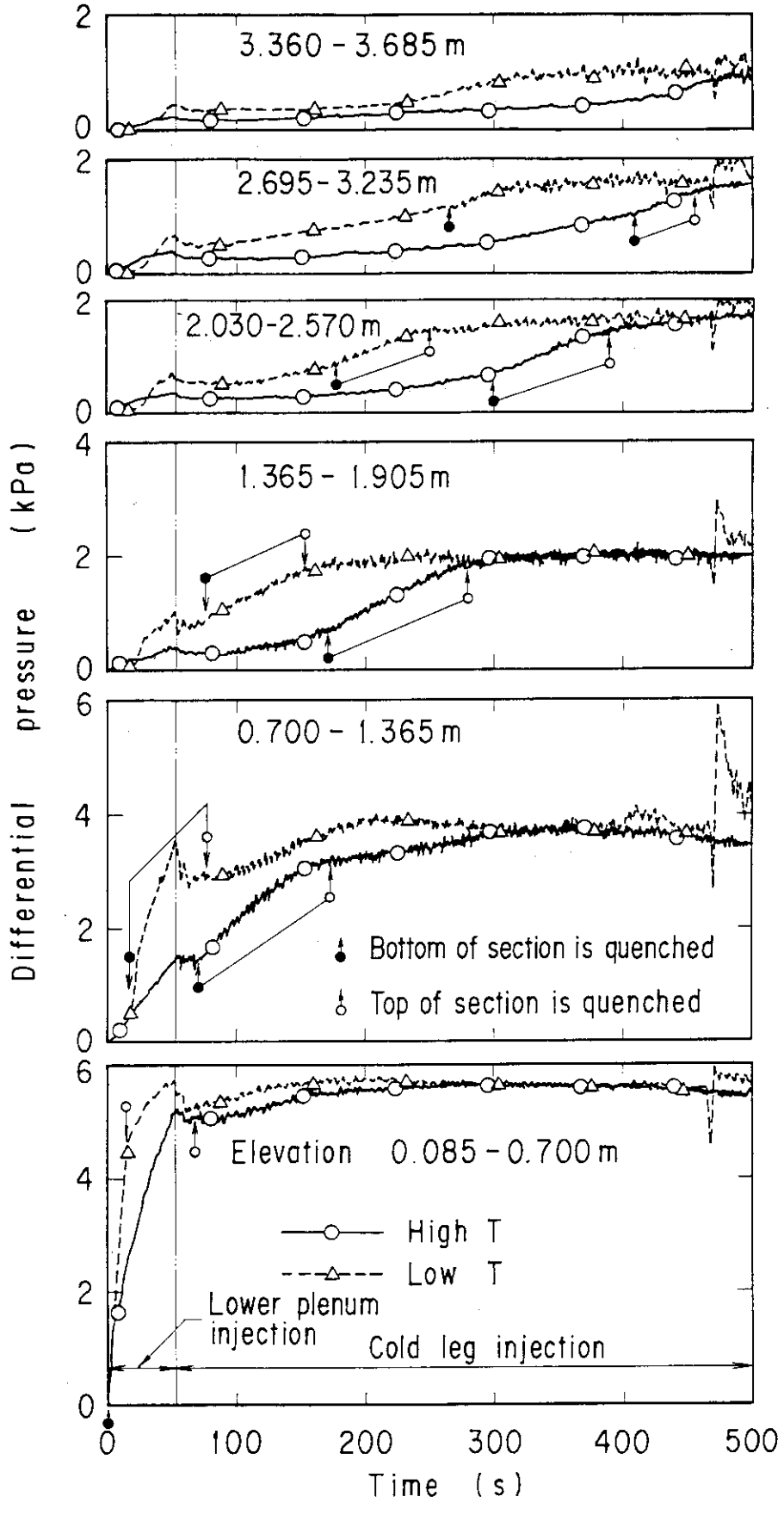

Fig. 13 Axial core differential pressures in Bundle 4

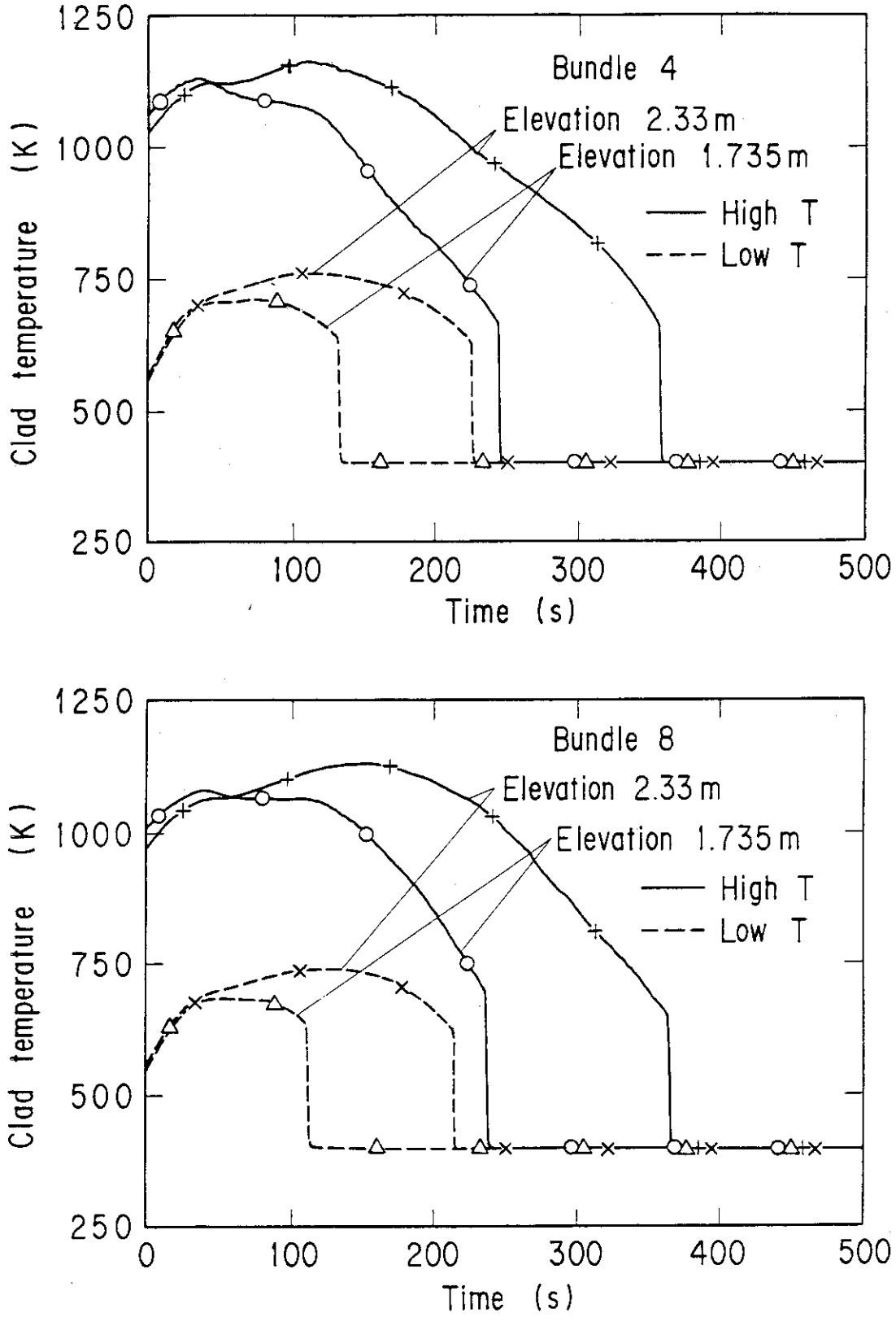

Fig. 14 Clad temperature at elevations of 1.735 and 2.330 m in Bundles 4 and 8

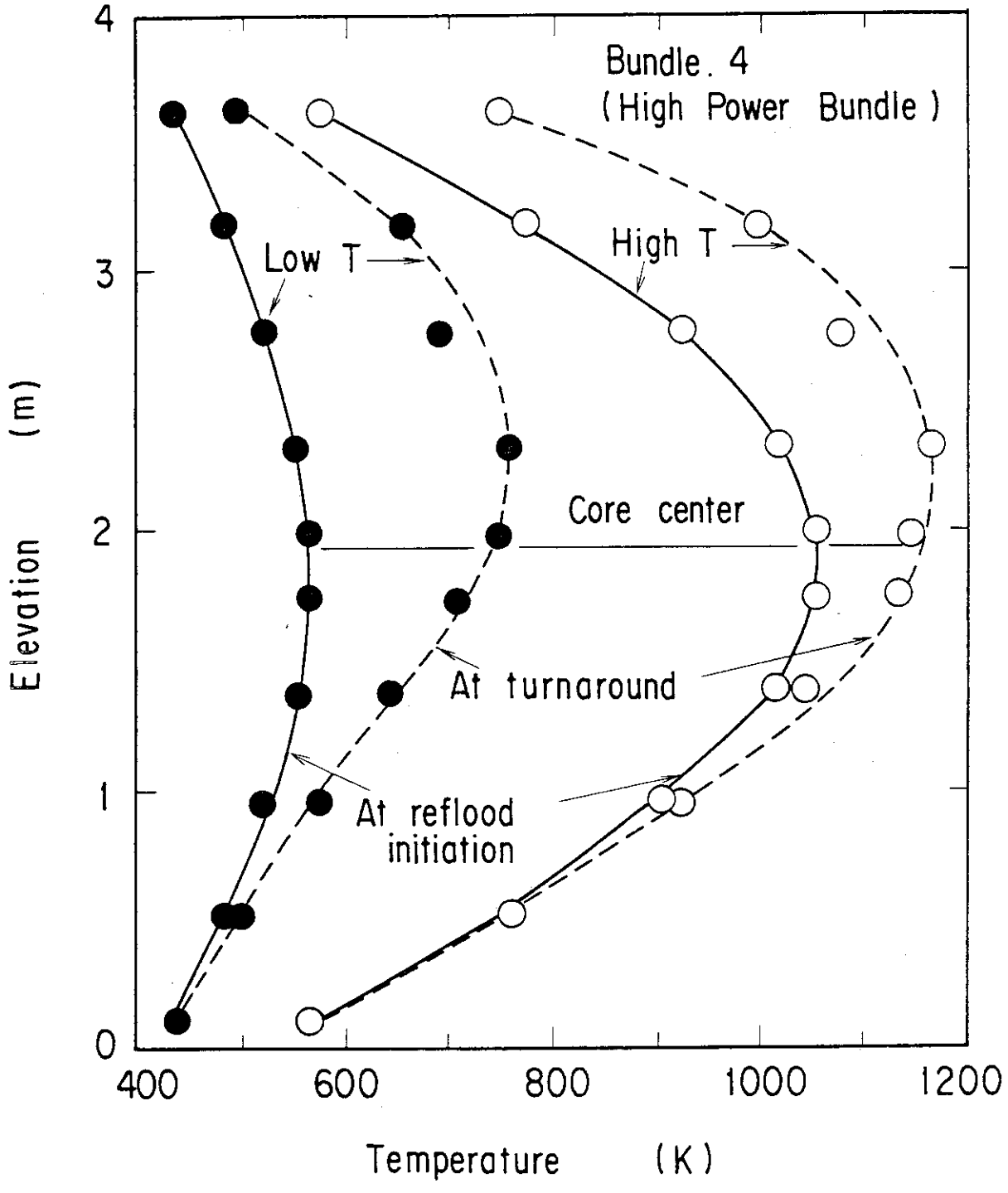

Fig. 15 Axial distribution of clad temperature at reflood initiation and turnaround

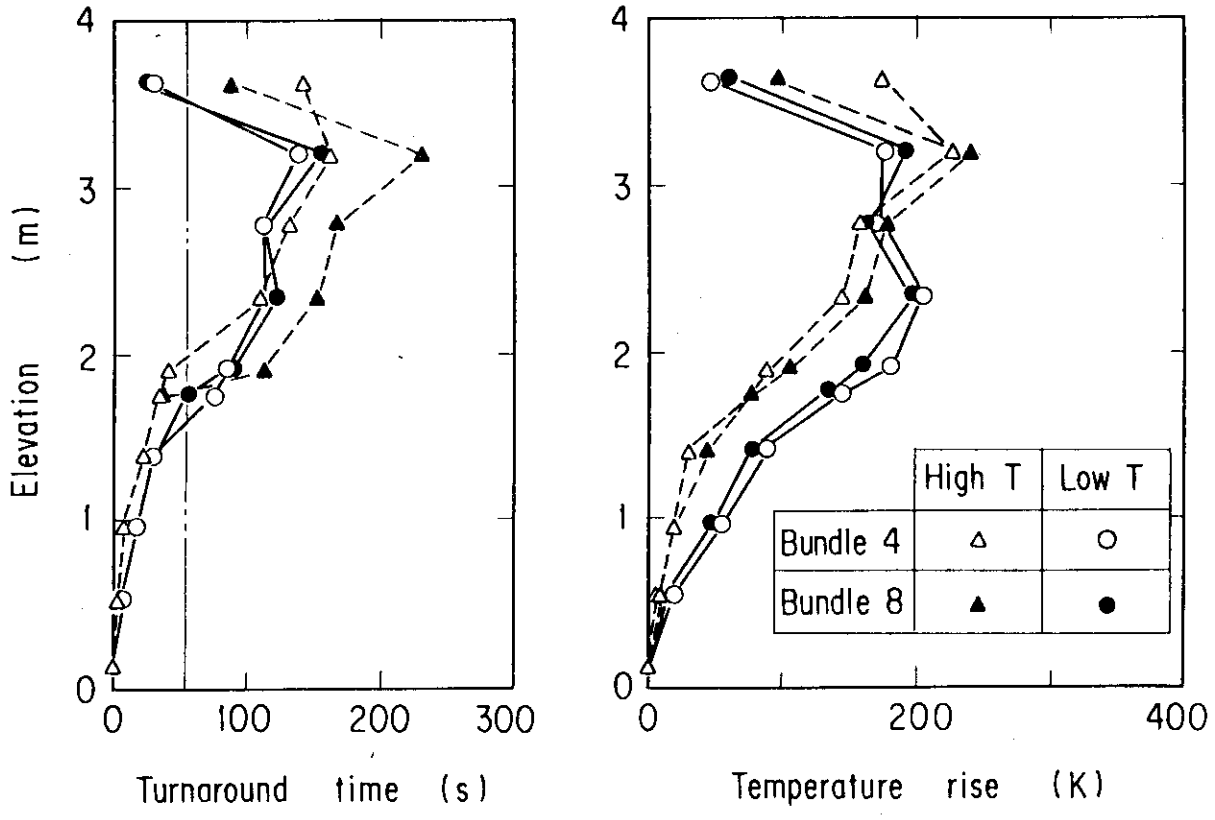

Fig. 16 Turnaround time and temperature rise in Bundles 4 and 8

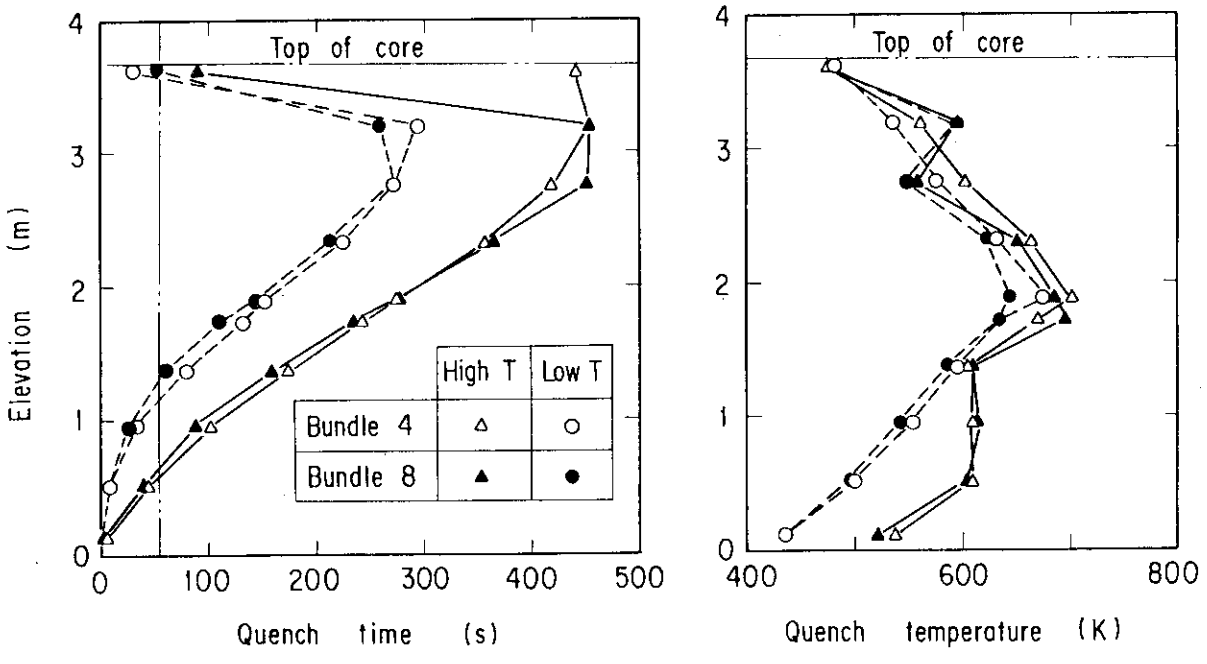

Fig. 17 Quench time and temperature in Bundles 4 and 8

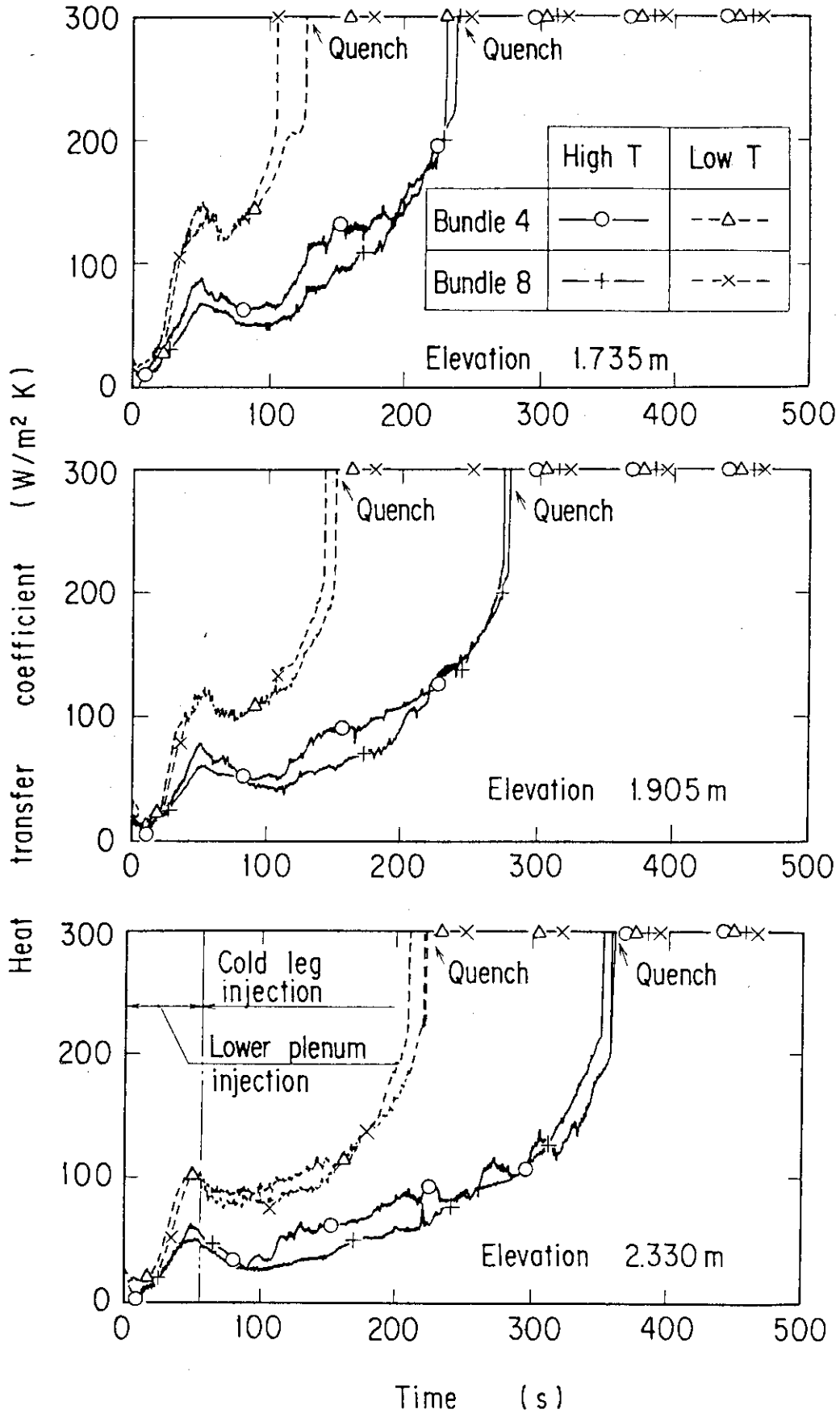

Fig. 18 Heat transfer coefficient at elevations of 1.735, 1.905 and 2.330 m in Bundles 4 and 8

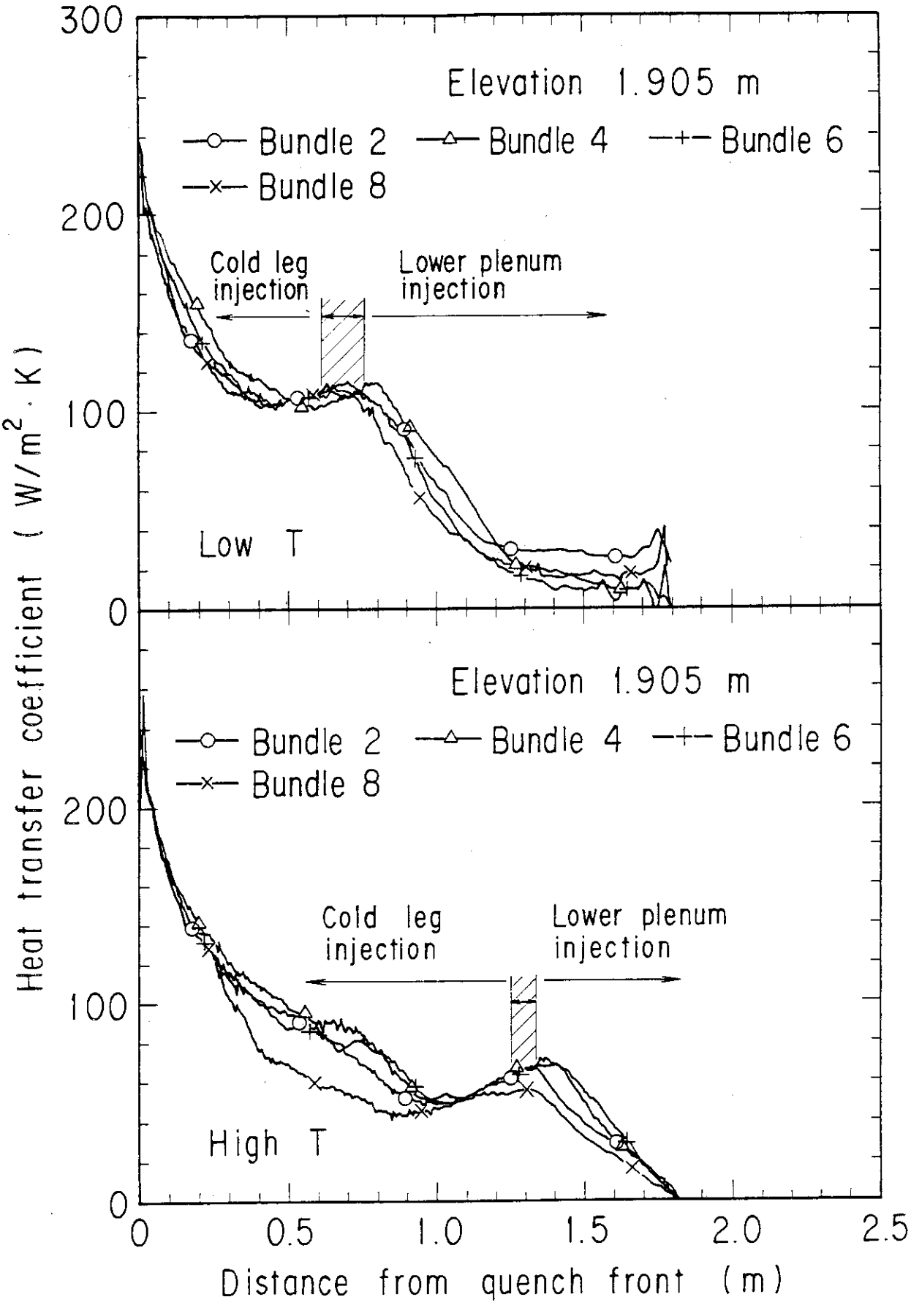

Fig. 19 Heat transfer coefficient at elevation of 1.905 m in terms of distance from quench front

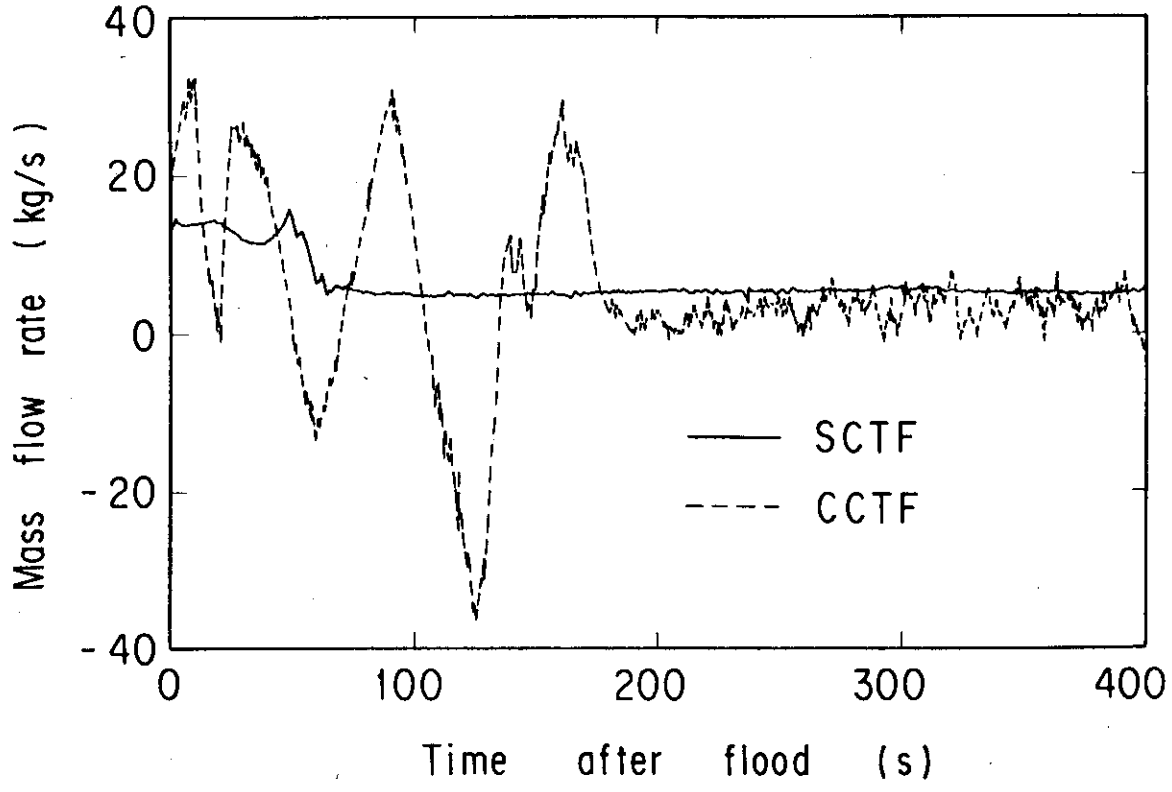

Fig. 20 Comparison of core inlet mass flow rate between CCTF and SCTF

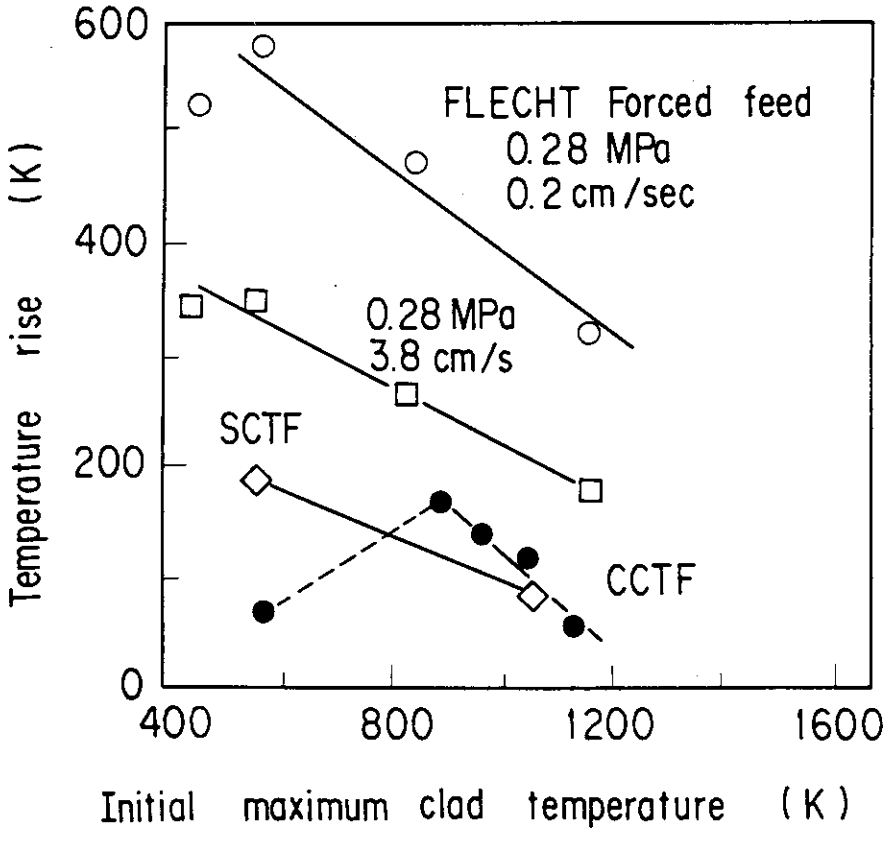

Fig. 21 Effect of initial clad temperature on temperature rise

Appendix A Brief Description of the Slab Core Test Facility(SCTF)

A.1 Test Facility

The Slab Core Test Facility is designed under the following design philosophy and design criteria:

a. Design Philosophy

(1) The facility should provide the capability to study the two-dimensional thermohydraulic behavior in a reactor pressure vessel especially due to the radial power distribution during the end of blowdown, refill and reflood pahses of a postulated LOCA in a PWR.

(2) To properly simulate the core heat transfer and hydrodynamics, a special emphasis is put on the proper simulation of the components in the pressure vessel. Provided as the components in the pressure vessel are the simulated core, downcomer, core baffle region, lower plenum, upper plenum and upper head. On the other hand, simplified primary coolant loops are also provided. Provided as the primary coolant loop components are a hot leg, an intact cold leg, broken cold legs and a steam/water separator which is to simulate single steam phase flow downstream of a steam generator and to measure the flow rate of carryover water coming from the upper plenum.

b. Design Criteria

(1) The reference reactor to be simulated in SCTF is the Trojan reactor in the United States which is a four-loop 3300 MWt PWR. The Ooi reactor etc. in Japan are also referred which are of the similar type to the Trojan reactor except the provision of UHI system.

(2) A full scale radial and axial section of core with single bundle width of the pressurized water reactor is provided as the simulated core of SCTF.

(3) The simulated core consists of 8 bundles arranged in a row. Each bundle has electrically heated rods simulating fuel rods and non-heated rods with 16×16 array, with the diameter and the pitch for Trojan which has 15×15 rod array.

(4) The flow area and fluid volume of components are scaled down based on the nominal core flow area scaling, 1/21.

(5) To properly simulate the flow behavior of carryover water or entrainment, the elevations of hot leg and cold legs are designed

to be the same as the PWR as much as possible.

(6) A honeycomb structure is used for side walls with surface plates which accomodates the slab core, the upper plenum and the upper part of lower plenum, so as to minimize the effect of walls on the core heat transfer and hydrodynamics.

(7) To investigate the effect of flow resistance in the primary loop are provided the orifices of which dimension is changeable.

(8) The maximum allowable temperature of the simulated fuel rods is 900°C (1173 K) and the maximum allowable pressure of the facility is 0.6 MPa.

(9) The facility is equipped with the hot leg equivalent to four hot legs connecting the upper plenum and the steam/water separator, the intact cold leg equivalent to three intact cold legs connecting the steam/water separator and the downcomer and the two broken cold legs, one is for the steam/water separator side and another for the pressure vessel side.

(10) The ECCS consists of an accumulator (Acc), a low pressure coolant injection (LPCI) system and a combined injection system.

(11) ECC water injection ports are at the cold leg, the hot leg, the upper plenum, the downcomer, the lower plenum and above the upper core support plate. These ports are to be chosen according to the objective of the test.

(12) For better simulation of lower plenum flow resistance, simulated fuel rods do not penetrate through the bottom plate of the lower plenum but terminate at below the bottom of the core.

(13) For measurements in the pressure vessel including core, the feature of the slab geometry of the pressure vessel is utilized as much as possible. Design and arrangement of the instruments are done so as to be able to carry out installation, calibration and removal of the instruments.

(14) View windows are provided where flow pattern recognition is important. Their locations are the interface between the core and the upper plenum, the hot leg, the pressure vessel side broken cold leg and the downcomer.

(15) Blocked bundle test is carried out in Core-I in order to investigate the effect of ballooned fuel rods and unblocked normal bundle test follows in the Core-II and -III.

(16) Types of break simulated are cold leg break and hot leg break.

(17) The components and systems such as the containment tanks and ECC water supply system in CCTF are shared with SCTF to the maximum extent.

The overall schematic diagram of SCTF is shown in Fig. A-1. The principal dimensions of the facility is shown in Table A-1, and the comparison of dimensions between SCTF and the reference PWR is shown in Fig. A-2.

A.1.1 Pressure Vessel and Internals

The pressure vessel is of slab geometry as shown in Fig. A-3. The height of the components in the pressure vessel is almost the same as the reference reactor's, and the flow area and the fluid volume of each component are scaled down based on the nominal core flow area scaling, 1/21.

The core consists of 8 bundles arranged in a row and each bundle includes heater rods and non-heated rods with 16×16 array. The core is enveloped by the honeycomb thermal insulator which is attached on the back surface of core wall plate.

The downcomer is located at one end of the pressure vessel which corresponds to the periphery of the actual reactor pressure vessel. The core baffle region located between the core and the downcomer is basically isolated for Core-II to minimize uncertainty in actual core flow. However, some leak holes are still existing. For better understanding, the cross section of the pressure vessel at the elevation of midplance of the core is shown in Fig. A-4.

The design of upper plenum internals is based on that for the new Westinghouse 17×17 array fuel assemblies. The internals consist of control rod guide tubes, support columns and orifice plates which are attached to the upper core support plate (UCSP). The UCSP has some open holes without internals. Those arrangement is shown in Fig. A-5. The radius of each internal is scaled down based on the factor of 8/15 of an actual reactor. Baffle plates are inserted in the guide tubes. The elevation and the configuration of baffle plates are shown in Figs. A-6 and A-7.

The heights of the hot leg and cold legs are designed as close to the reference PWR as possible. However, in order to avoid the interference of the nozzles in the downcomer, the heights of nozzles for the

broken cold leg and the intact cold leg are shifted down compared to that of the hot leg as shown in Fig. A-3.

A.1.2 Simulated Core

The simulated core for the SCTF Core-II consists of 8 heater rod bundles arranged in a row. Each bundle has 234 electrically heated rods and 22 non-heated rods. The dimensions of the heater rods are based on 15×15 fuel rods bundle for a PWR and the heated length and the outer diameter of each heater rod are 3.66 m and 10.7 mm, respectively. A heater rod consists of a nichrome heater element, boron nitride (BN) or magnesium oxide (MgO) depending on elevation in the heated zone and Nichrofer 7216 (equivalent to Inconel 600) sheath. The sheath thickness is about 1.0 mm and is thicker than the actual fuel cladding because of the requirements for thermocouple installation. The heater element is a helical coil and has a 17 step chopped cosine axial power profile as shown in Fig. A-8. The peaking factor is 1.4.

Non-heated rods are either pipes or solid rods of stainless steel with 13.8 mm O.D. The heater rods and non-heated rods are fixed at the top of the core allowing downward expansion. In Fig. A-9, relative elevation of rods and spacers is shown.

For better simulation of flow resistance in the lower plenum the simulated fuel rods end in the lower plenum and do not penetrate through the bottom plate of the lower plenum as shown in Fig. A-9.

A.1.3 Primary Loops and ECCS

Primary loops consist of a hot leg equivalent to four hot legs in area, a steam/water separator for simulating single steam phase flow downstream of the steam generator and for measuring flow rate of carry over water, an intact cold leg equivalent to three intact loops, a broken cold leg on the pressure vessel side and a broken cold leg on the steam/water separator side. These two broken cold legs are connected to two containment tanks through break valves, respectively. The arrangement of the primary loops is shown in Fig. A-10. The flow area of each loop is scaled down based on the core flow area scaling, 1/21. It should be emphasized that the cross section of the hot leg is an elongated circle with an actual height to realize proper flow pattern in the hot leg. The steam/water separator has a steam generator inlet

plenum simulator to correctly simulate the flow characteristics of carryover water into the U-tubes. The cross section of the hot leg and the configuration of the steam genrator inlet plenum simulator are shown in Fig. A-11.

A pump simulator and a loop seal part are provided for the intact cold leg. The arangement of the intact cold leg is shown in Fig. A-12. The pump simulator consists of the casing and duct simulators and an orifice plate as shown in Fig. A-13. The loop resistance is adjusted with the orifice plates attached to the intact cold leg, the steam/water separator side and pressure vessel side broken cold legs and the pump simulator.

ECCS consists of the Acc and an LPCI systems. Injection ports are located as already described in the design criteria section. Besides, the UCSP water extraction system and the UCSP water injection system are provided for combined injection tests.

A.1.4 Containment Tanks and Auxiliary System

Two containment tanks are provided to SCTF. The containment tank-I is connected with the downcomer through the pressure vessel side broken cold leg and the containment tank-II is connected with the steam/water separator through the steam/water separator side broken cold leg. Especially in the containment tank-I, carryover water from the downcomer is measured by the differentiation of the liquid level. These containment tanks and auxiliary system such as a pressurizer for injecting water from the Acc tanks, etc. are shared with CCTF.

A.2 Instrumentation

The instrumentation in SCTF has been provided both by JAERI and USNRC. The JAERI-provided instrumentation includes the measurement of temperatures, pressures, differential pressures, liquid levels, flow velocities, and heating powers. USNRC has provided film probes, impedance probes, string probes, liquid level detectors (LLDs), fluid distribution grids (FDGs), turbine meters, drag disks, densitometers, spool pieces and video optical probes. Location of each instrument is shown in Figs. A-14 through A-32.

A.3 Mass Balance Calculation

The mass flow rate at the core inlet, $\dot{m}_F$ shown in Fig. A-33, was estimated by the mass balance in the SCTF system assuming the quasi-steady state conditions. The following mass accumulation rates in various parts, $\dot{m}_K$, were estimated by the time differentiation of the measured differential pressure ΔP_K:

$$\dot{m}_K = \frac{1}{g} \cdot \frac{d}{dt} (\Delta P_K) \, S_K \, ,$$

where K = Ci (core, i = 1 ~ 8),
Ui (upper plenum, i = 1 ~ 8),
Ei (end box, i = 1 ~ 8),
B (baffle region),
UB (upper plenum above baffle region),
L (lower plenum),
D (downcomer),
H (hot leg),
CI (containment tank-I) and
SW (steam/water separator).

The total steam flow rate generated in the core was estimated by the sum of mass flow rates at intact cold leg, $\dot{m}_I$, and at broken cold leg (steam/water separator side), $\dot{m}_{BS}$, measured by the ventury flow meters assuming single-phase steam flow conditions, which was confirmed by the differential pressure along the vertical direction in those pipings. Condensation due to the subcooled ECC water at intact cold leg was estimated by the difference between $\dot{m}_I$ and $\dot{m}_{I\,II}$, where $\dot{m}_{I\,II}$ is the mass flow rate from the containment tank I to the containment tank-II measured by the orifice flow meter.

The core inlet mass flow rate $\dot{m}_F$ can then be expressed considering the upstream mass balance from the core inlet as

$$\dot{m}_F = \dot{m}_{SL} + \dot{m}_{SI} + \dot{m}_I - \dot{m}_{I\,II} - \dot{m}_L - \dot{m}_D - \dot{m}_{CI} \, ,$$

where $\dot{m}_{SL}$ and $\dot{m}_{SI}$ are the supplied ECC water mass flow rate into the lower plenum and the intact cold leg, respectively. The core inlet mass flow rate can also be estimated considering the downstream mass balance from the core inlet as

$$\dot{m}'_F = \sum_{i=1}^{8} (\dot{m}_{ci} + \dot{m}_{ui} + \dot{m}_{Ei}) + \dot{m}_B + \dot{m}_{UB} + \dot{m}_H + \dot{m}_{SW} + \dot{m}_{OW} + \dot{m}_I + \dot{m}_{SB} ,$$

where $\dot{m}_{OW}$ is the overflowing water mass flow rate from the steam/water separator.

A.4 Calculation Method of Steam Generation Rate

The steam generation rate in the core was calculated with a heat balance calculation code "STEAM". The heat flux at the surface of heater rods was calculated with a heat transfer calculation code "HEATT"[12] developed for the SCTF test analysis. The temperature dependence of physical properties is considered but the axial heat conduction is neglected in this code.

The following assumptions were made in the calculation.

(1) The heat flux from the heater rods is totally absorbed in the fluid.

(2) The core inlet flow rate is equally divided into each of 8 bundles.

(3) The steam and water mixture is always saturated.

The core is divided into 8 bundles and 10 elevations.

The steam generation rate in each of 80 cells is calculated by

$$S_{ij} = \frac{1}{h_{fg}} \{q_{ij} A - m_i C_{p\ell} \Delta T_{sub}^{i}\} \qquad (A3\text{-}1)$$

where i = Bundle i

j = elevation j

S_{ij} = steam generation rate in this cell

q_{ij} = heat flux

A = $234\pi D \cdot \Delta H_j$ (Heat transfer area)

D = heater rod diameter

ΔH_j = height of this cell

m_i = core inlet mass flow rate in Bundle i

$C_{p\ell}$ = specific heat capacity of saturated water at the pressure in the lower plenum (PTO1A11)

ΔT_{sub}^{i} = subcooling of core inlet water in Bundle i

h_{fg} = latent heat of evaporation at the pressure in the core center (PT01D11)

The core inlet mass flow rate is assumed to be equally distributed in each bundle and given by

$$m_i = \frac{1}{8} W_{in} \qquad \text{(A3-2)}$$

where the W_{in} is the total core inlet mass flow rate obtained by the mass balance calculation described in A.3.

The ΔT_{sub}^{i} is obtained by using the following Data:

$$\Delta T_{sub}^{i} = T_{sat} - (TWO1i11 + TWO1i41)/2 \qquad \text{(A3-3)}$$

where T_{sat} = saturation temperature at the pressure in the lower plenum (PT01A11)

TWO1i11 and TOW1i41 are the fluid temperature at the bottom of heated part in Bundle i

The heat flux, q_{ij}, is calculated from the transient of heater rod surface temperature. In the STEAM code, two kinds of temperature transients can be selected. One is the temperature at the center of each bundle (TEji1C in Fig. A-14, j = 01 ~ 10, i = 1 ~ 8). Another is the average temperature in each bundle at the same elevation. Figure A-34 shows a comparison of total steam generation rate obtained by these two methods in Test S2-06. As shown in this figure, the difference of these two method is less than about 8 %. If not specially commented, the average temperature transient is used in the steam generation calculation.

Two kinds of vertical nording models are involved in the STEAM code. One is a even division between two adjacent thermocouple locations ("Even" division). Another type of division is made so that the heat flux in each cell accuratelly represent the average heat flux of the cell by considering the stepwise axial power profile shown in Fig. A-8 ("Step" division). Figure A-35 shows the vertical nording models of these two division methods. The difference of the total steam generation rates obtained by these two methods is less than about 8 % as shown in Fig. A-36. If not specially commented, the "Step"

division method is used in the steam generation calculation. The "Even" division method is mainly used for the evaluation of steam flow rate at each elevation.

Since the heat flux shows a very high peak value when the thermocouple is quenched, the heat flux is averaged for the calculation of steam generation rate when the quench front exists in the cell. The averaging method is classified into two cases.

(1) In case of: $t_{j-1} < t_q < t_j$ or $t_j < t_q < t_{j-1}$

where t_q = quench time at thermocouple location

t_{j-1} = quench time at the bottom of cell j

t_j = quench time at the top of cell j

$$q\,A = \sum_{k=0}^{m} q(t_m) \cdot 234\pi D\Delta H_j/(m+1) \qquad \text{(A3-4)}$$

where $m = |t_j - t_{j-1}|/\Delta t$, $\Delta t = 0.5$ s

$$t_m = t + 0.5\left(\frac{\Delta H_j^{\,2}}{\Delta H_j^{\,1} + \Delta H_j^{\,2}}\, m - k\right)$$

$\Delta H_j^{\,1}$ = distance between thermocouple elevation and bottom of cell

$\Delta H_j^{\,2}$ = distance between thermocouple elevation and top of cell

When t is between t_{j-1} and t_j, eq. (A3-4) is used in eq. (A3-1).

(2) In case of: $t_j<t_{j-1}<t_q$, $t_{j-1}<t_j<t_q$, $t_q<t_j<t_{j-1}$ or $t_q<t_{j-1}<t_j$

$$qA = \sum_{k=0}^{m} q(t_m) \cdot 234\pi D\Delta H_j/(m+1) \qquad \text{(A3-5)}$$

where $m = |t_j - t_{j-1}|/\Delta t$, $\Delta t = 0.5$ s

$t_m = t + 0.5(m - k)$

When t is between t_{j-1} and t_j, eq. (A3-5) is used in eq. (A3-1). For the other time, eq. (A3-4) is used in eq. (A3-1).

The quench time at the bottom of the core is set to the initiation time of bottom reflooding. The quench time at the top of the core is obtained by extraporating the quench times at elevations 10 and 9.

A.5 Calculation Method of Horizontal Differential Pressure

The measurement locations of the horizontal differential pressures in the core are shown in Fig. A-26. In addition, the vertical differential pressures were measured at various locations as shown in Fig. A-25. The horizontal differential pressures which were not measured directly can be obtained by combining these measured horizontal and vertical differential pressures. Figure A-37 shows the locations and Tag ID's of calculated horizontal differential pressures together with the locations of measured horizontal and vertical differential pressures. The calculation method for the additional horizontal differential pressures is shown in Table A-3. The Tag ID's used in this table are explained in Figs. A-25, A-26 and A-37.

Table A-1 Principal Dimensions of Test Facility

1.	Core Dimension	
(1)	Quantity of Bundle	8 Bundles
(2)	Bundle Array	1×8
(3)	Bundle Pitch	230 mm
(4)	Rod Array in a Bundle	16×16
(5)	Rod Pitch in a Bundle	14.3 mm
(6)	Quantity of Heater Rod in a Bundle	234 rods
(7)	Quantity of Non-Heated Rod in a Bundle	22 rods
(8)	Total Quantity of Heater Rods	234×8=1872 rods
(9)	Total Quantity of Non-Heated Rods	22×8=176 rods
(10)	Effective Heated Length of Heater Rod	3660 mm
(11)	Diameter of Heater Rod	10.7 mm
(12)	Diameter of Non-Heated Rod	13.8 mm
2.	Flow Area & Fluid Volume	
(1)	Core Flow Area (Nominal)	0.227 m^2
(2)	Core Fluid Volume	0.92 m^3
(3)	Baffle Region Flow Area	0.10 m^2
(4)	Baffle Region Fluid Volume (Nominal)	0.36 m^3
(5)	Effective Core Flow Area Based on the Measured Level-Volume Relationship Shown in Fig. 4-7 Including Gap between Core Barrel and Pressure Vessel Wall and Various Penetration Holes	0.35 m^2
(6)	Downcomer Flow Area	0.121 m^2
(7)	Upper Annulus Flow Area	0.158 m^2
(8)	Upper Plenum Horizontal Flow Area	0.525 m^2
(9)	Upper Plenum Fluid Volume	1.16 m^3
(10)	Upper Head Fluid Volume	0.86 m^3
(11)	Lower Plenum Fluid Volume	1.38 m^3
(12)	Steam Generator Inlet Plenum Simulator Flow Area	0.626 m^2
(13)	Steam Generator Inlet Plenum Simulator Fluid Volume	0.931 m^3
(14)	Steam Water Separator Fluid Volume	5.3 m^3
(15)	Flow Area at the Top Plate of Steam Generator Inlet Plenum Simulator	0.195 m^2
(16)	Hot Leg Flow Area	0.0826m^2
(17)	Intact Cold Leg Flow Area (Diameter = 297.9 mm)	0.9697m^2
(18)	Broken Cold Leg Flow Area (Diameter = 151.0 mm)	0.0179m^2

Table A-1 (Continued)

(19) Containment Tank-I Fluid Volume	30	m^3
(20) Containment Tank-II Fluid Volume	50	m^3
(21) Flow Area of Exhausted Steam Line from Containment Tank-II to the Atmosphere	see Ref. (1)	

3. Elevation & Height

(1) Top Surface of Upper Core Support Plate (UCSP)	0	mm
(2) Bottom Surface of UCSP	- 76	mm
(3) Top of the Effective Heated Length of Heater Rod	- 393	mm
(4) Bottom of the Skirt in the Lower Plenum	-5270	mm
(5) Bottom of Intact Cold Leg	+ 724	mm
(6) Bottom of Hot Leg	+1050	mm
(7) Top of Upper Plenum	+2200	mm
(8) Bottom of Steam Generator Inlet Plenum Simulator	+1933	mm
(9) Centerline of Loop Seal Bottom	-2281	mm
(10) Bottom Surface of End Box	- 185.1	mm
(11) Top of the Upper Annulus of Downcomer	+2234	mm
(12) Height of Steam Generator Inlet Plenum Simulator	1595	mm
(13) Height of Loop Seal	3140	mm
(14) Inner Height of Hot Leg Pipe	737	mm
(15) Bottom of Lower Plenum	-5770	mm
(16) Top of Upper Head	+2887	mm

Table A-2 Total, lower and upper heights of each cell for calculation of steam generation rate

(a) "Even"division method

Elev. No.	ΔH_j (m)	ΔH_j^1 (m)	ΔH_j^2 (m)
10	0.255	0.215	0.04
9	0.430	0.215	0.215
8	0.430	0.215	0.215
7	0.4275	0.2125	0.215
6	0.2975	0.085	0.2125
5	0.2625	0.1775	0.085
4	0.3925	0.215	0.1775
3	0.430	0.215	0.215
2	0.420	0.205	0.215
1	0.315	0.110	0.205

(b) "Step" division method

Elev. No.	ΔH_j (m)	ΔH_j^1 (m)	ΔH_j^2 (m)
10	0.205	0.165	0.04
9	0.630	0.365	0.265
8	0.220	0.155	0.065
7	0.660	0.385	0.275
6	0.115	0.075	0.040
5	0.115	0.020	0.095
4	0.660	0.325	0.335
3	0.220	0.115	0.105
2	0.630	0.315	0.315
1	0.205	0.110	0.095

ΔH_j = total height of each cell (elev. No. j)

ΔH_j^1 = distance between thermocouple elevation and bottom of cell (elev. No. j)

ΔH_j^2 = distance between thermocouple elevation and top of cell (elev. No. j)

Table A-3 Calculation method for additional horizontal differential pressures using measured horizontal and vertical differential pressures

(1) elev.1 (-0.142 m) for Run 601 ~ 619

HD01C11 = DT01D11 + HD05C11 - DT01D21

HD01C21 = DT01D21 + HD05C21 - DT01D41

HD01C12 = HD01C11 + HD01C21

HD01C41 = DT01D41 + DT04D41 - DT01D61

HD01C61 = DT01D61 + HD05C61 - DT01D81

HD01C42 = HD01C41 + HD01C61

(1)' elev.1 (-0.142 m) for Run 620 ~ 625

HD01C11 = DT01D11 + HD05C11 - DT01D21

HD01C21 = DT00D11 - HD01C11

HD01C12 = DT00D11

HD01C41 = DT00D41

HD01C61 = DT00D42 - DT00D41

HD01C42 = DT00D42

(2) elev.2 (0.085 m)

HD02C21 = DT01S21 + HD03C21 - DT01S41

HD02C41 = DT01S41 + DT02S41 + HD04C41 - DT01S61

HD02C61 = DT01S61 + HD04C61 - DT02S81 - DT01S81

HD02C42 = HD02C41 + HD02C61

(3) elev.3 (0.7 m) for Run 601 ~ 619

HD03C21 = DT02S21 + DT03D22 - DT02S41

HD03C42 = DT02S41 + HD04C42 - DT02S81

(3)' elev.3 (0.7 m) for Run 620 ~ 625

HD03C21 = DT02D22

HD03C42 = DT02D42

(4) elev.4 (1.365 m)

HD04C21 = DT03D22

HD04C41 = DT03S41 + DT04D41 - DT02S61

HD04C61 = DT02S61 + HD05C61 - DT03S81

HD04C42 = HD04C41 + HD04C61

(5) elev.5 (1.905 m)

HD05C11 = DT04D11 - HD05C21

HD05C21 = DT03D22 + DT03S41 - DT03S21

HD05C12 = DT04D11

HD05C41 = DT04D42

HD05C61 = DT04D41 - DT04D42

HD05C42 = DT04D41

(6) elev.6 (2.03 m)

HD06C21 = DT04S21 + DT05D21 - DT04S41

HD06C42 = DT04S41 + HD07C42 - DT04S81

(7) elev.7 (2.57 m)

HD07C21 = DT05D21

HD07C42 = DT05G41 + HD08C42 - DT05G81

(8) elev.8 (2.695 m)

HD08C21 = DT05D21 + DT05G41 - DT05G21

HD08C42 = DT05S41 + DT06D41 - DT05S81

(9) elev.9 (3.235 m)

HD09C11 = DT06D11 - HD09C21

HD09C21 = HD08C21 + DT05S41 - DT05S21

HD09C12 = DT06D11

HD09C41 = DT04D41 + DT03S61 - DT05S41 - DT05G41 - DT04S41 - DT04G41

HD09C61 = DT06D41 - HD09C41

HD09C42 = DT06D41

(10) elev.10 (3.36 m)

HD10C42 = DT06S41 + HD11C42 - DT06S81

(11) elev.11 (3.685 m)

HD11C41 = HD09C41 + DT04S61 - DT06S41 - DT06G41

HD11C61 = HD11C42 - HD11C41

HD11C42 = DT07G41 + HD12C42 - DT07G81

(12) elev.12 (3.821 m)

HD12C11 = HD05C11 + DT02D21 - DT02D11

HD12C21 = HD05C21 + DT02C41 - DT02D21

HD12C12 = HD12C11 + HD12C21

HD12C41 = DT04D41 + DT02D61 - DT02D41

HD12C61 = HD05C61 + DT02D81 - DT02D61

HD12C42 = HD12C41 + HD12C61

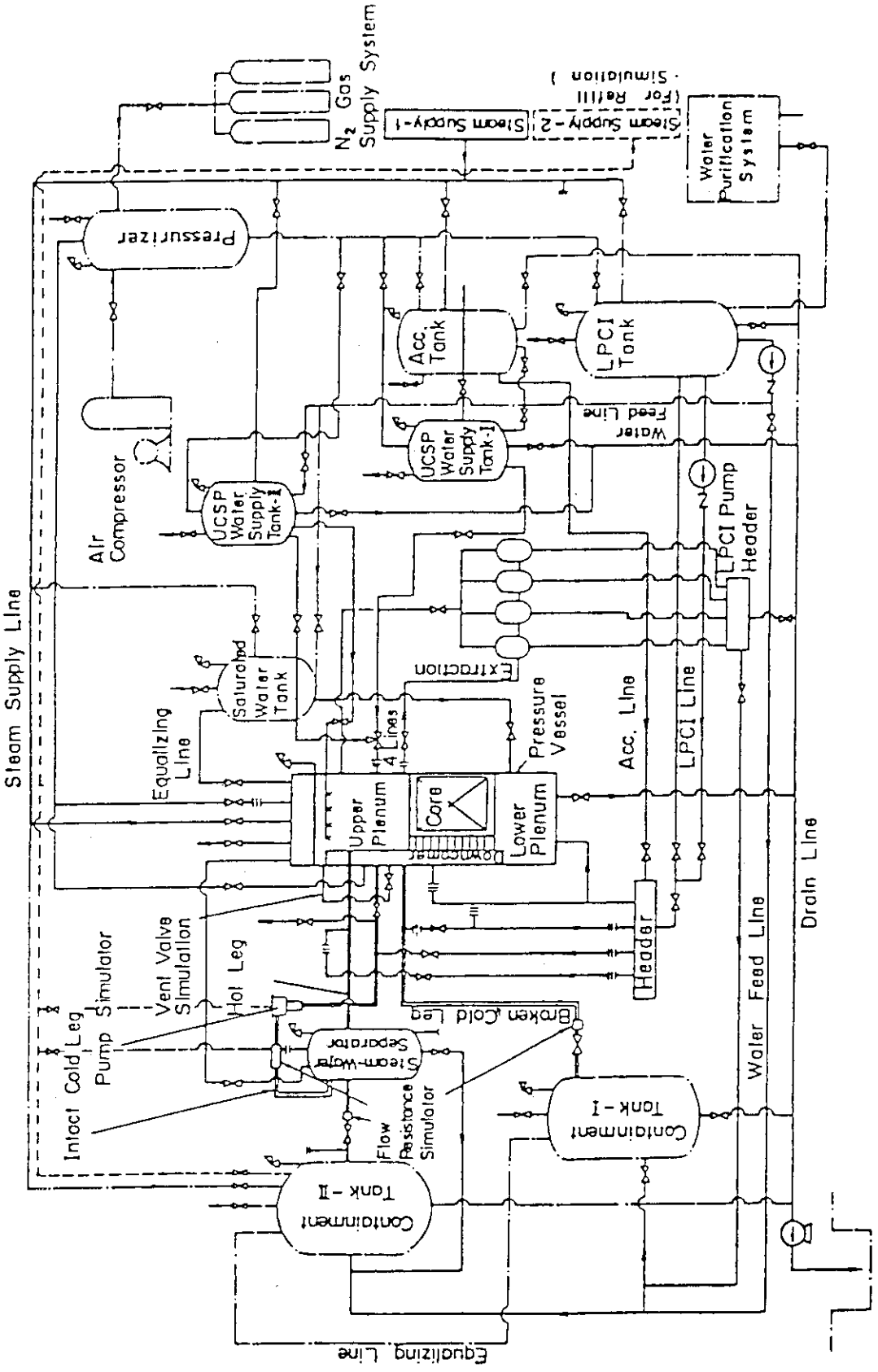

Fig. A-1 Schematic Diagram of Slab Core Test Facility

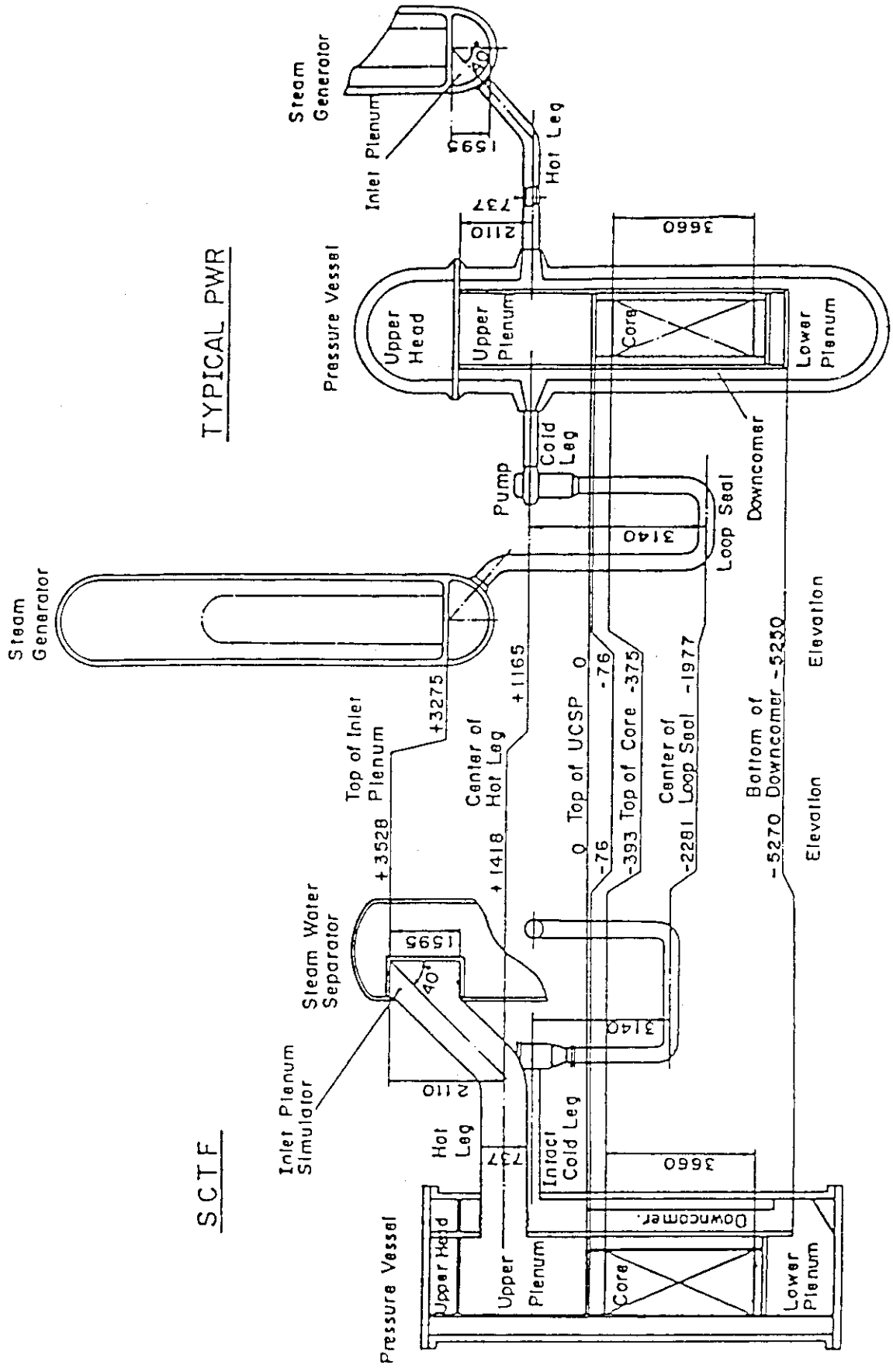

Fig. A-2 Comparison of Dimensions between SCTF and a Reference PWR

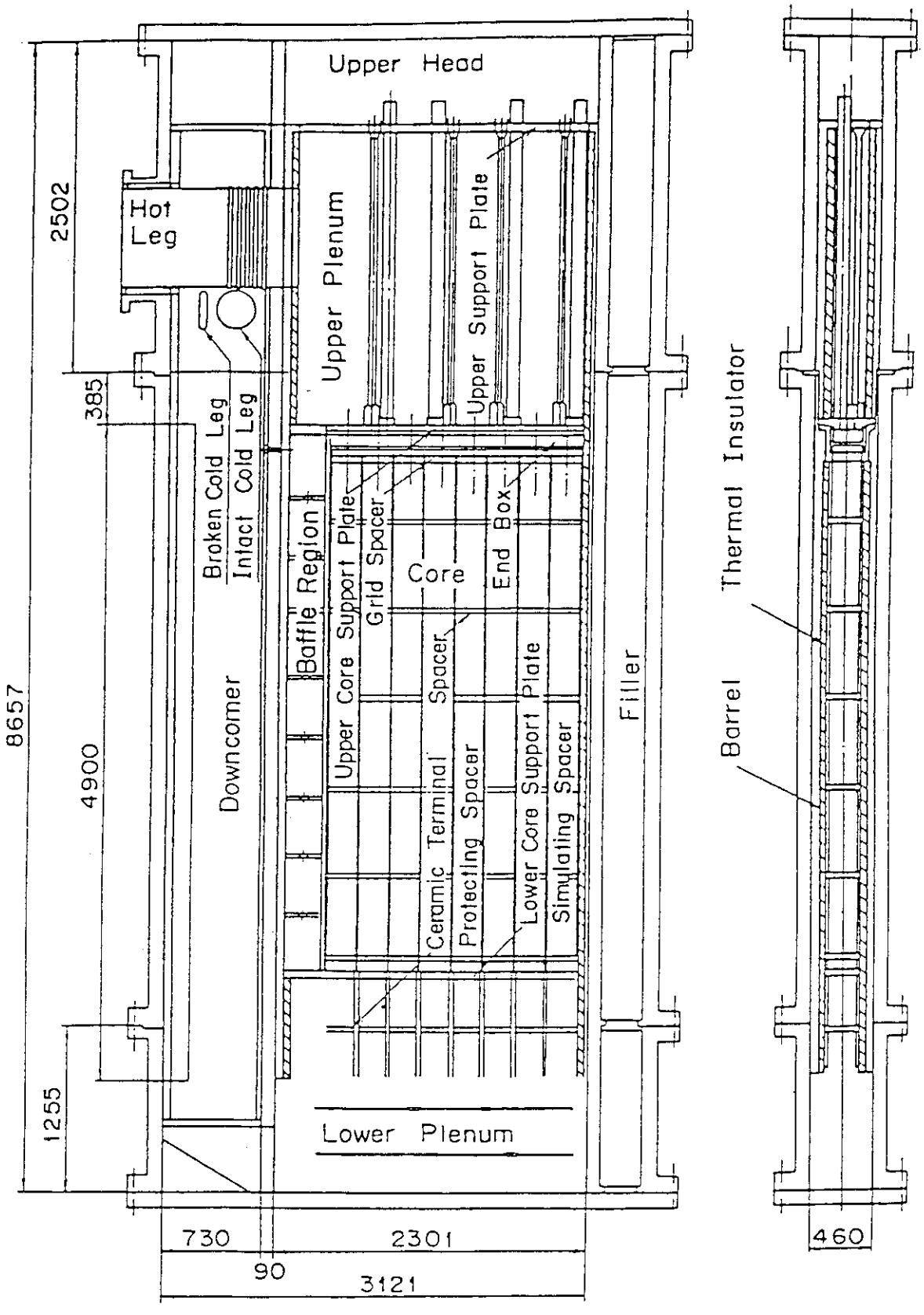

Fig. A-3 Vertical Cross Section of the Pressure Vessel

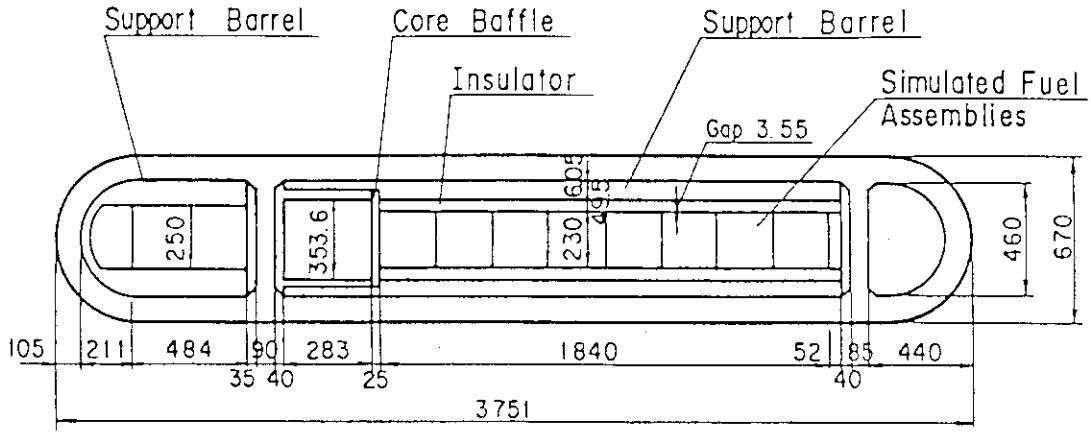

Fig. A-4 Horizontal Cross Section of the Pressure Vessel (1)

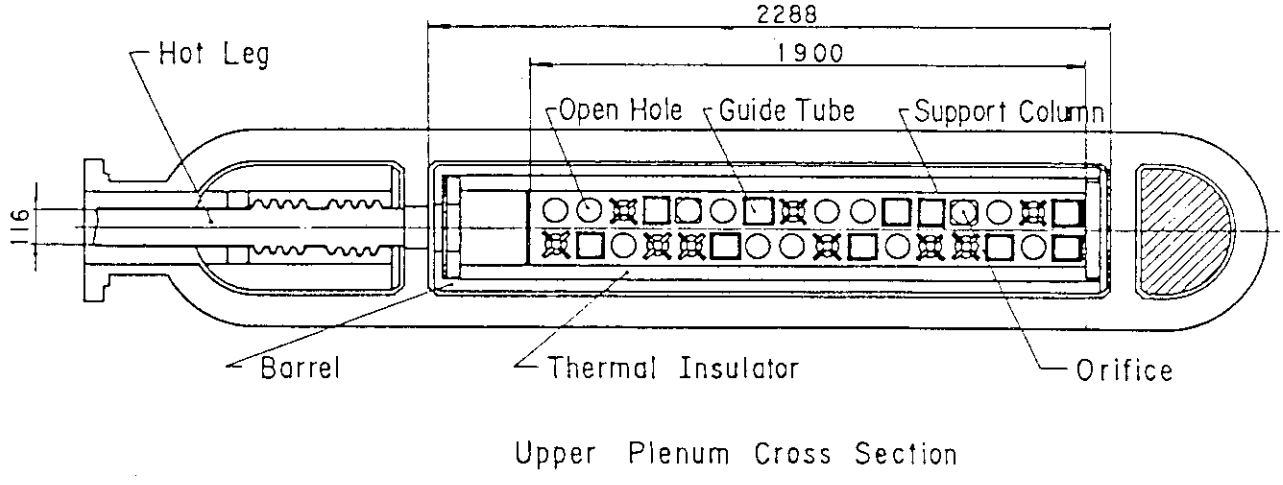

Fig. A-5 Horizontal Cross Section of the Pressure Vessel (2)

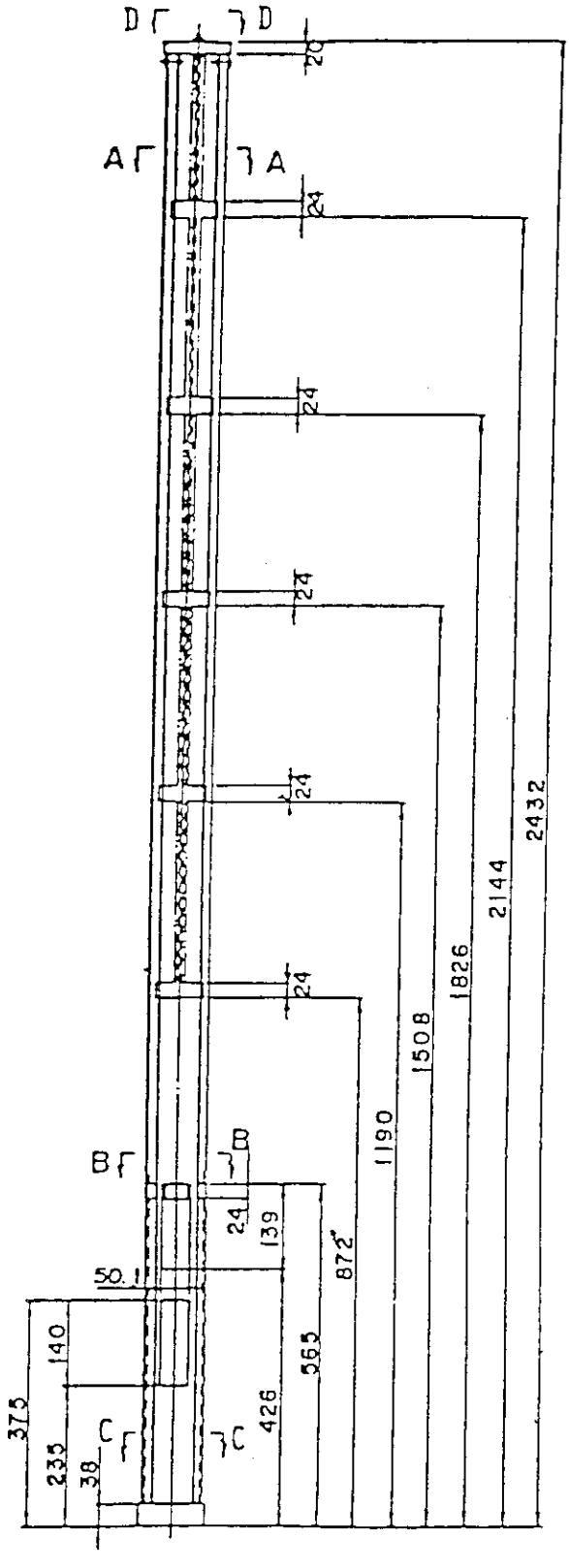

Fig. A-6 Dimension of Guide Tube (1)

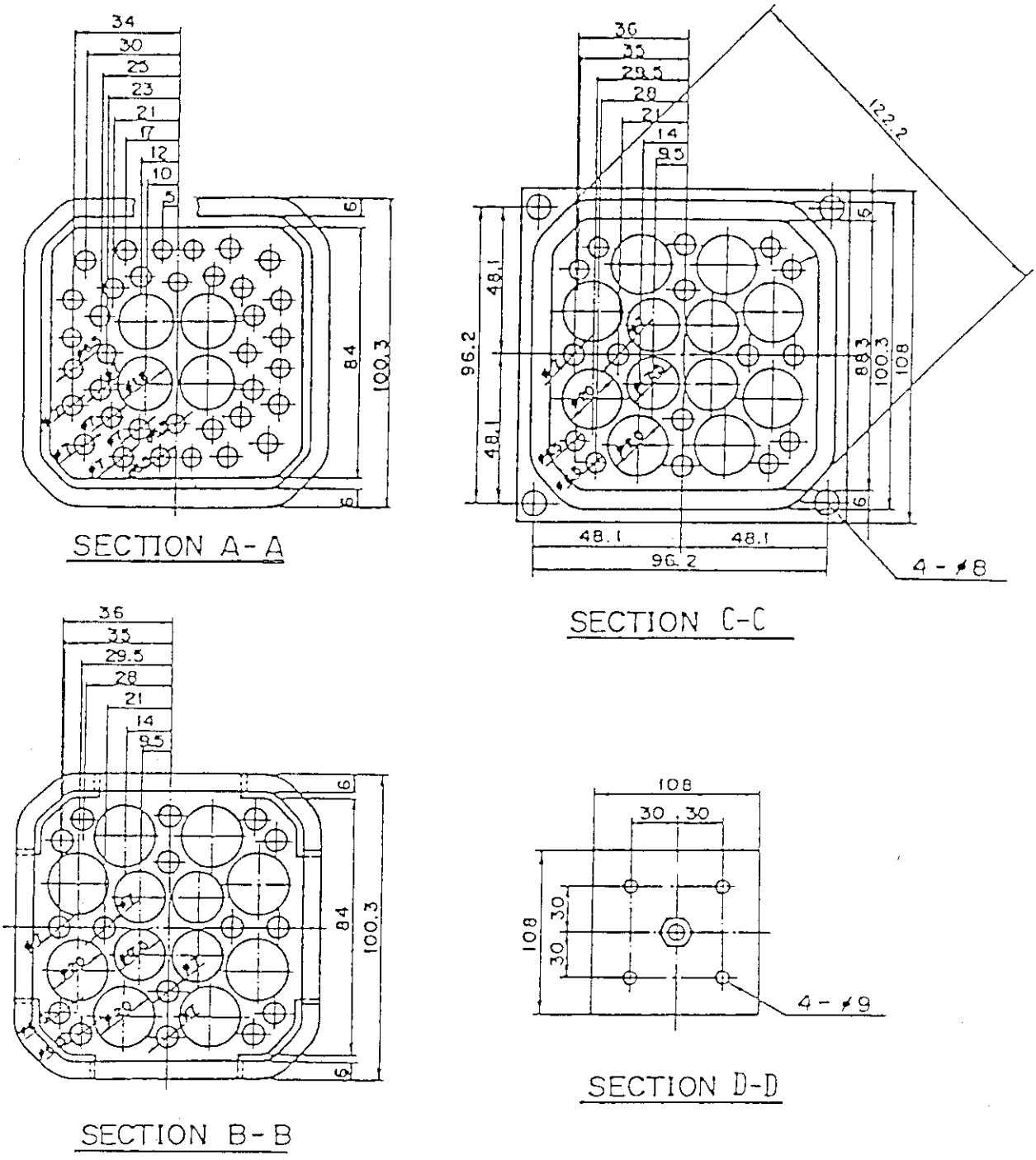

Fig. A-7 Dimension of Guide Tube (2)

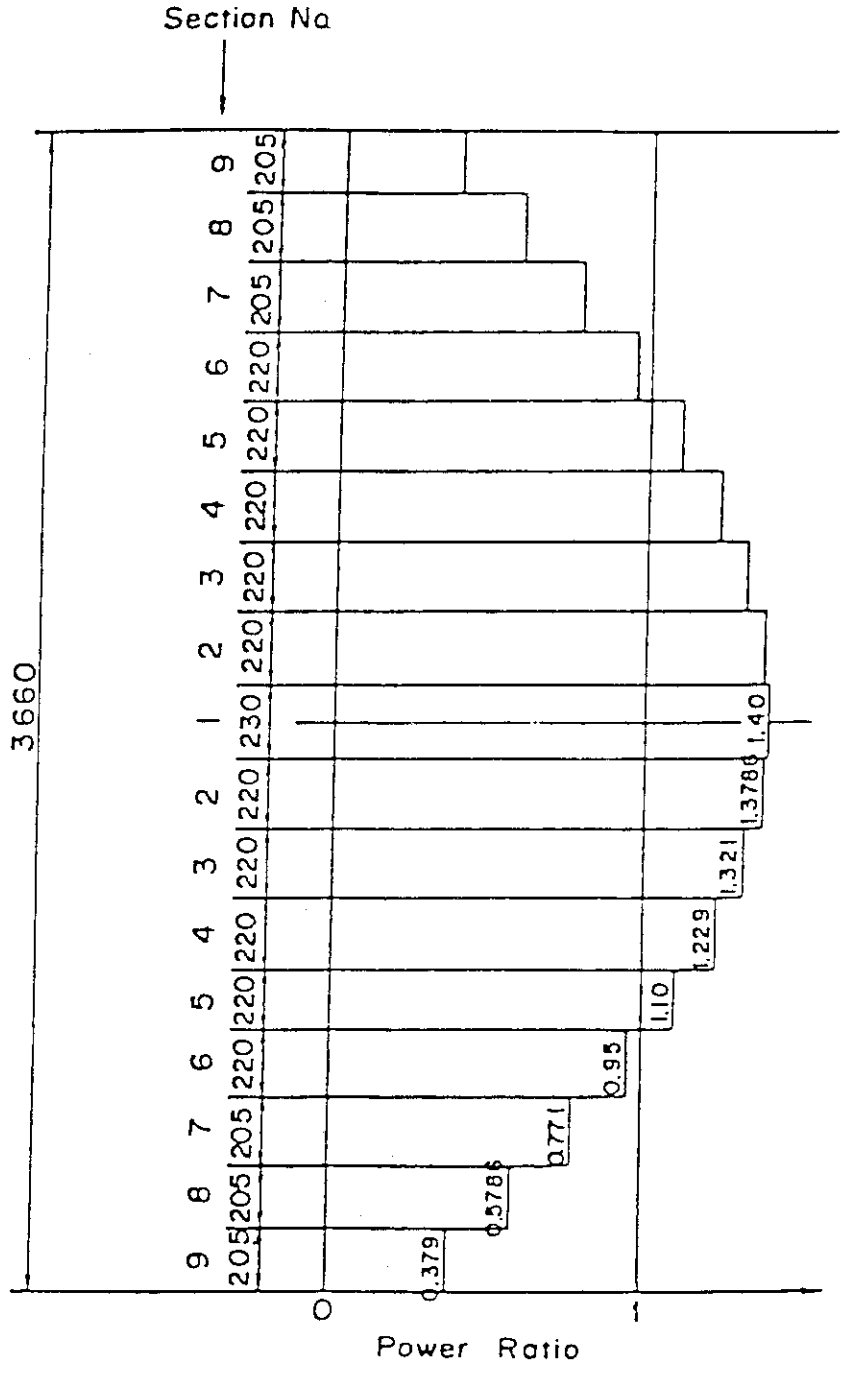

Fig. A-8 Axial Power Distribution of Heater Rod

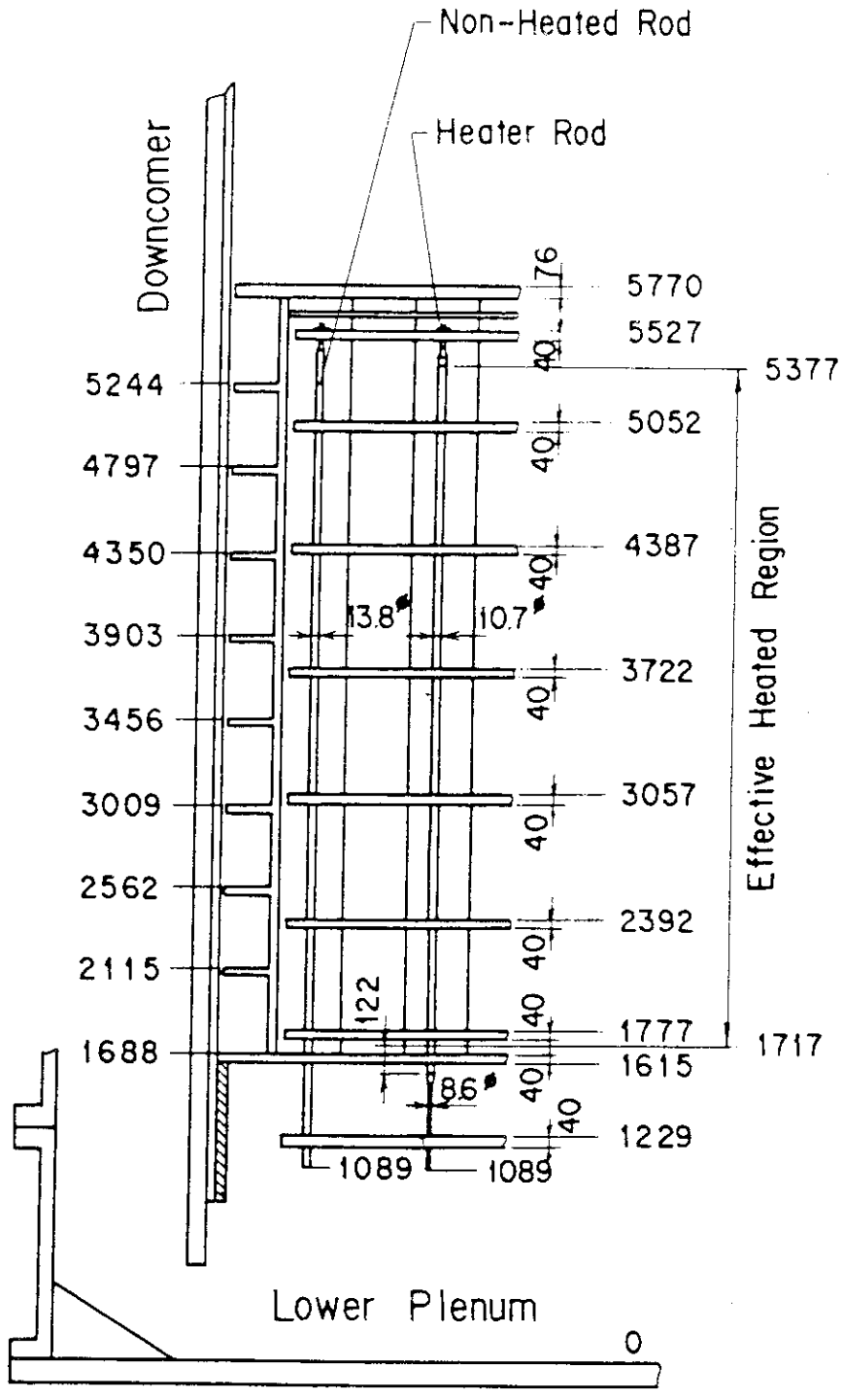

Fig. A-9 Relative Elevation and Dimension of the Core in SCTF

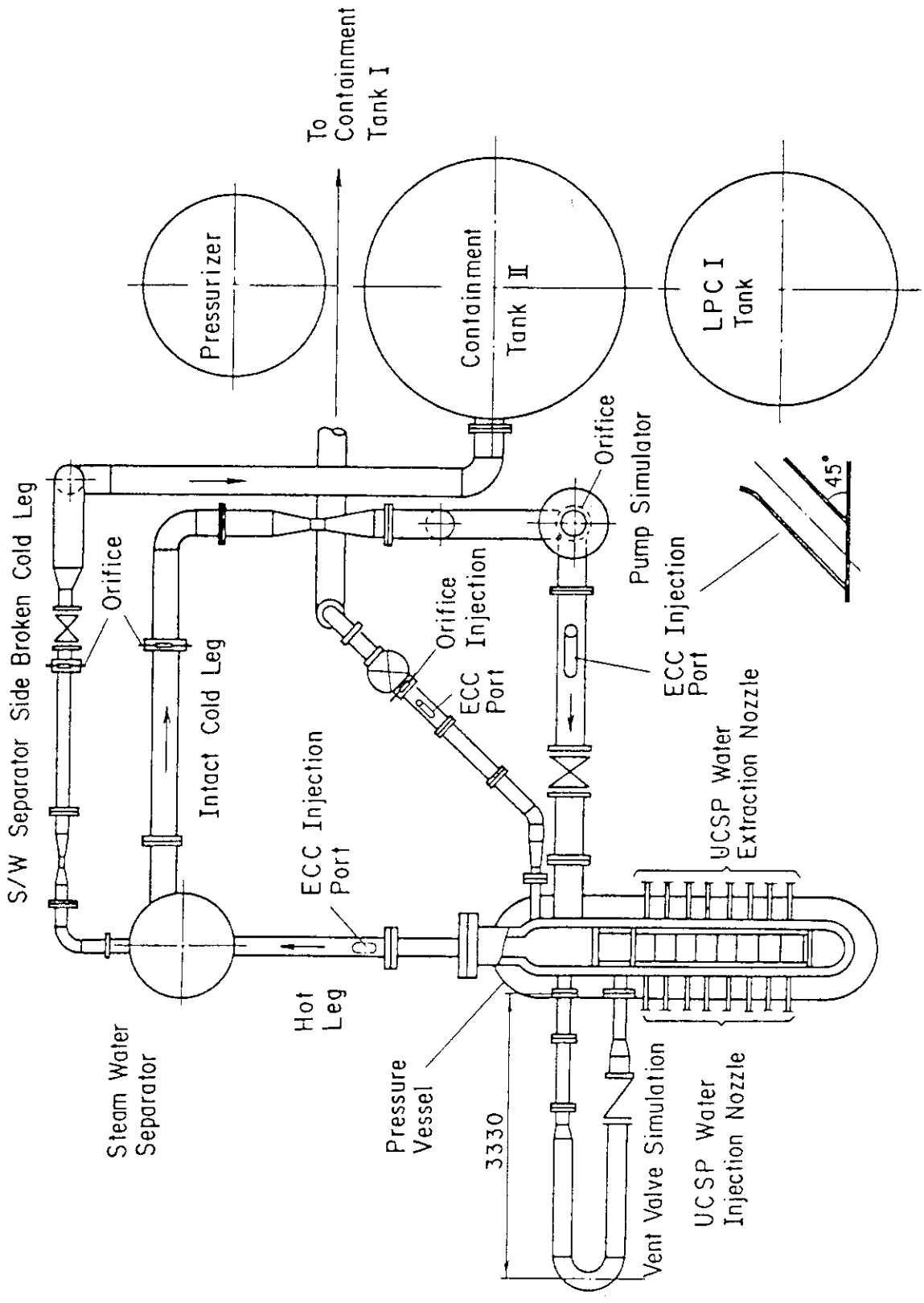

Fig. A-10 Overview of the Arrangements of the SCTF

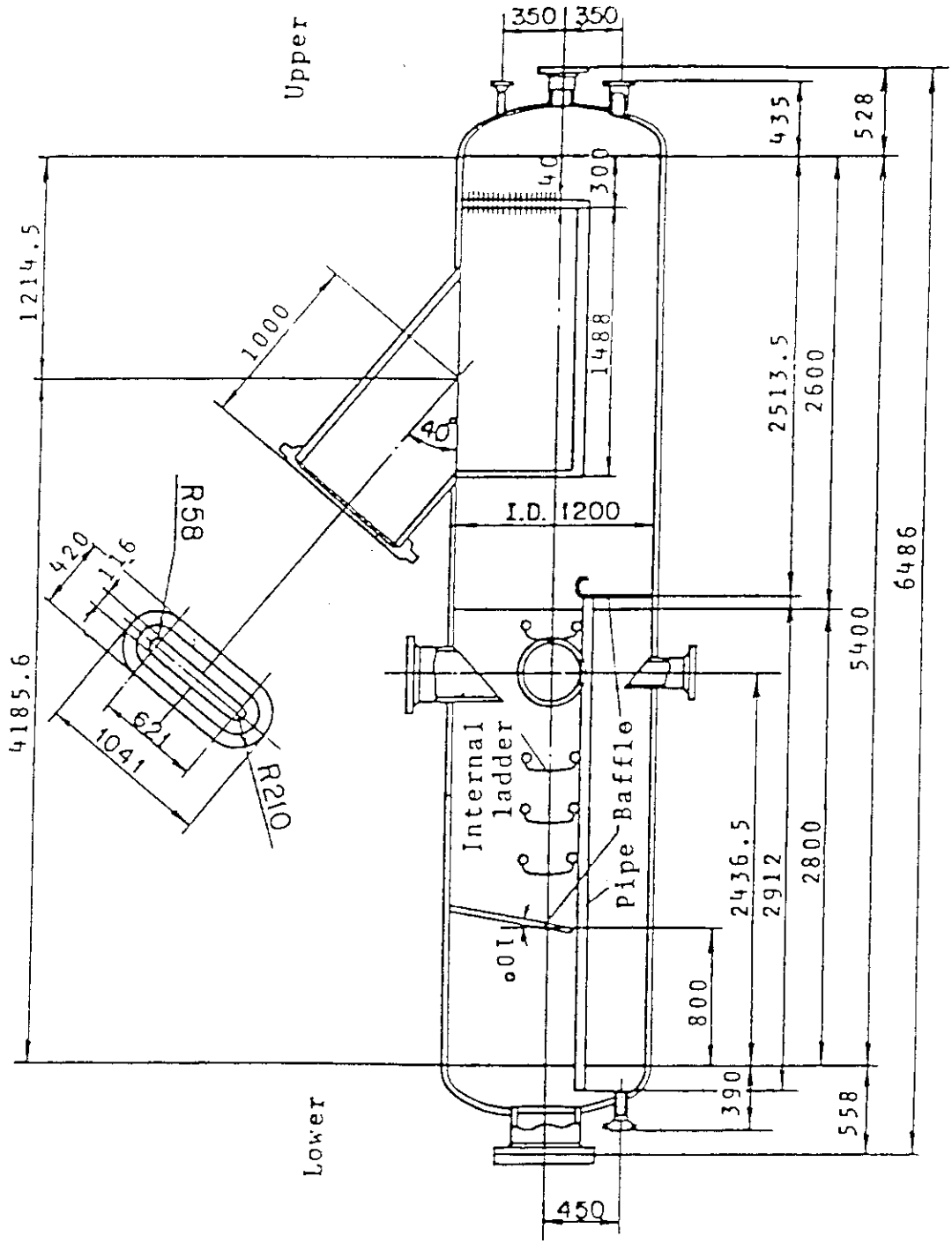

Fig. A-11 Steam/Water Separator

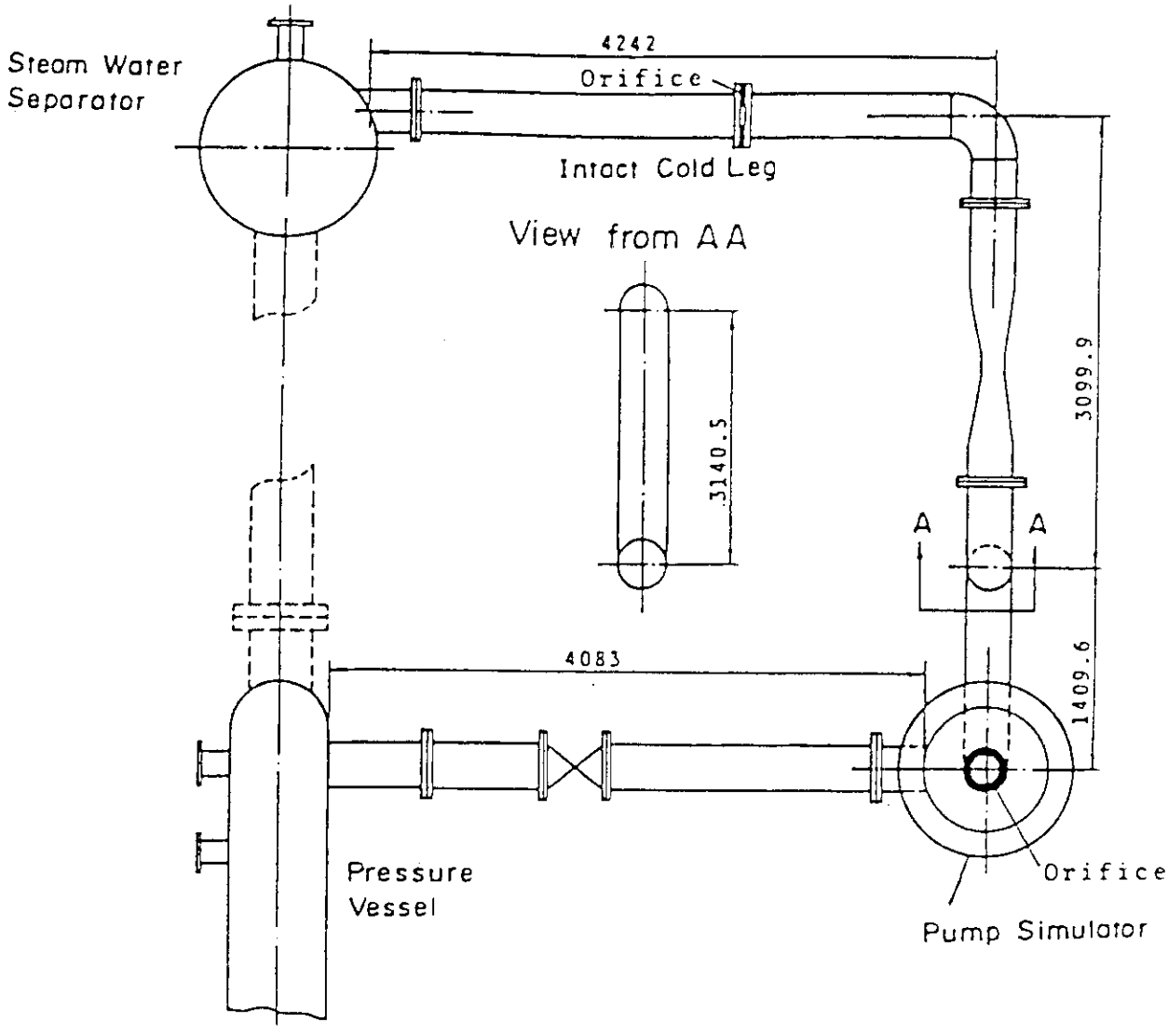

Fig. A-I2 Arrangement of Intact Cold Leg

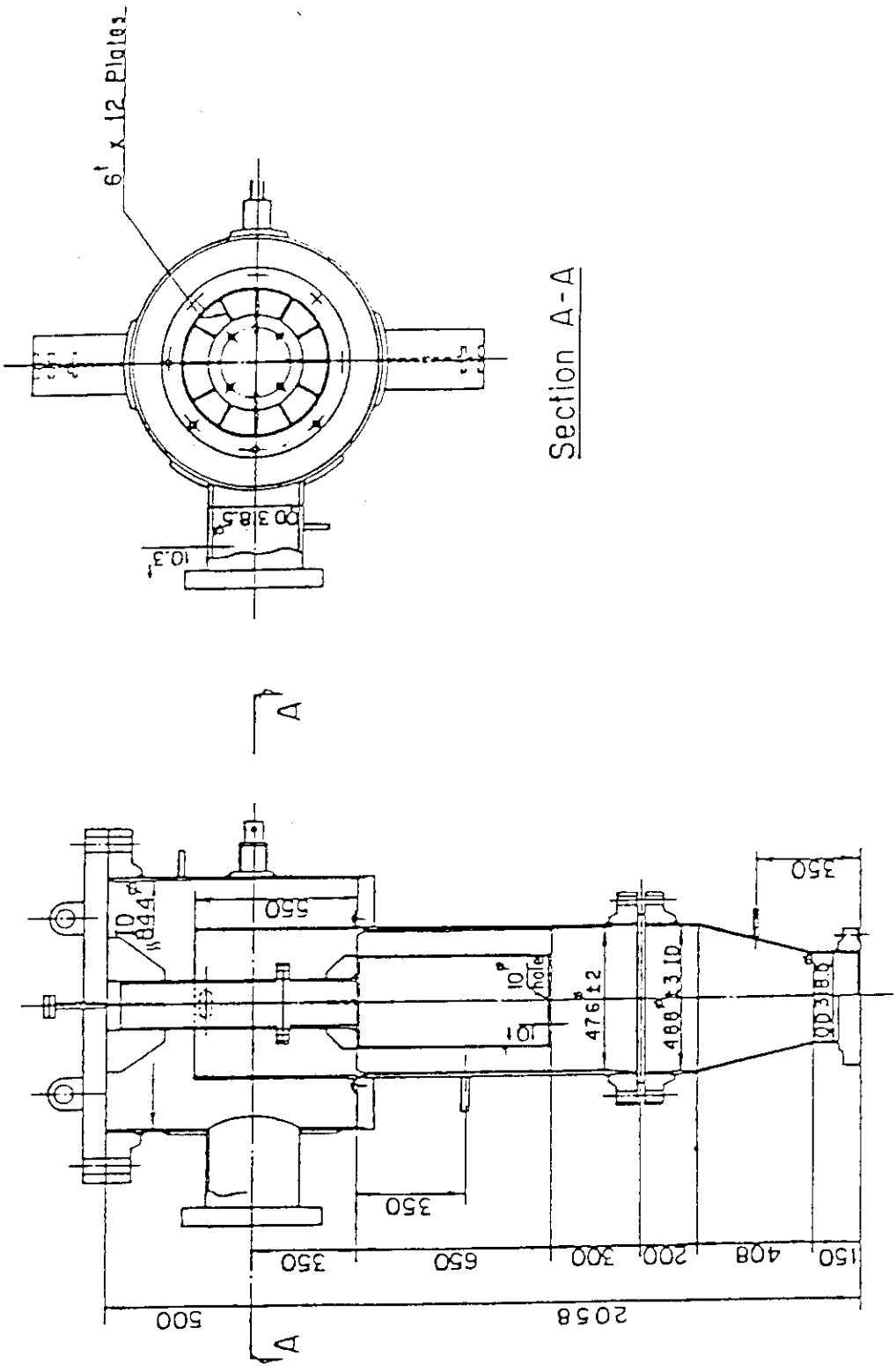

Fig. A-13 Configuration and Dimension of Pump Simulator

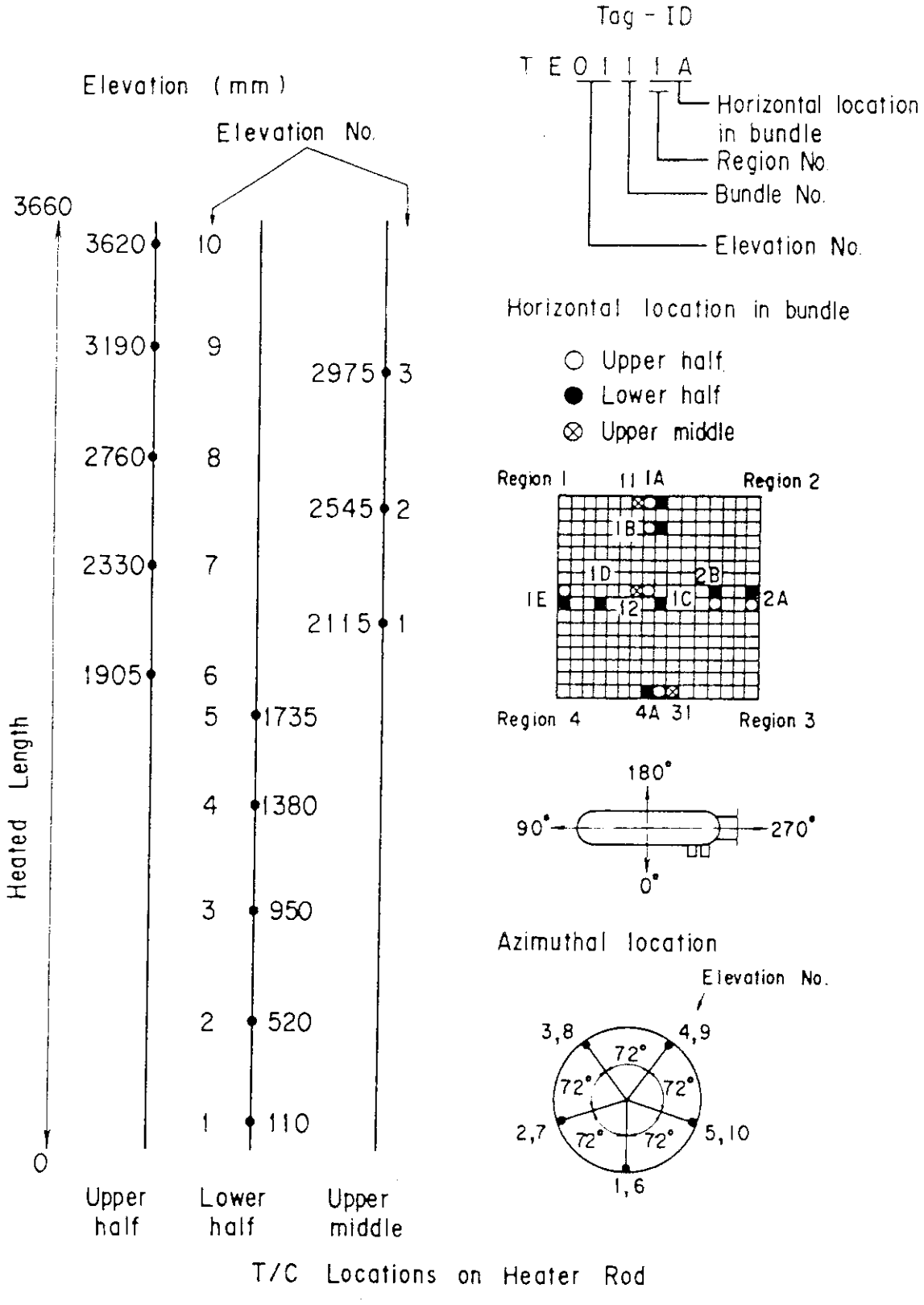

Fig. A-14 Thermocouple Locations of Heater Rod Surface Temperature Measurements

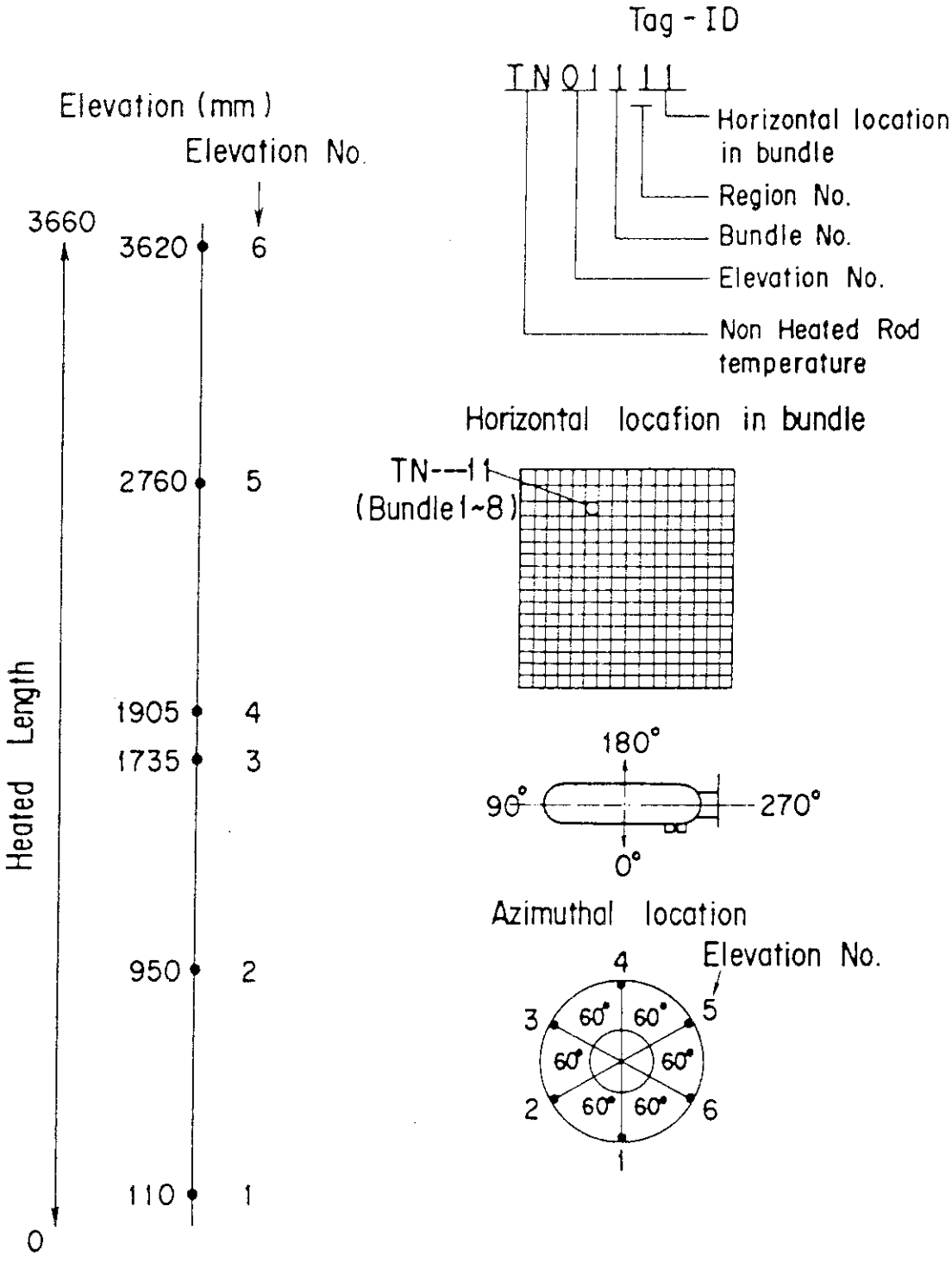

Fig. A-15 Thermocouple Locations of Non-Heated Rod Surface Temperature Measurements

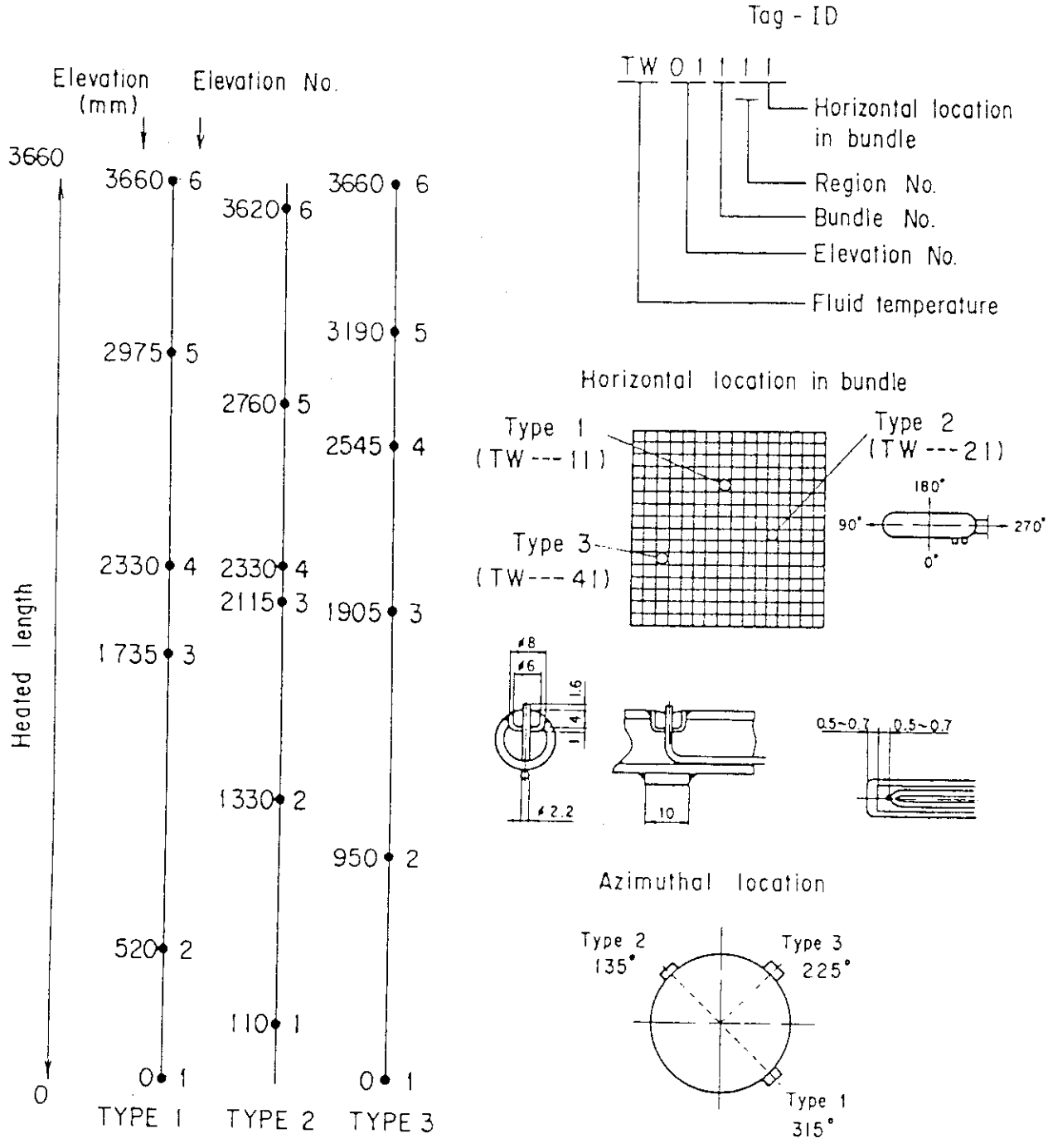

Fig. A-16 Thermocouple Locations of Fluid Temperature (Sputtering) Measurements in Core

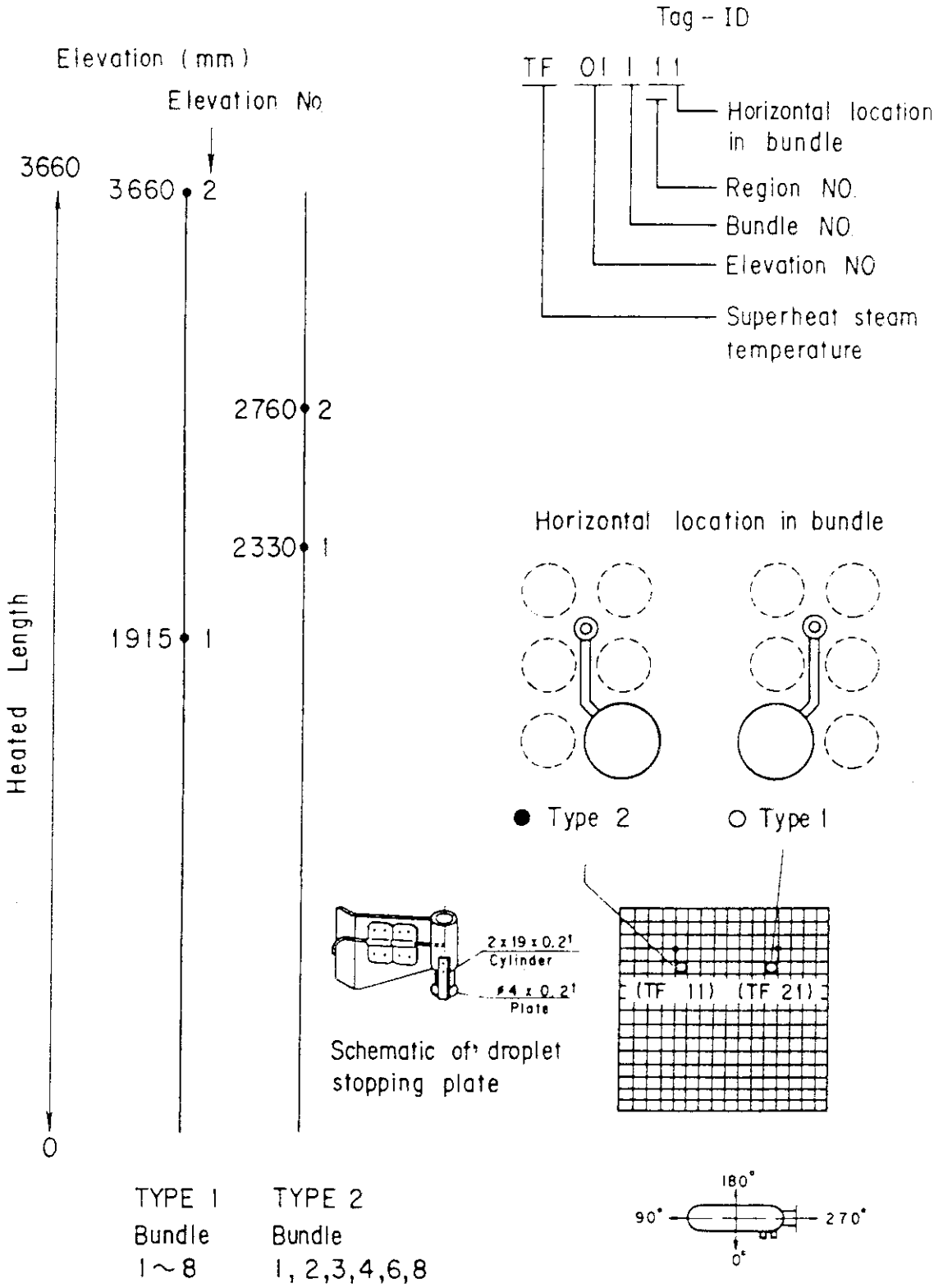

Fig. A-17 Thermocouple Locations of Steam Temperature Measurements in Core

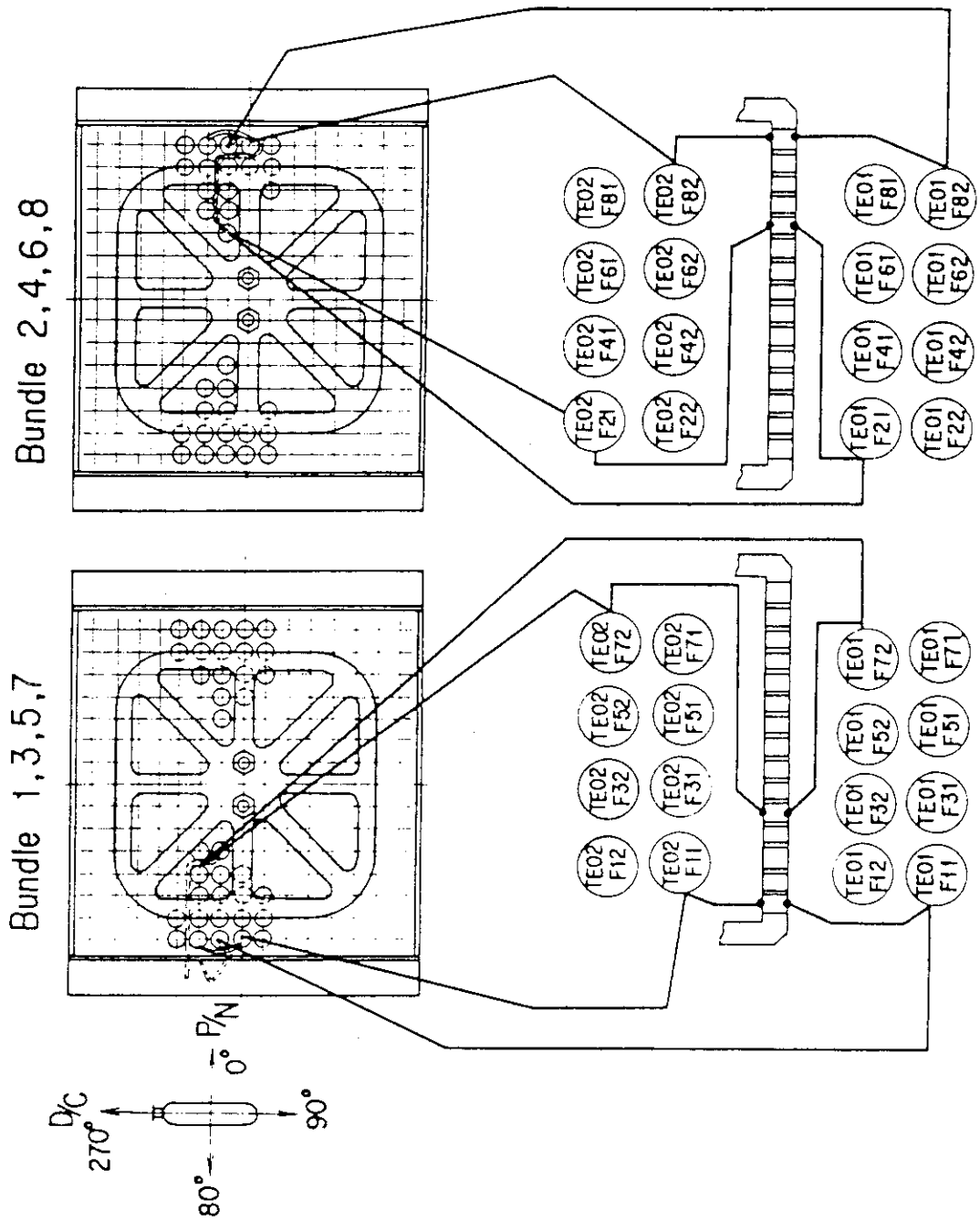

Fig. A-18 Thermocouple Locations of Fluid Temperature Measurement just above and below End Box Tie Plate

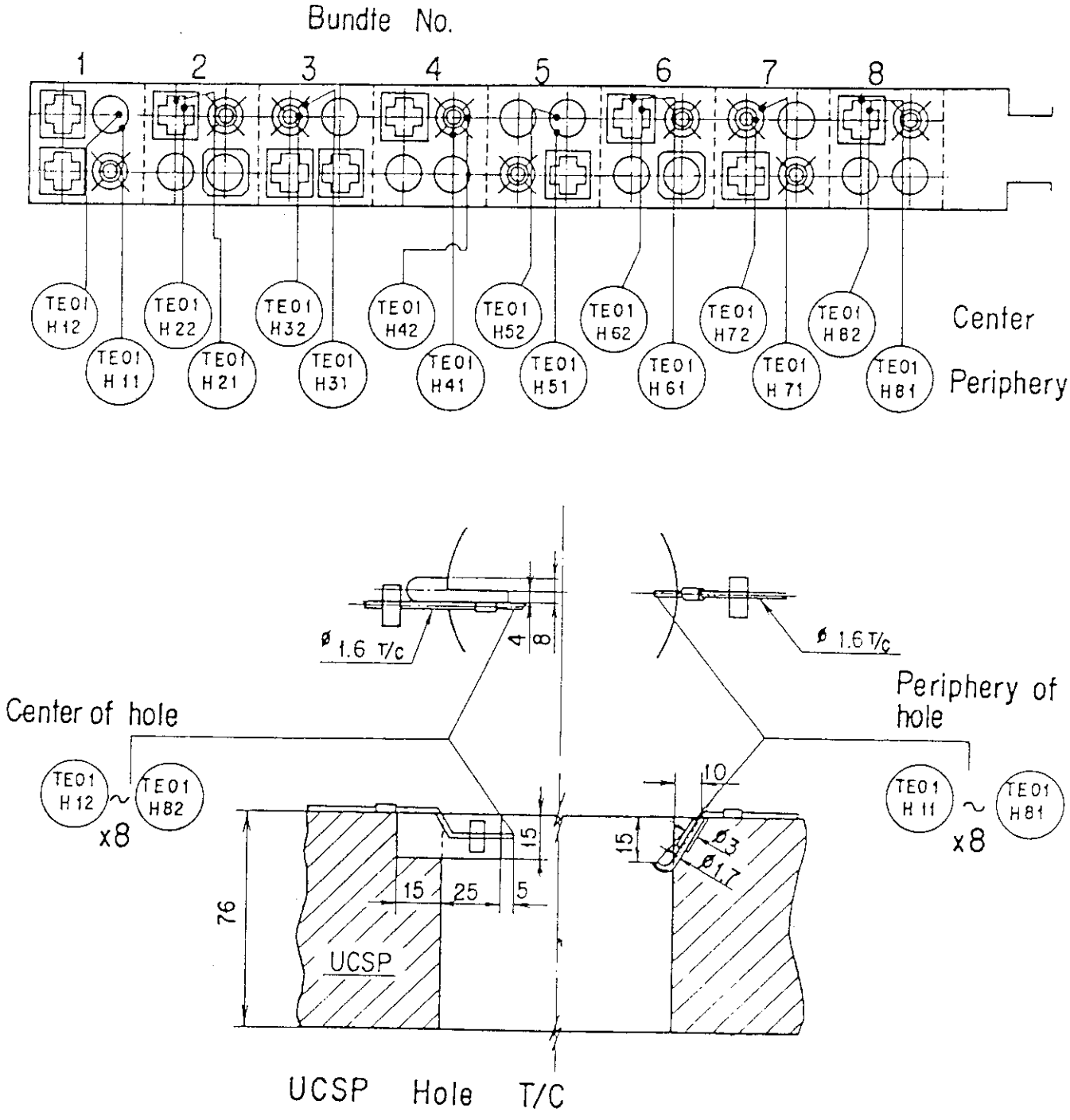

Fig. A-19 Thermocouple Locations of Fluid Temperature Measurements at Center and Periphery of UCSP Holes

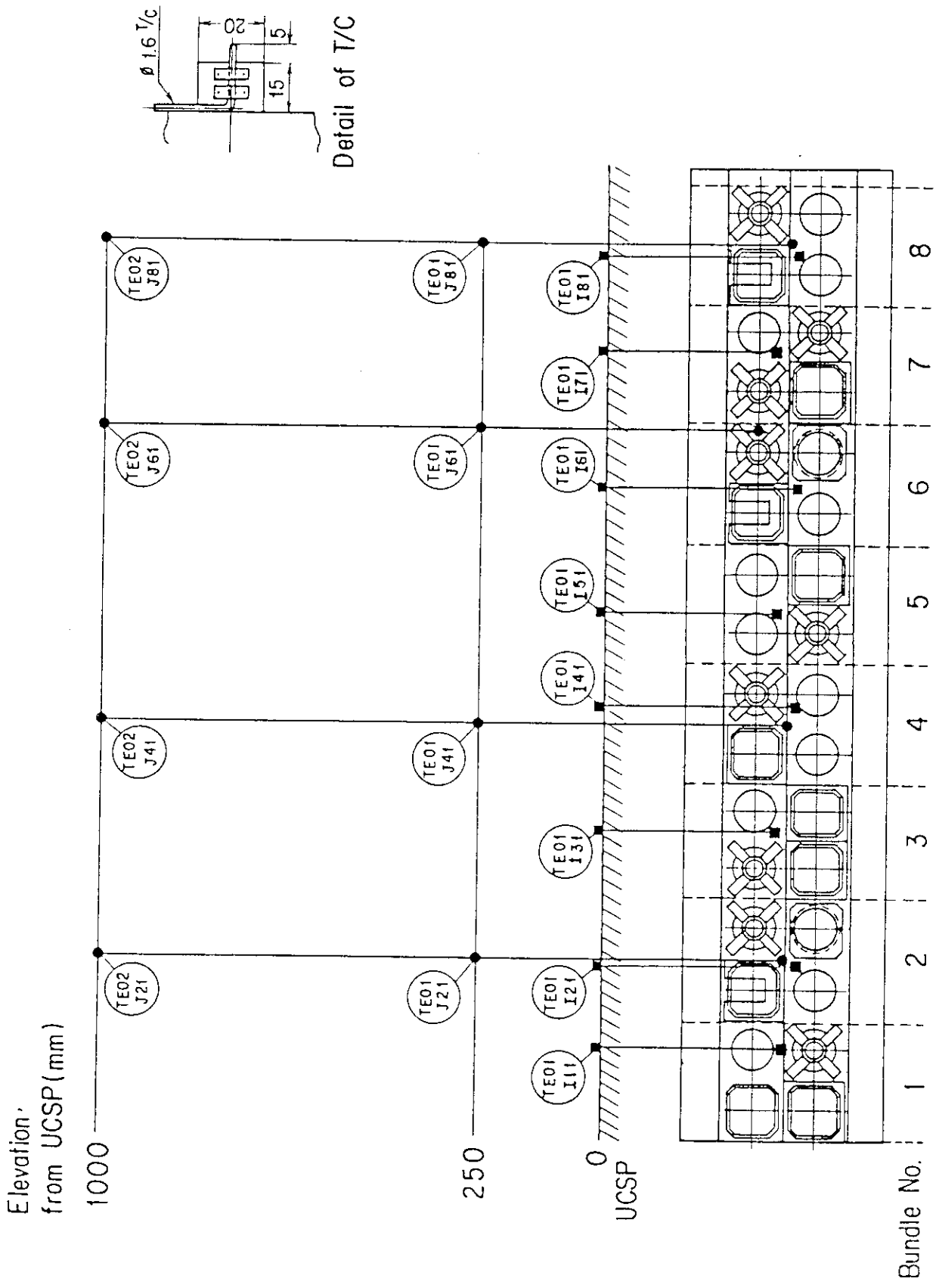

Fig. A-20 Thermocouple Locations of Fluid Temperature Measurements on and above UCSP

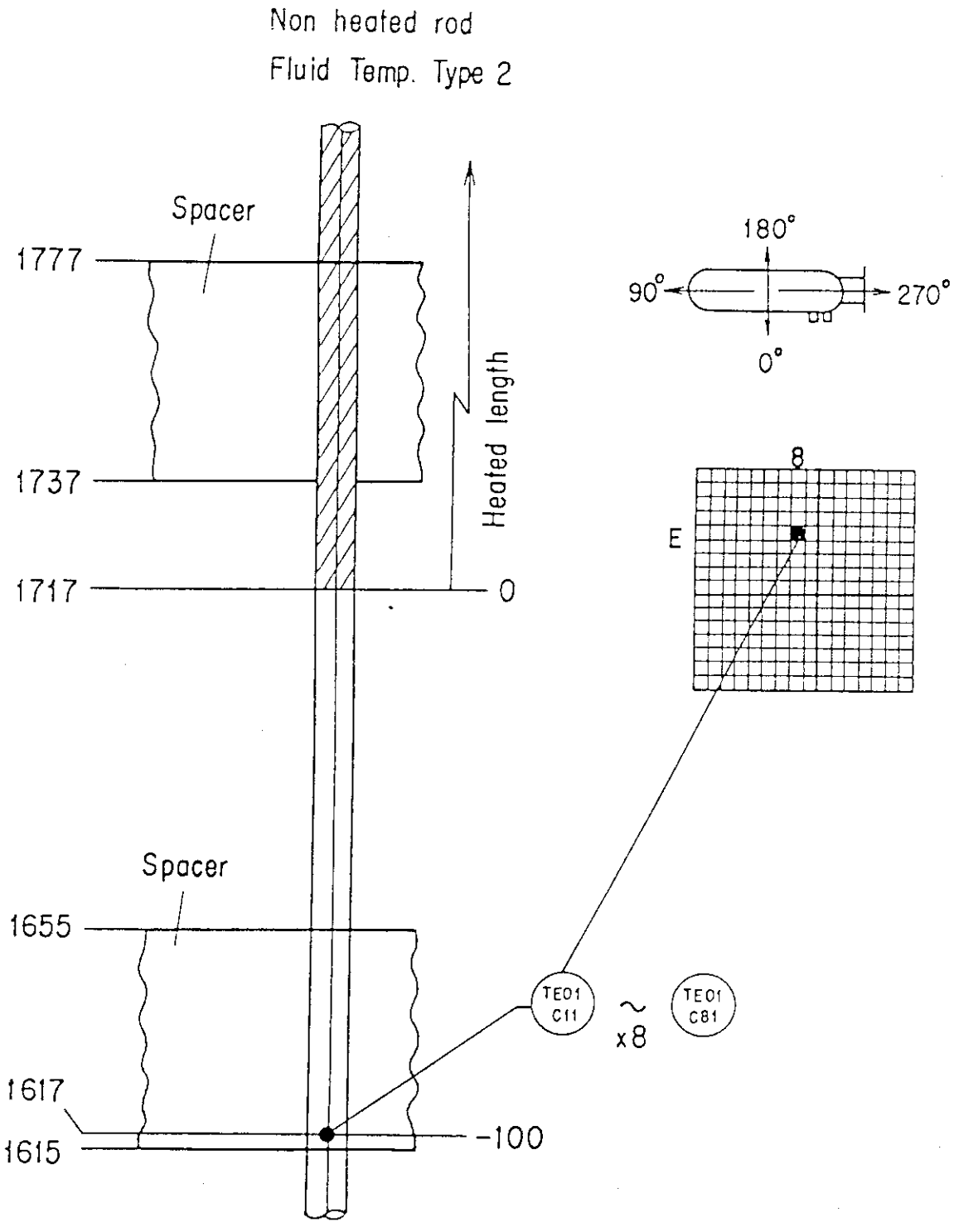

Fig. A-21 Thermocouple Locations of Fluid Temperature Measurements at Core Inlet

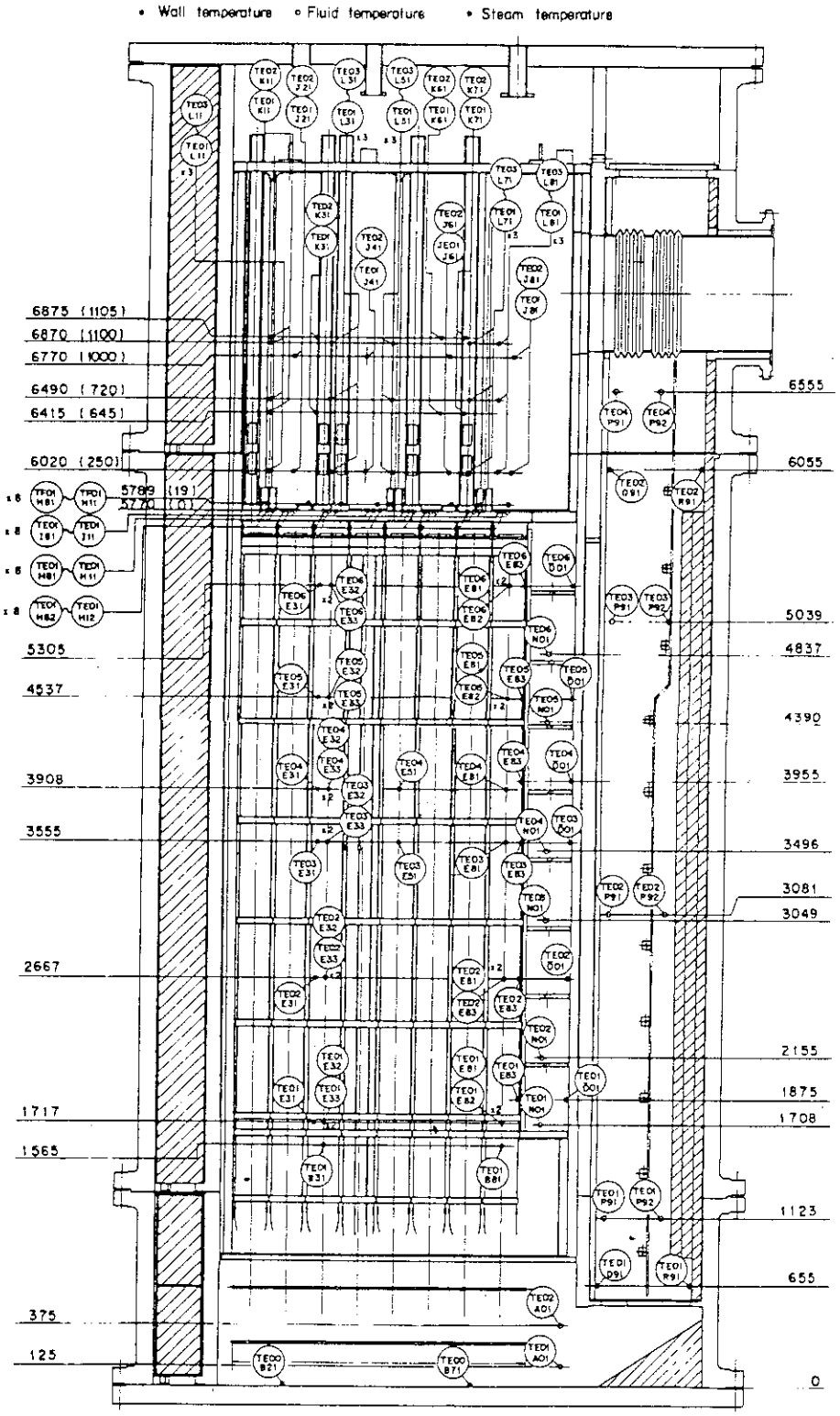

Fig. A-22 Thermocouple Locations of Temperature Measurements in Pressure Vessel except Core Region

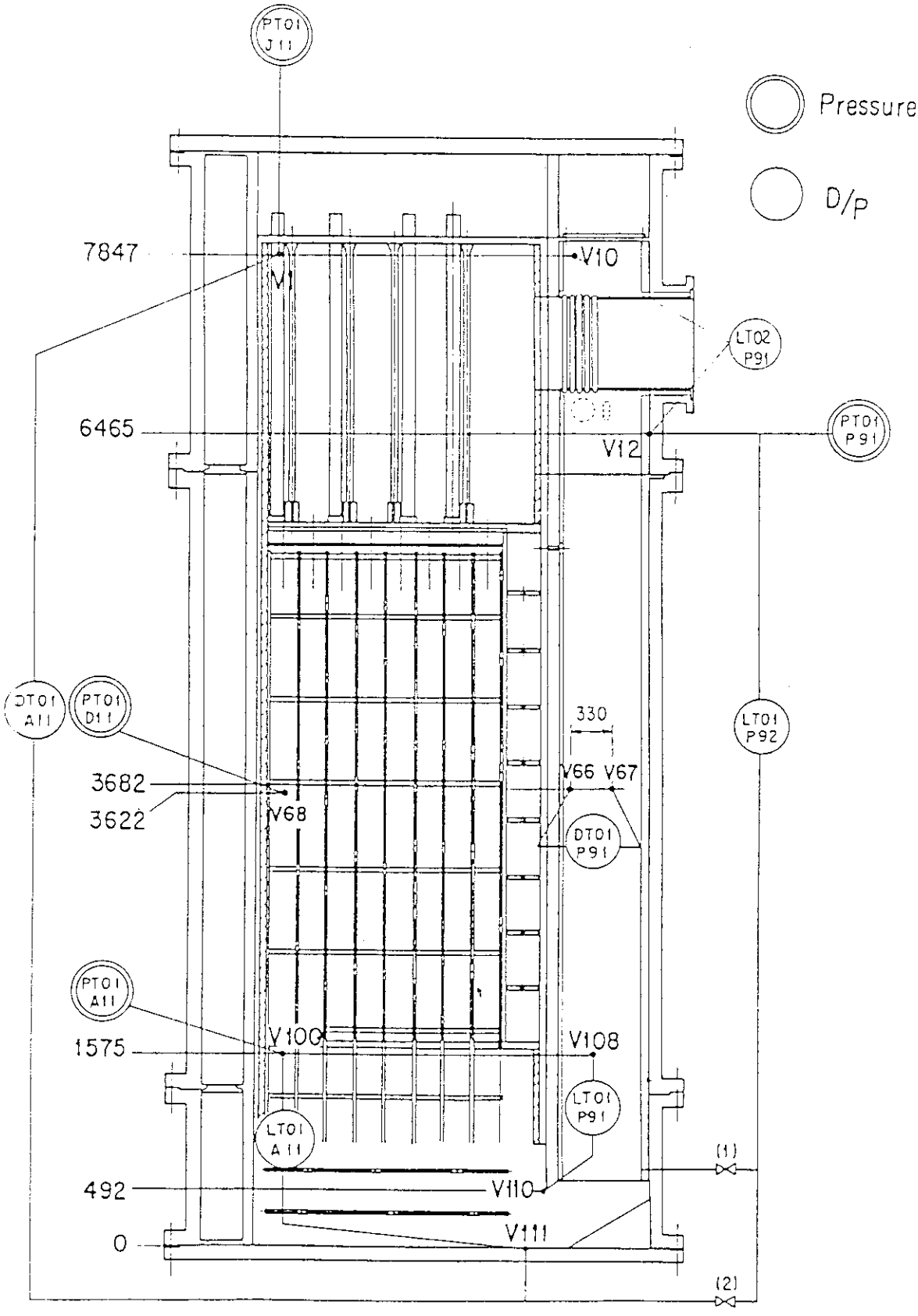

Fig. A-23 Location of Pressure Measurements in Pressure Vessel, Differential Pressure Measurements between Upper and Lower Plenums and Liquid Level Measurements in Downcomer and Lower Plenum

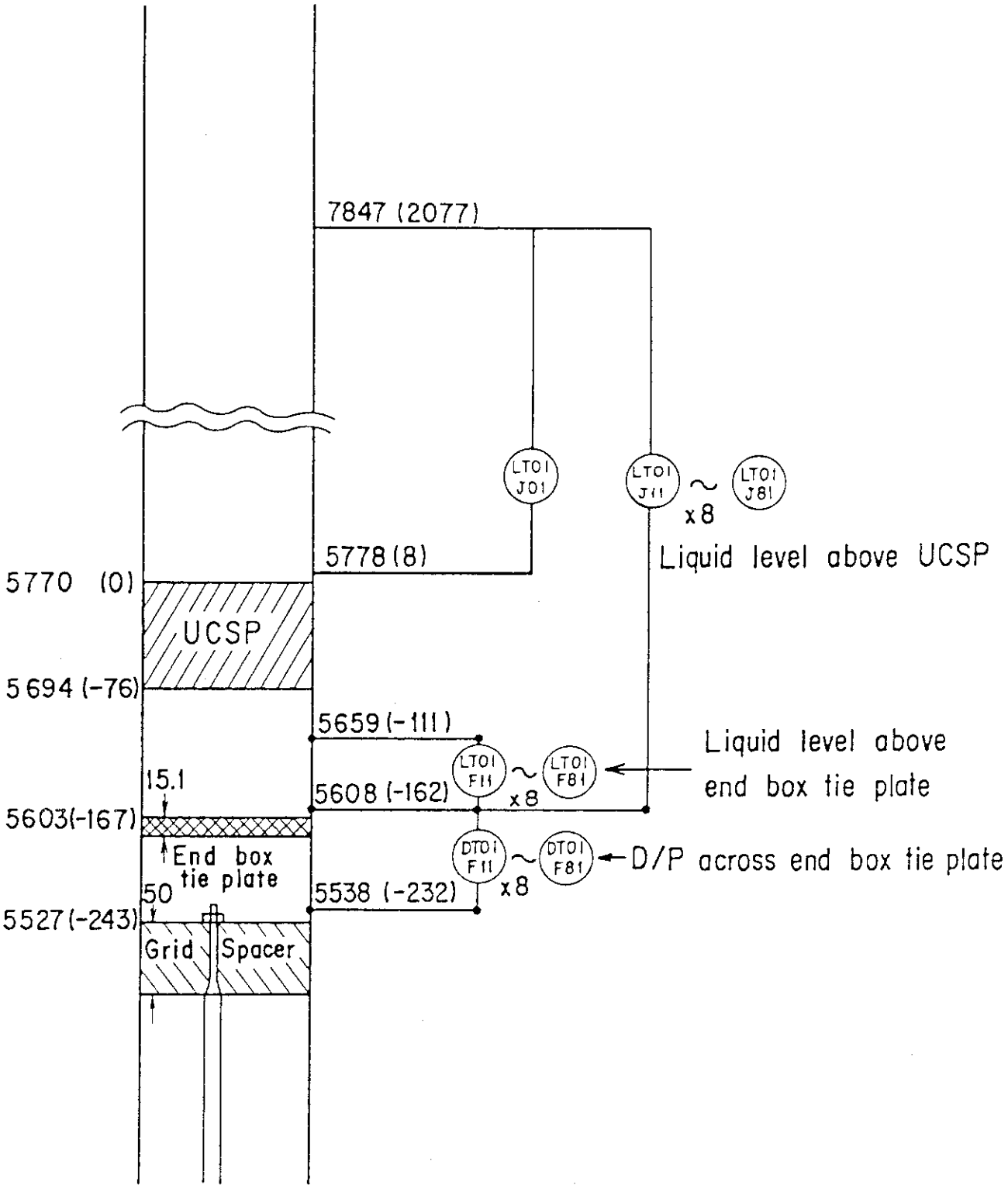

Fig. A-24 Locations of Differential Pressure Measurements across End Box Tie Plate and Liquid Level Measurements above UCSP and End Box Tie Plate

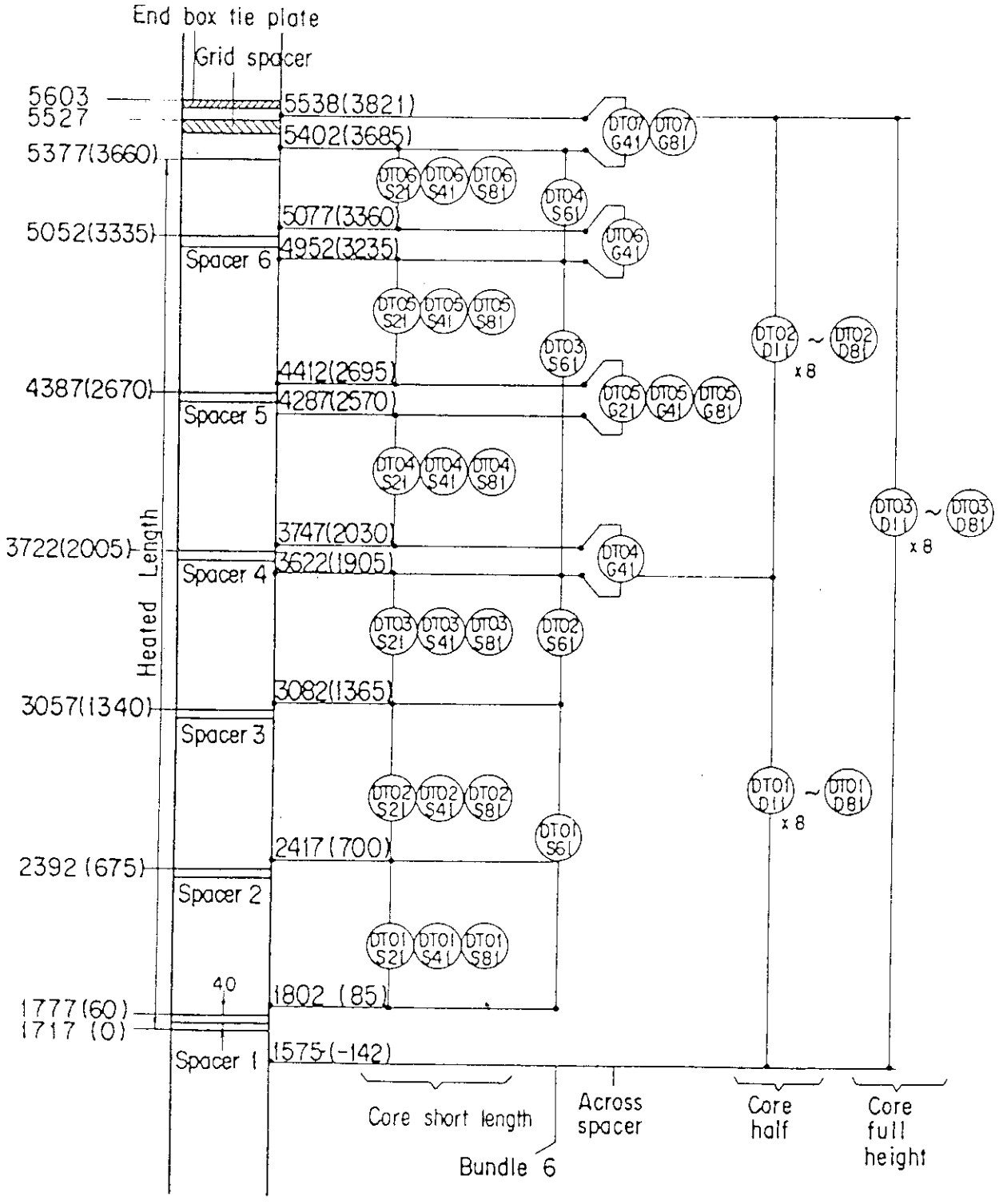

Fig. A-25 Locations of Vertical Differential Pressure Measurements in Core

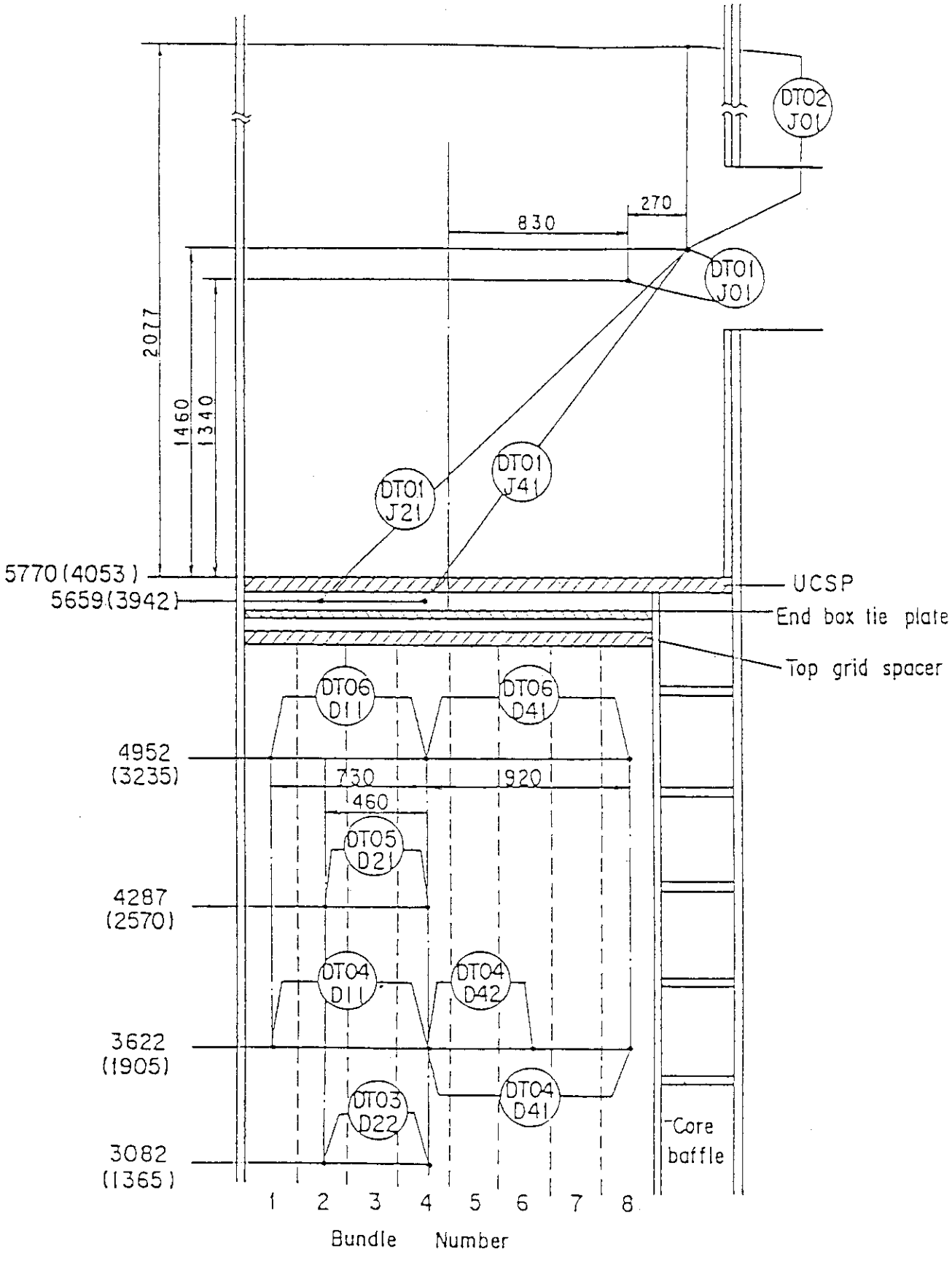

Fig. A-26 Measurement Locations of Horizontal Differential Pressures in Core and Differential Pressures in Upper Plenum

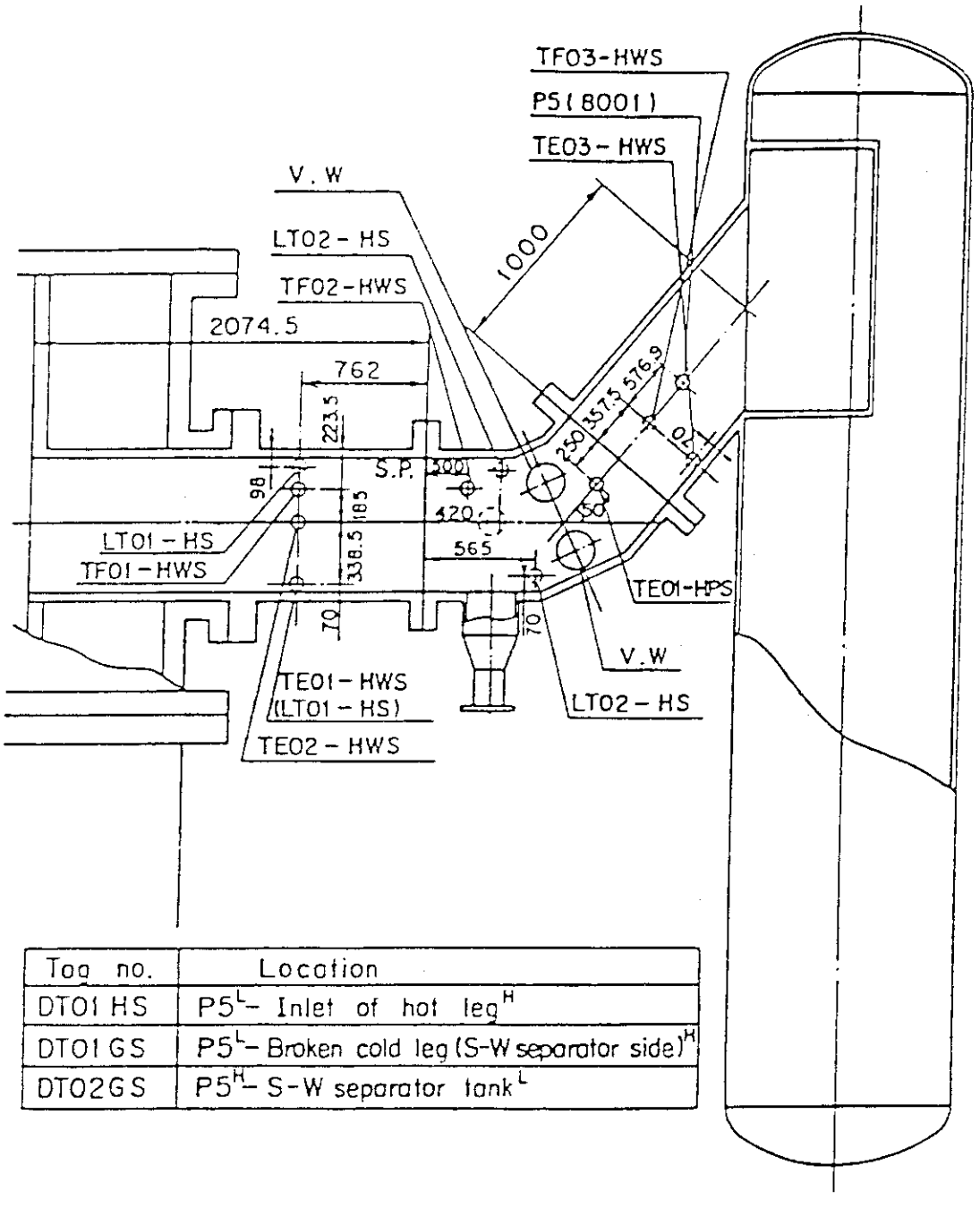

Tag no.	Location
DT01HS	P5[L]- Inlet of hot leg[H]
DT01GS	P5[L]- Broken cold leg (S-W separator side)[H]
DT02GS	P5[H]- S-W separator tank[L]

Fig. A-27 Locations of Hot Leg Instrumentation

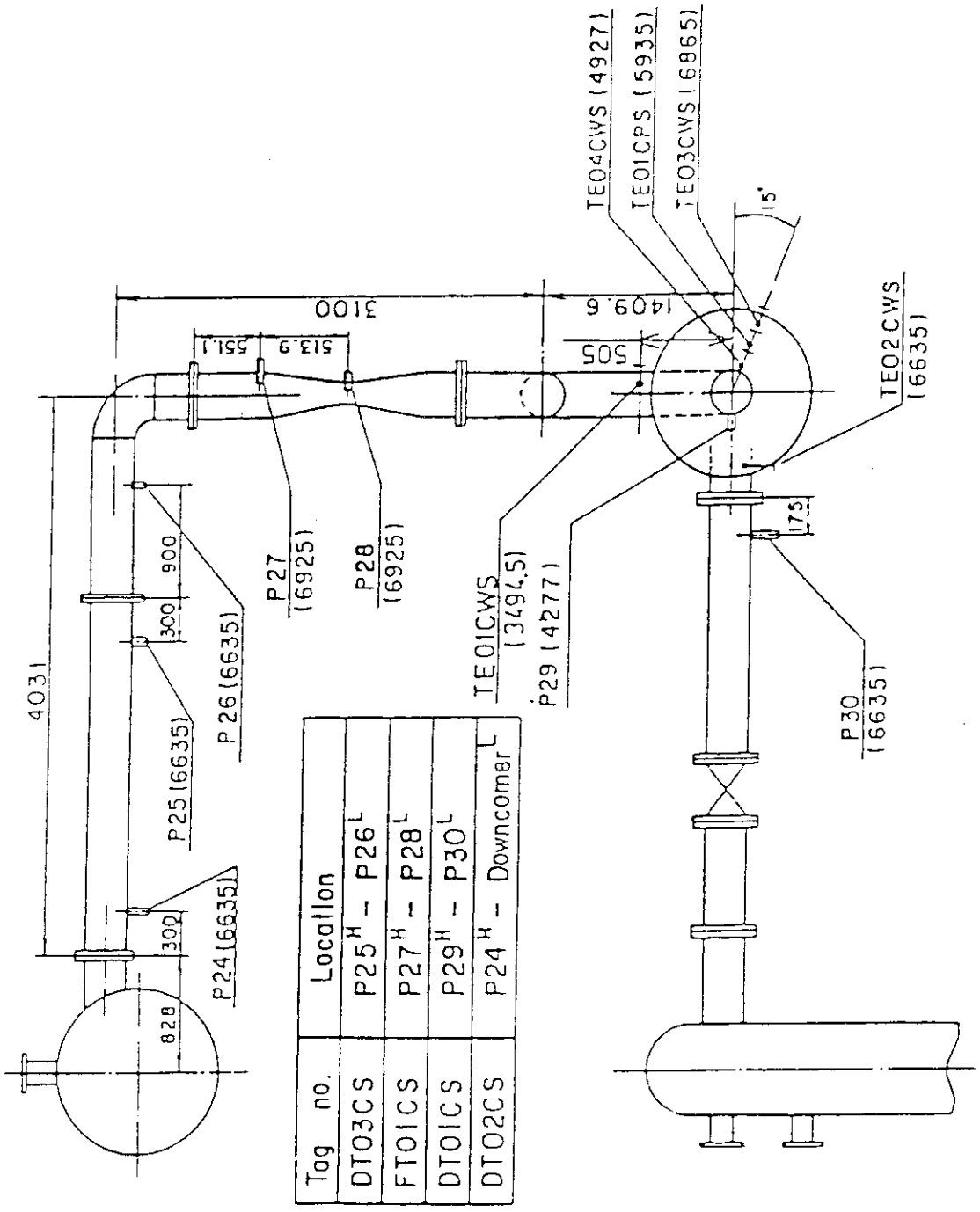

Fig. A-28 Locations of Intact Cold Leg Instrumentation

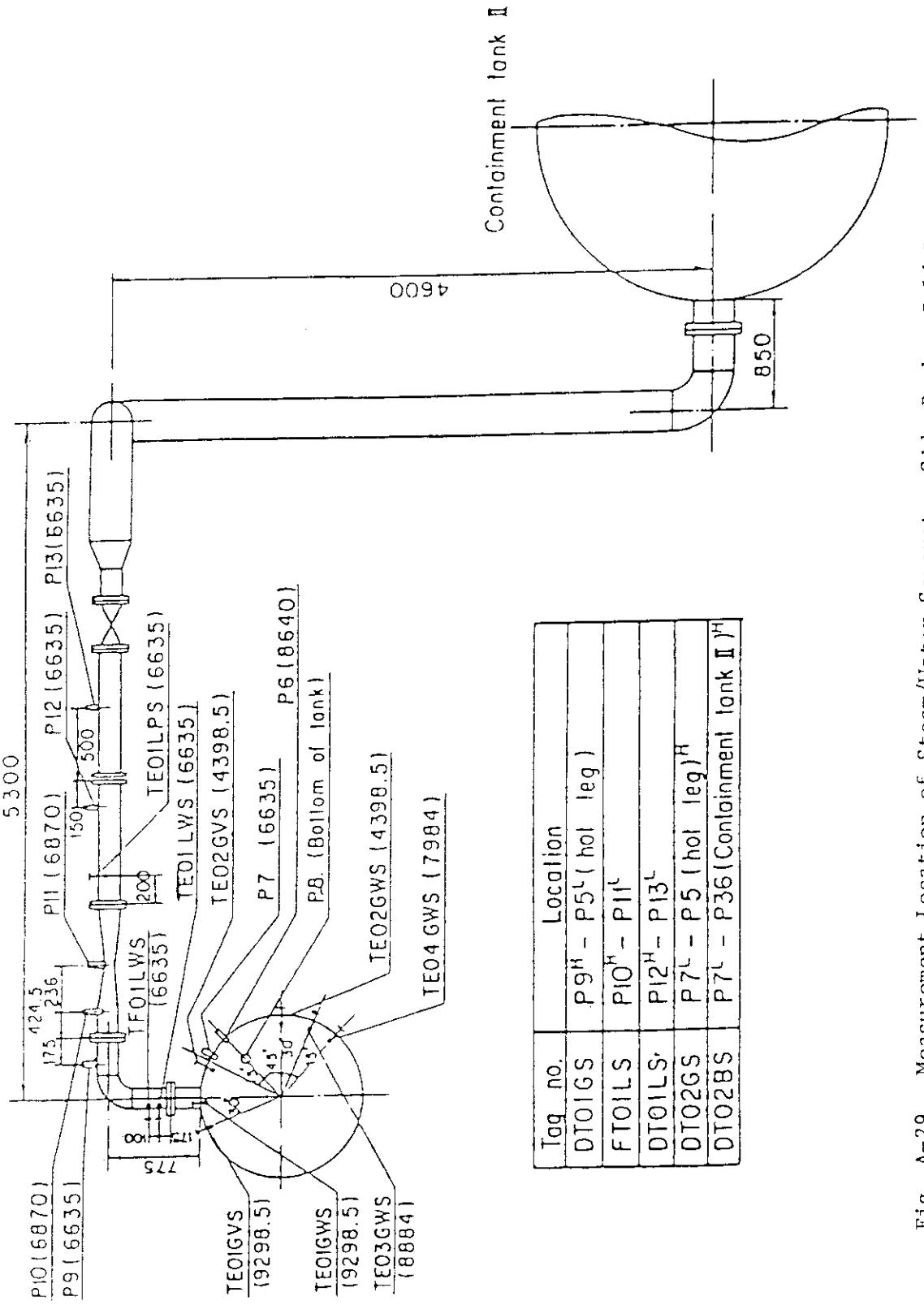

Tag no.	Location
DT01GS	$P9^H - P5^L$ (hot leg)
FT01LS	$P10^H - P11^L$
DT01LS	$P12^H - P13^L$
DT02GS	$P7^L - P5$ (hot leg)^H
DT02BS	$P7^L - P36$ (Containment tank II)^H

Fig. A-29 Measurement Location of Steam/Water Separator Side Broken Cold Leg

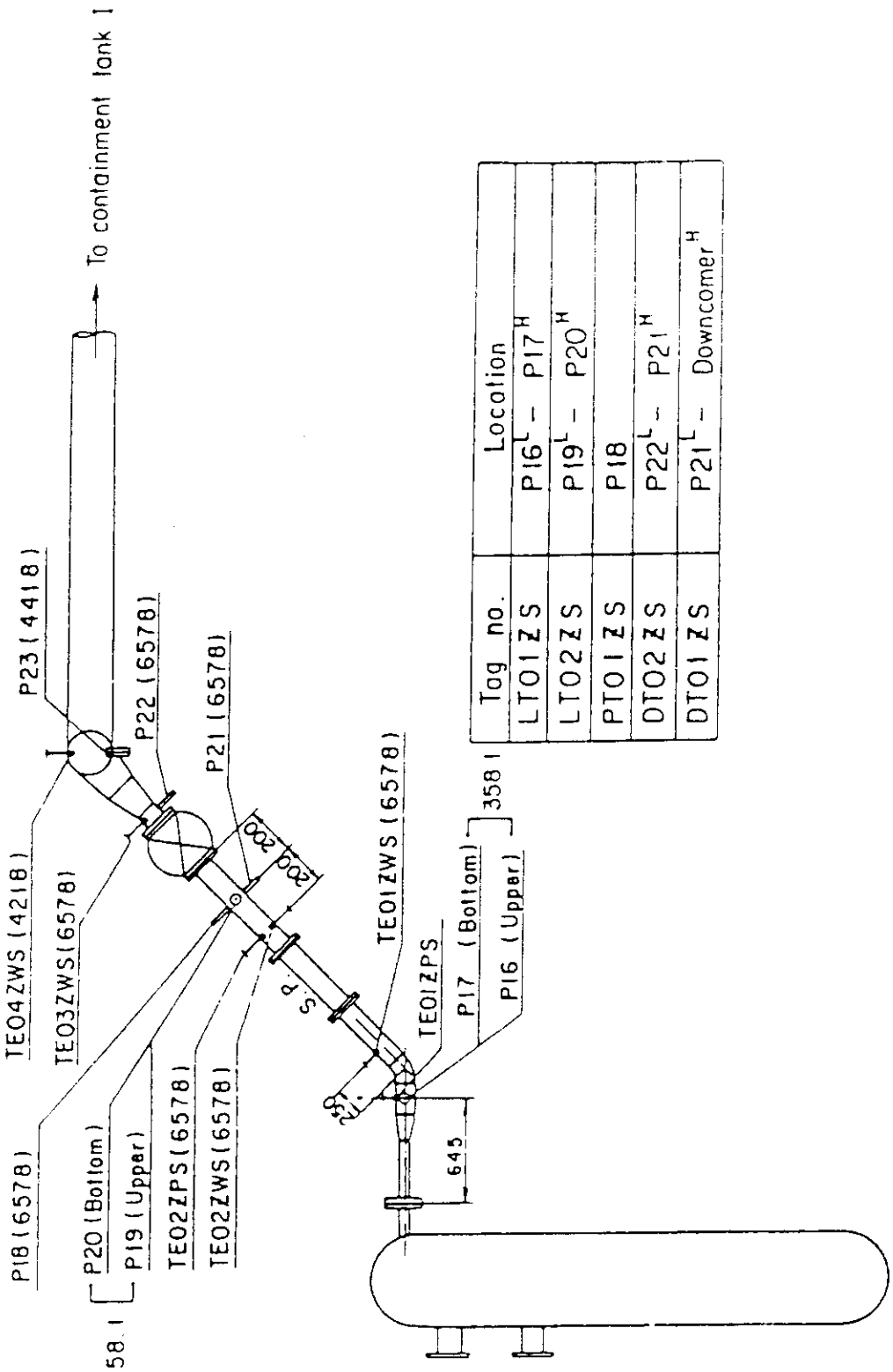

Fig. A-30 Measurement Location of Pressure Vessel Side Broken Cold Leg

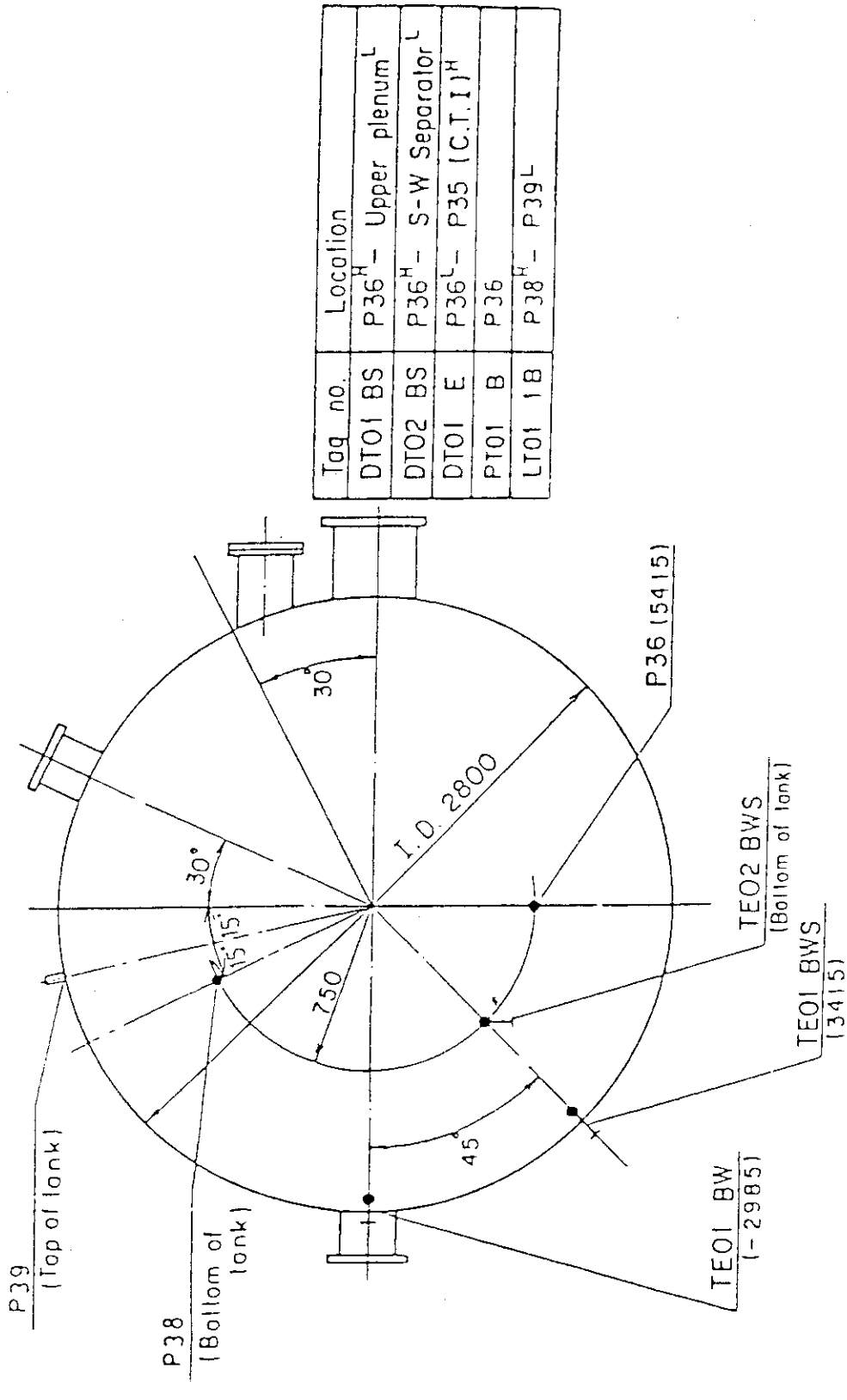

Fig. A-31 Locations of Containment Tank-II Instrumentation

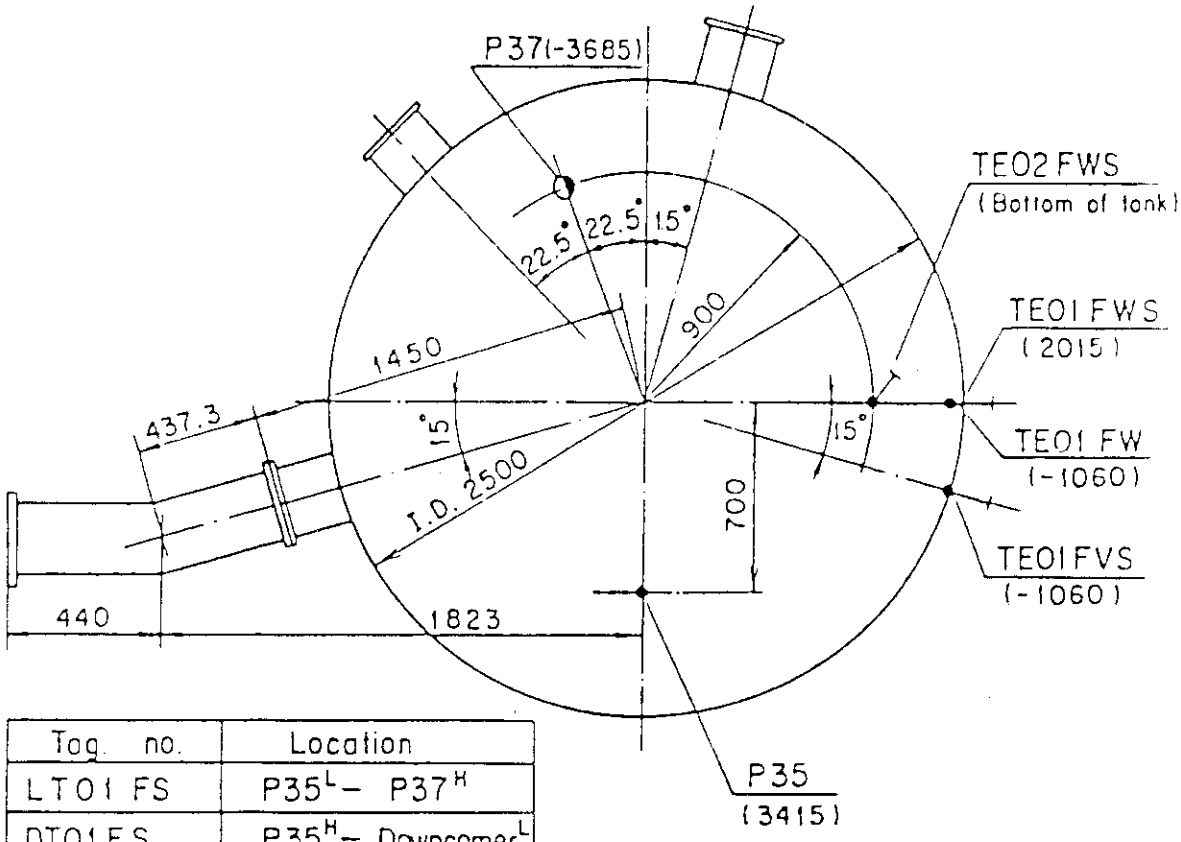

Tag. no.	Location
LT01 FS	$P35^{L}$ – $P37^{H}$
DT01 FS	$P35^{H}$ – $Downcomer^{L}$
DT01 E	$P35^{H}$ – P36 (C.T. II)
PT01 F	P35

Fig. A-32 Locations of Containment Tank-I Instrumentation

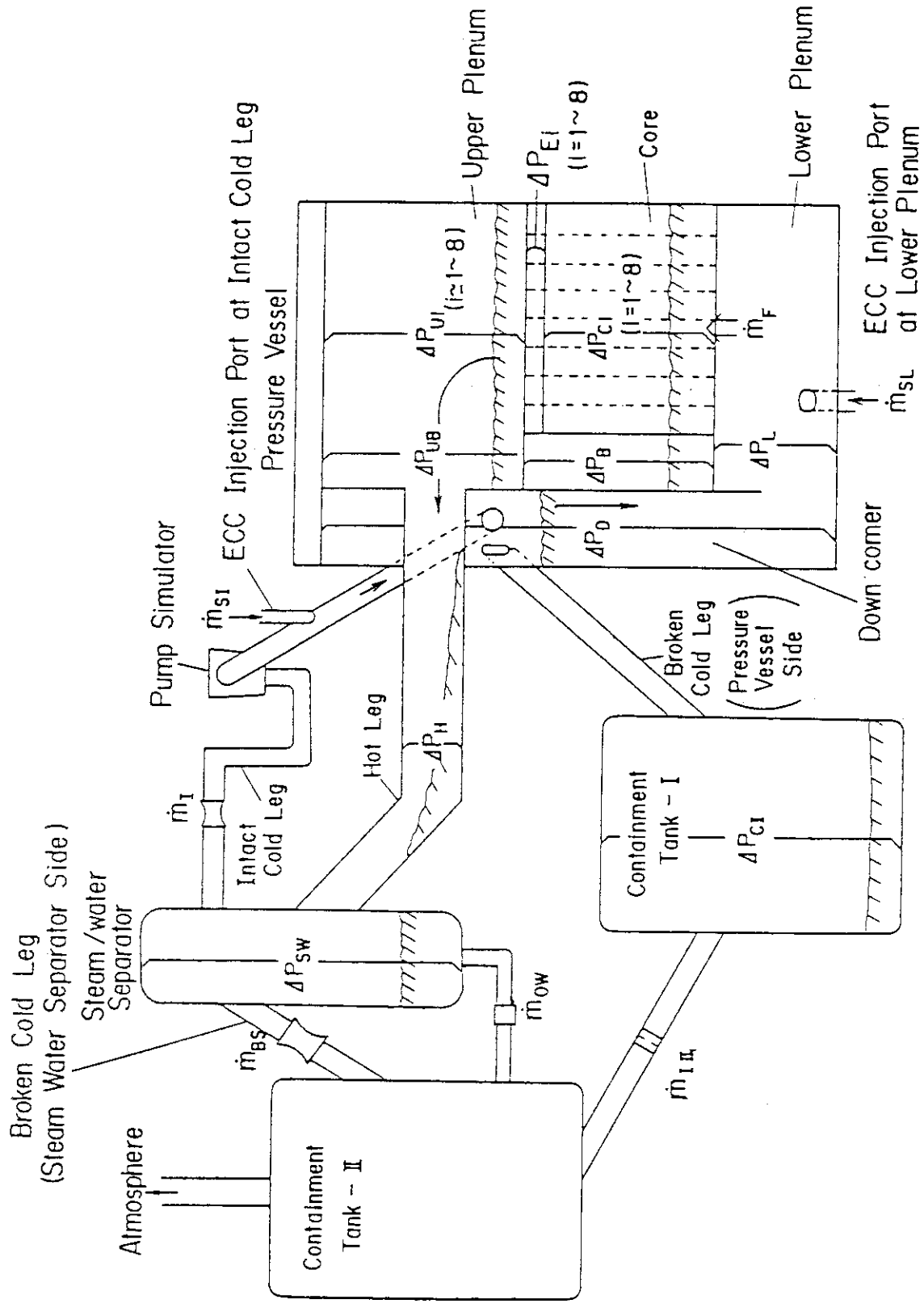

Fig. A-33 Schematic of SCTF and locations of differential pressure and mass flow rate measurements

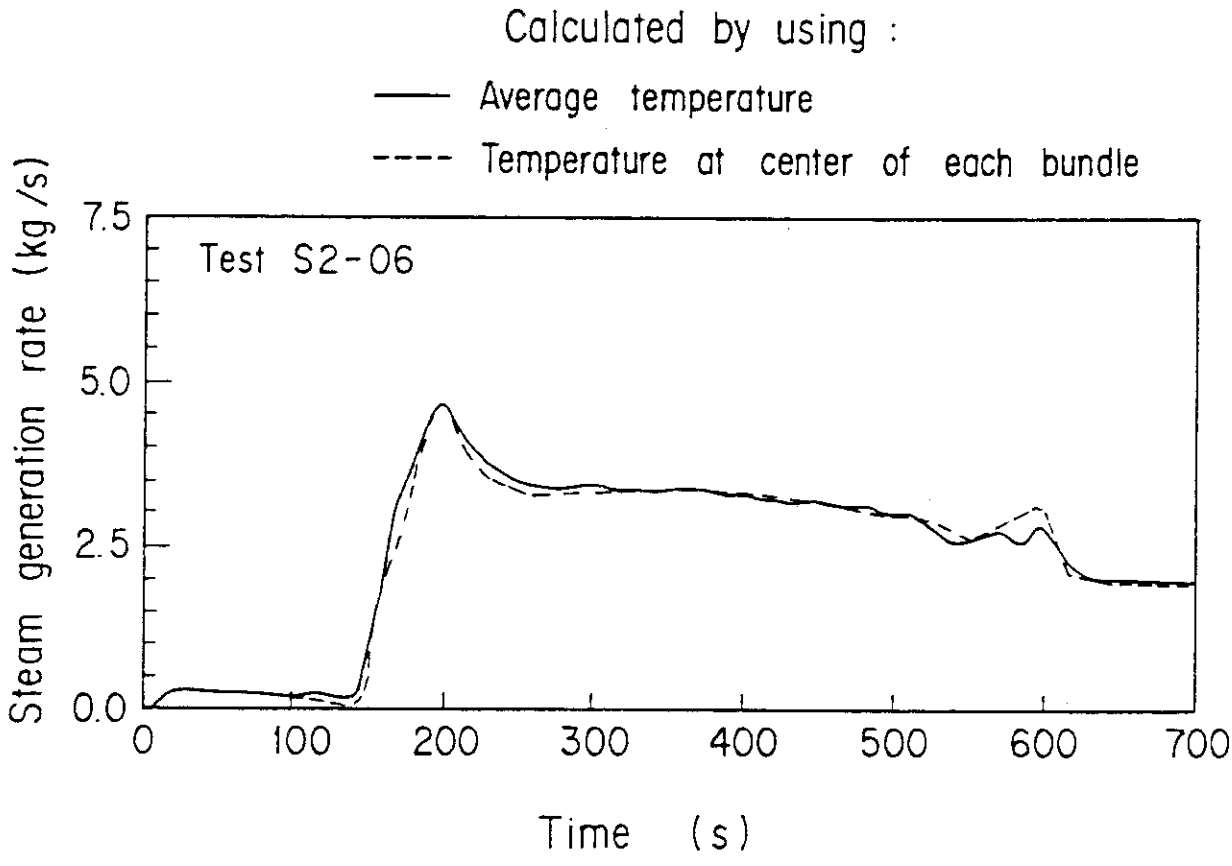

Fig. A-34 Effect of temperature data on steam generation calculation

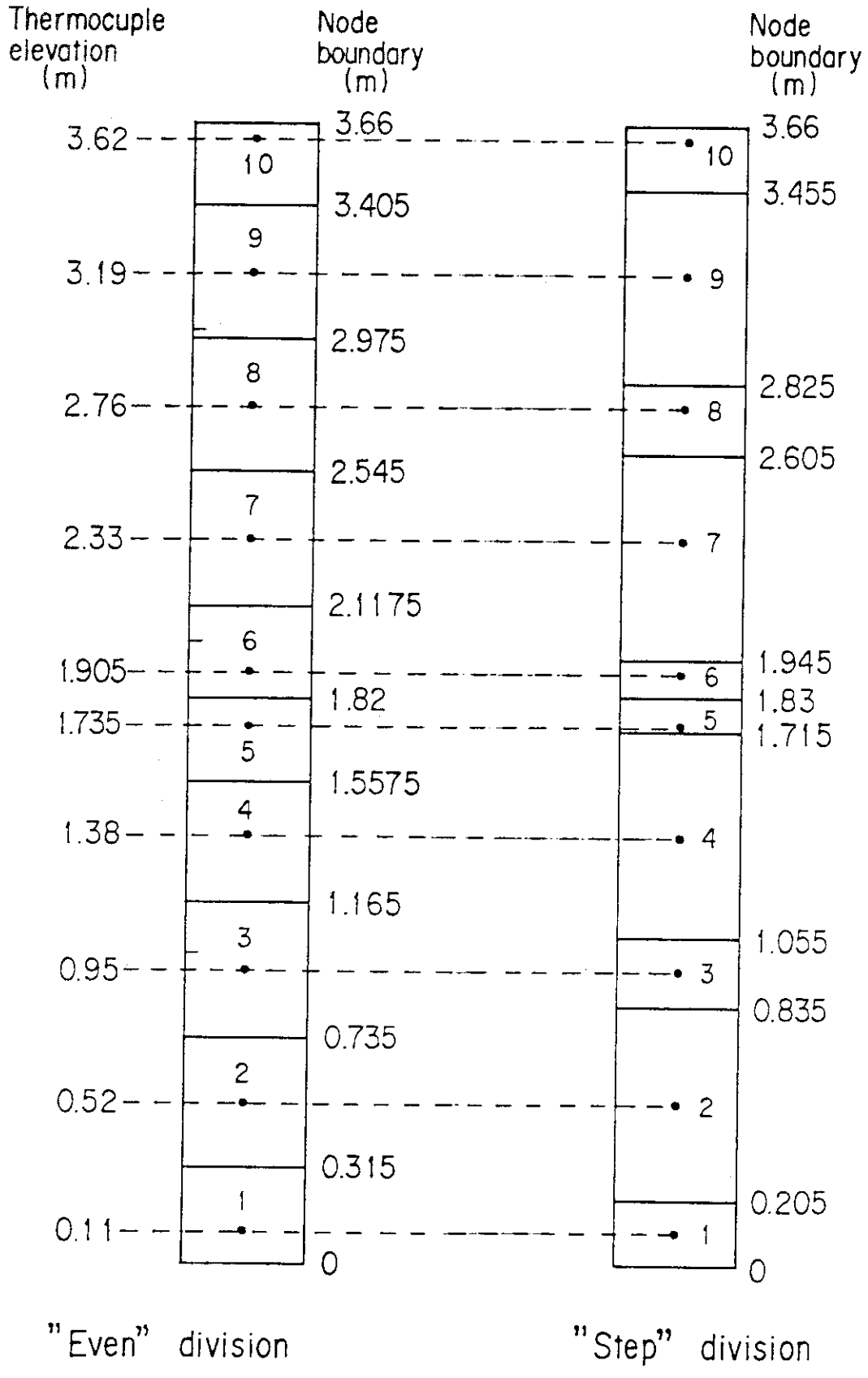

Fig. A-35 Two kinds of vertical noding models for steam generation calculation

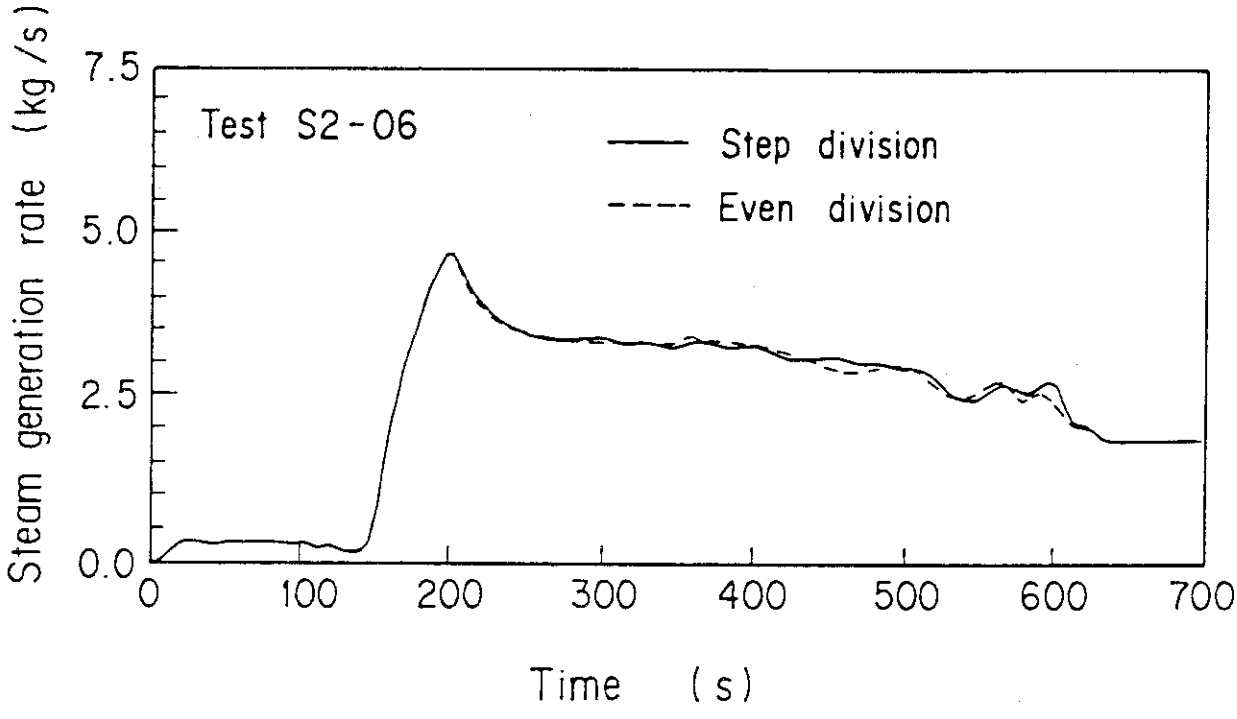

Fig. A-36 Effect of vertical noding models on steam generation calculation

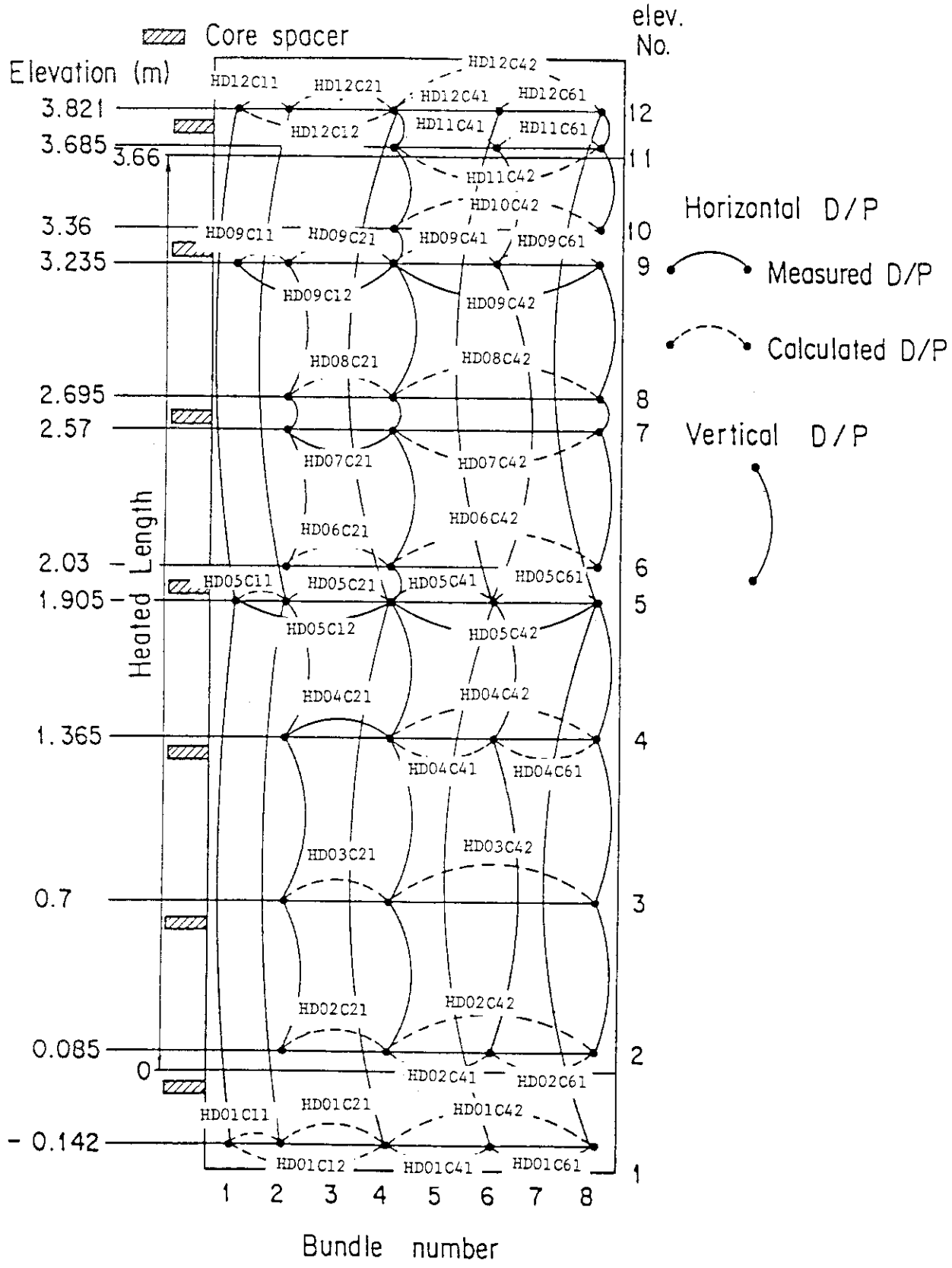

Fig. A-37 Locations of calculated horizontal differential pressures

Appendix B Selected Data for SCTF Test S2-09(Run 614)

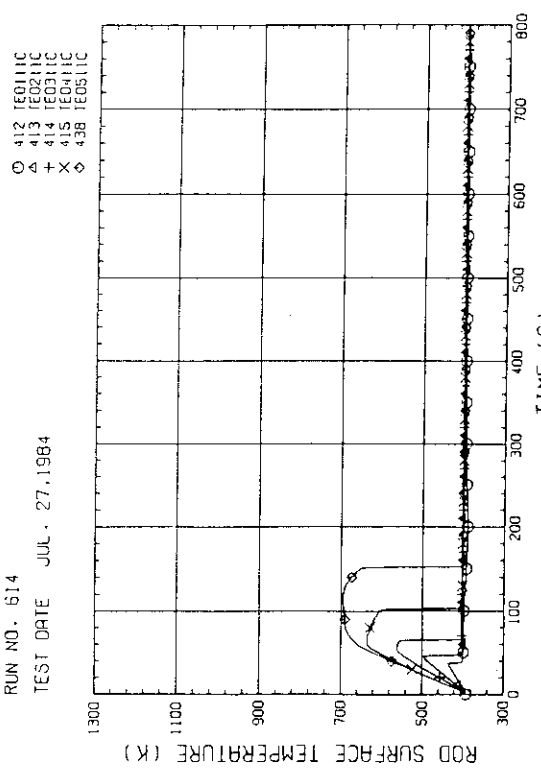

Fig. B-1 HEATER ROD TEMPERATURE (BUNDLE 1-1C, LOWER HALF)

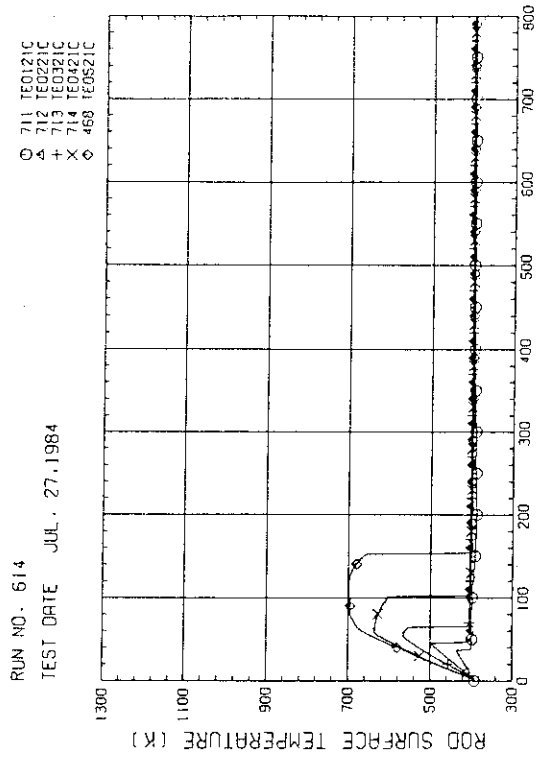

Fig. B-3 HEATER ROD TEMPERATURE (BUNDLE 2-1C, LOWER HALF)

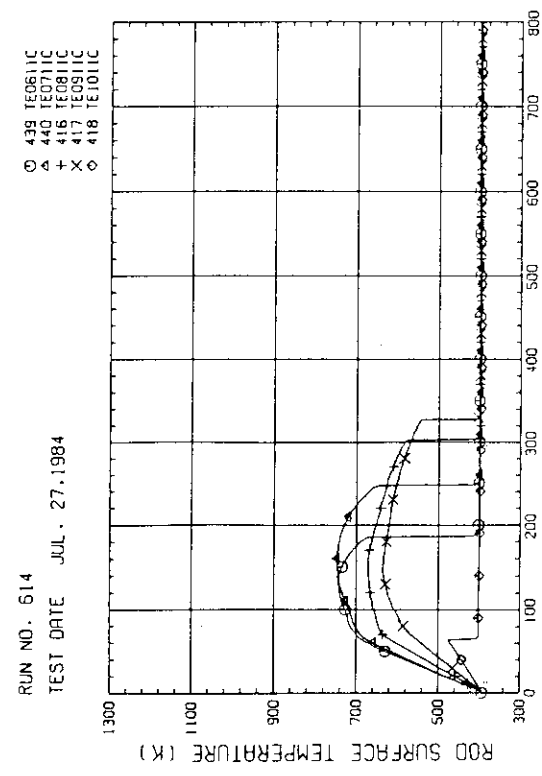

Fig. B-2 HEATER ROD TEMPERATURE (BUNDLE 1-1C, UPPER HALF)

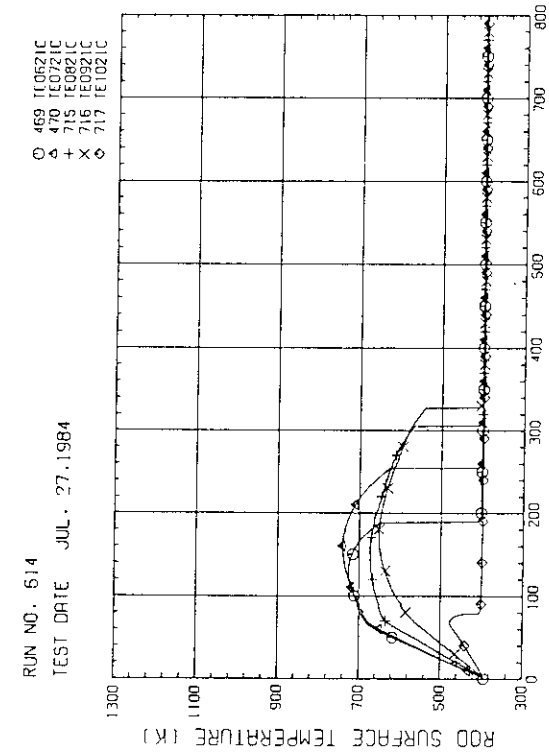

Fig. B-4 HEATER ROD TEMPERATURE (BUNDLE 2-1C, UPPER HALF)

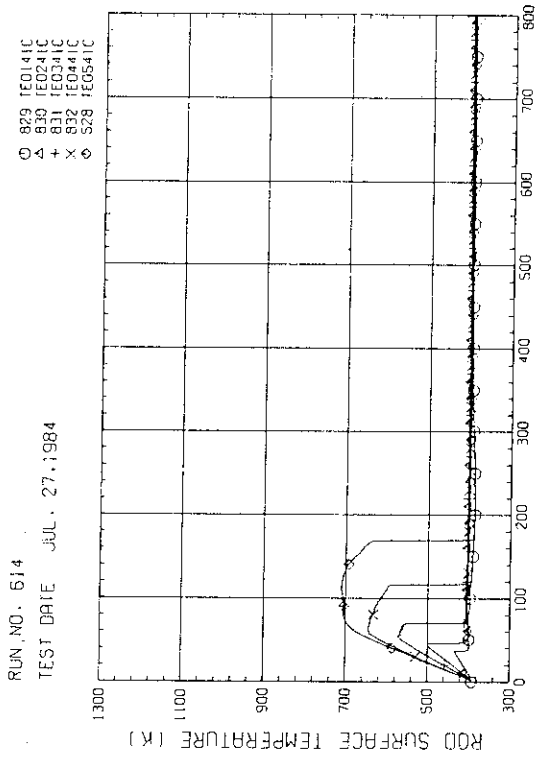

Fig. B-7 HEATER ROD TEMPERATURE (BUNDLE 4-1C, LOWER HALF)

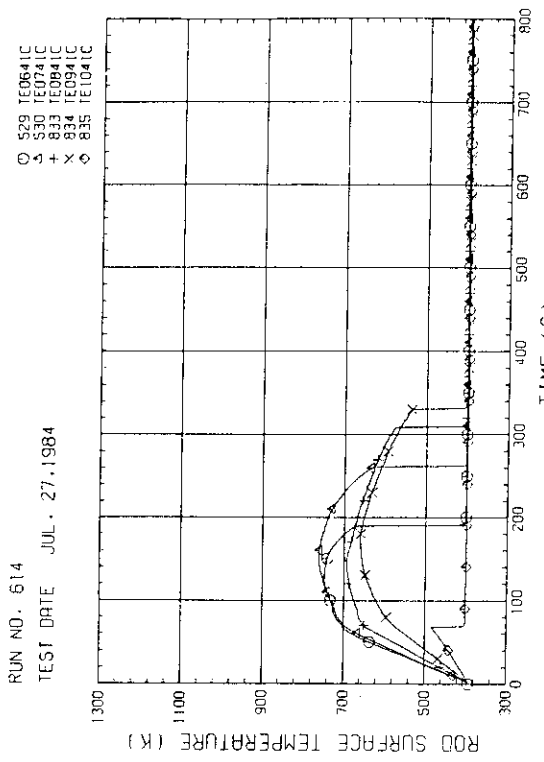

Fig. B-8 HEATER ROD TEMPERATURE (BUNDLE 4-1C, UPPER HALF)

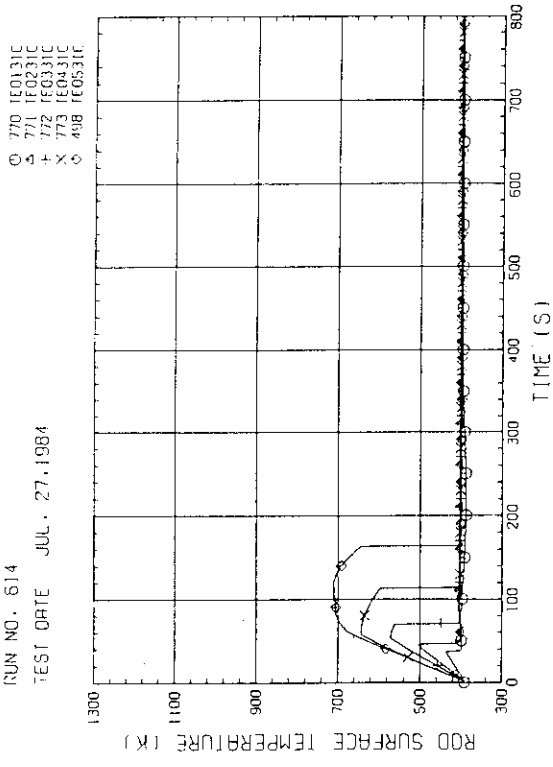

Fig. B-5 HEATER ROD TEMPERATURE (BUNDLE 3-1C, LOWER HALF)

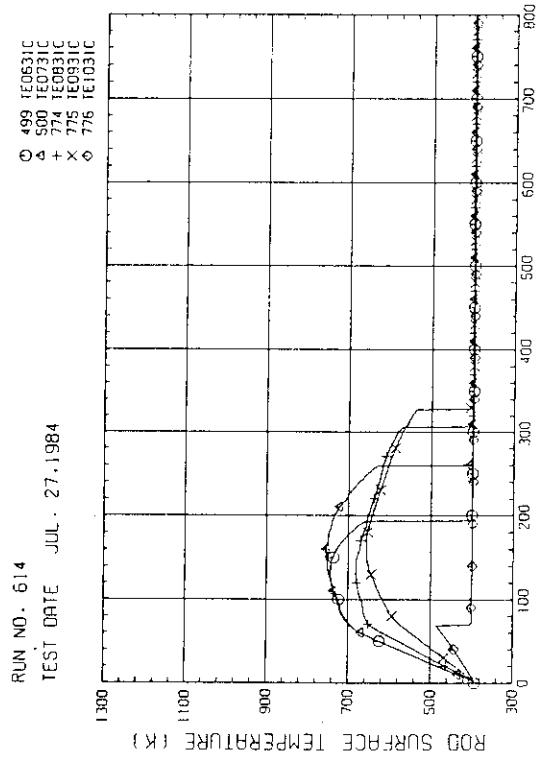

Fig. B-6 HEATER ROD TEMPERATURE (BUNDLE 3-1C, UPPER HALF)

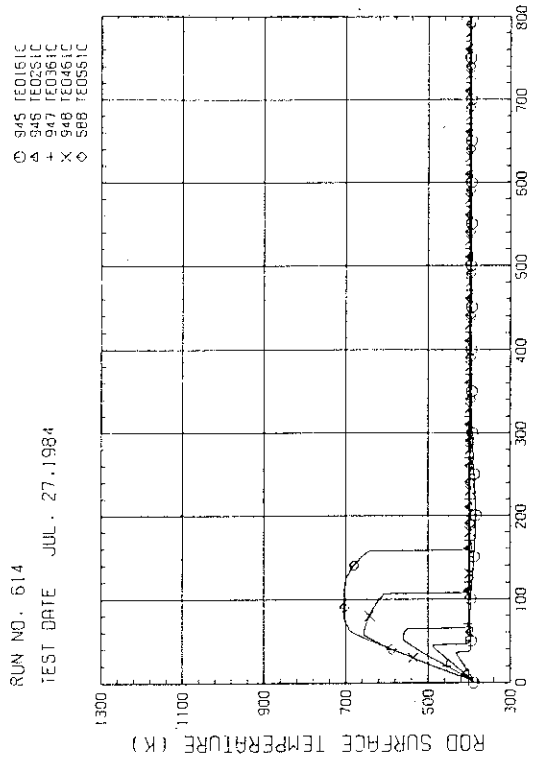

Fig. B-11 HEATER ROD TEMPERATURE (BUNDLE 6-1C, LOWER HALF)

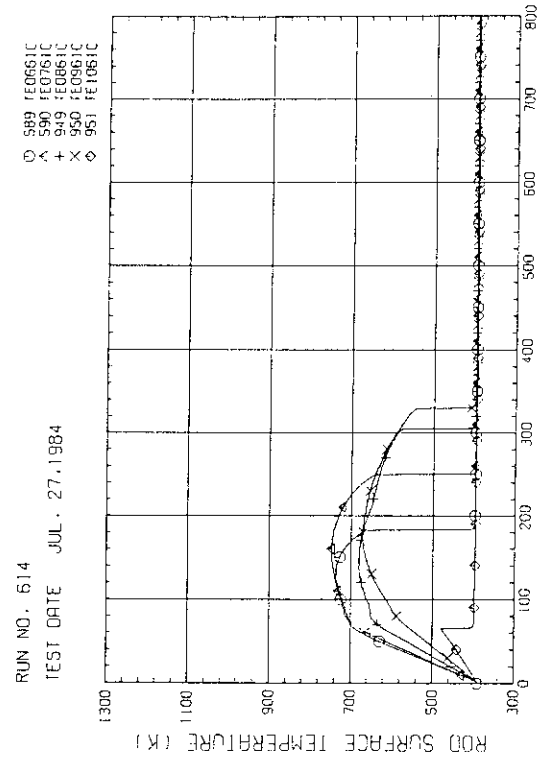

Fig. B-12 HEATER ROD TEMPERATURE (BUNDLE 6-1C, UPPER HALF)

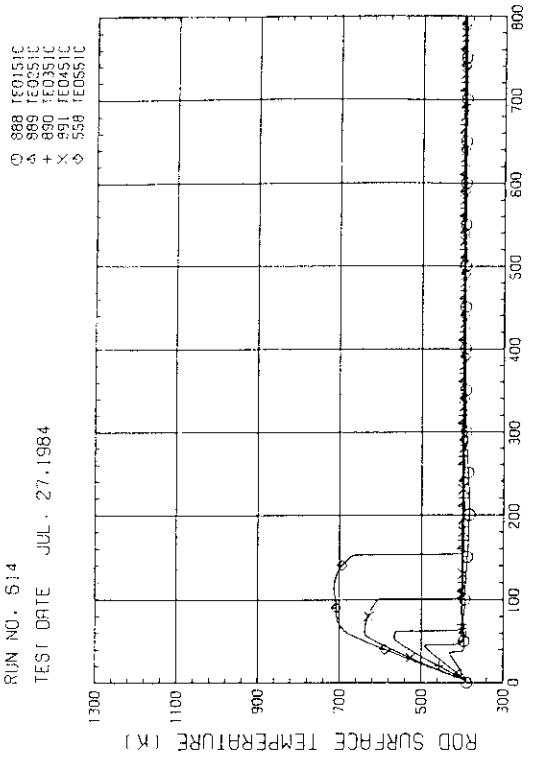

Fig. B-9 HEATER ROD TEMPERATURE (BUNDLE 5-1C, LOWER HALF)

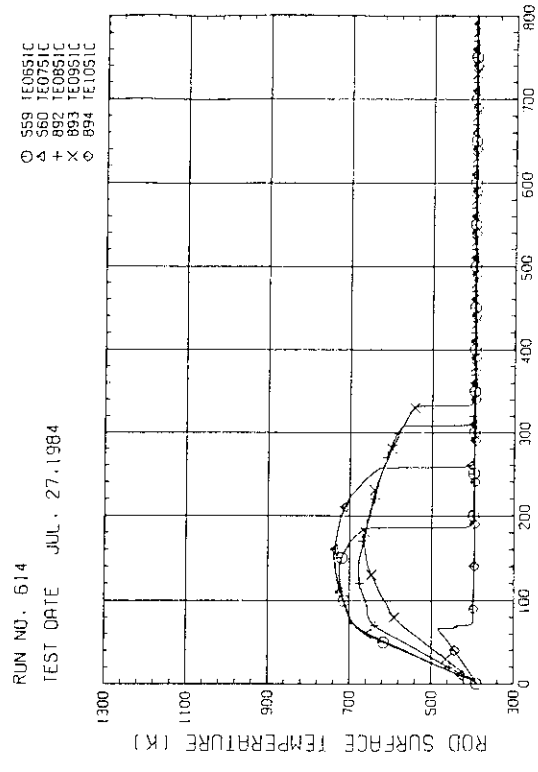

Fig. B-10 HEATER ROD TEMPERATURE (BUNDLE 5-1C, UPPER HALF)

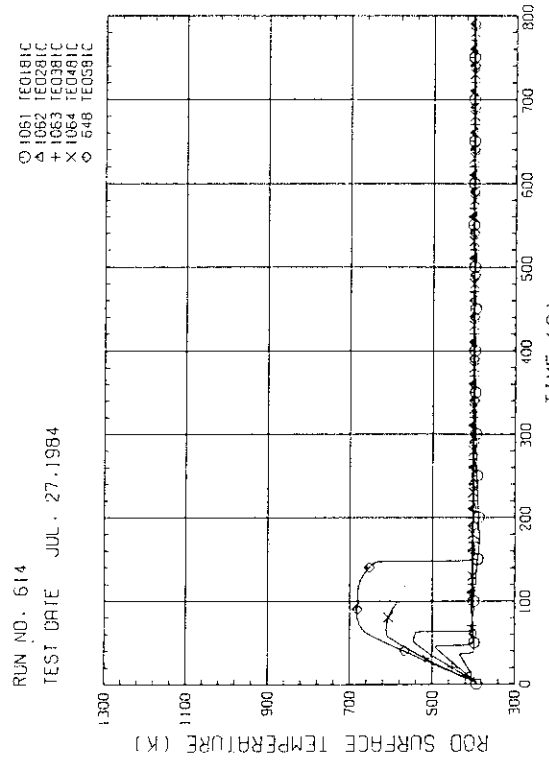

Fig. B-15 HEATER ROD TEMPERATURE (BUNDLE 8-IC, LOWER HALF)

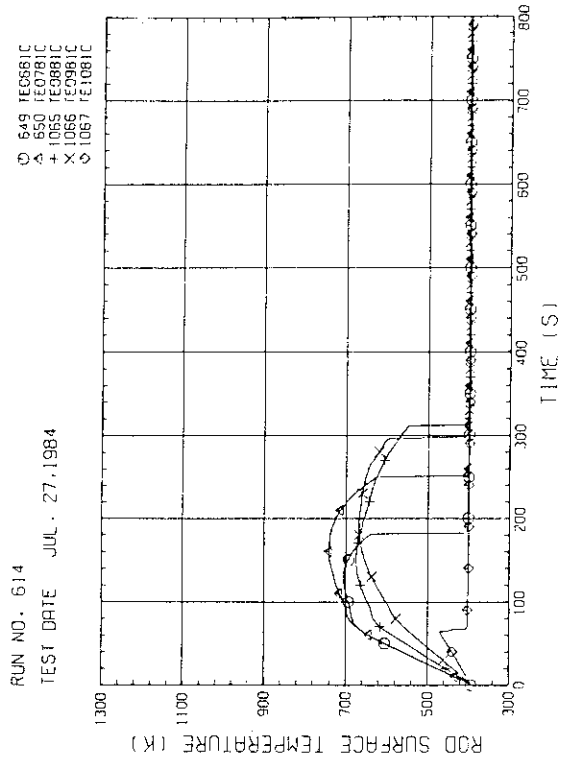

Fig. B-16 HEATER ROD TEMPERATURE (BUNDLE 8-IC, UPPER HALF)

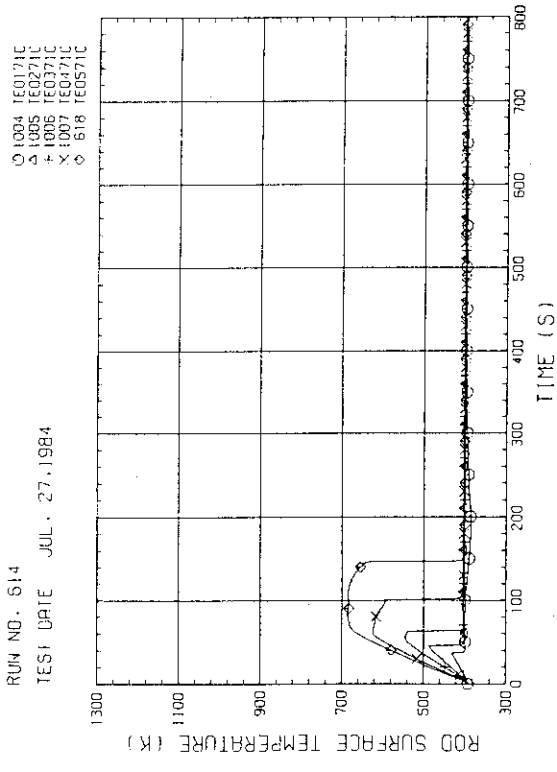

Fig. B-13 HEATER ROD TEMPERATURE (BUNDLE 7-IC, LOWER HALF)

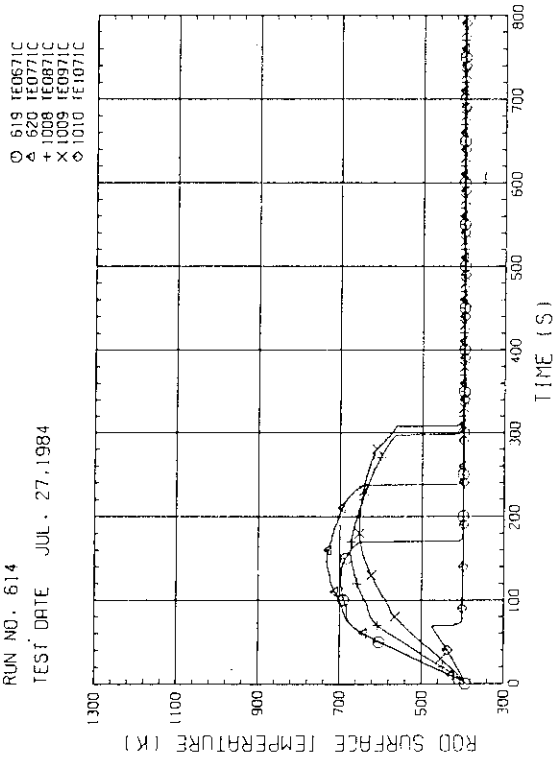

Fig. B-14 HEATER ROD TEMPERATURE (BUNDLE 7-IC, UPPER HALF)

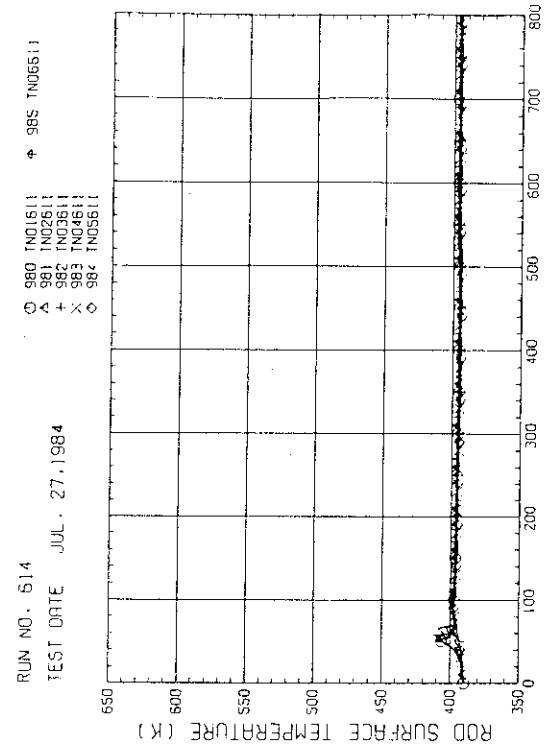

Fig. B-19 NON-HEATED ROD TEMPERATURE (BUNDLE 5-1)

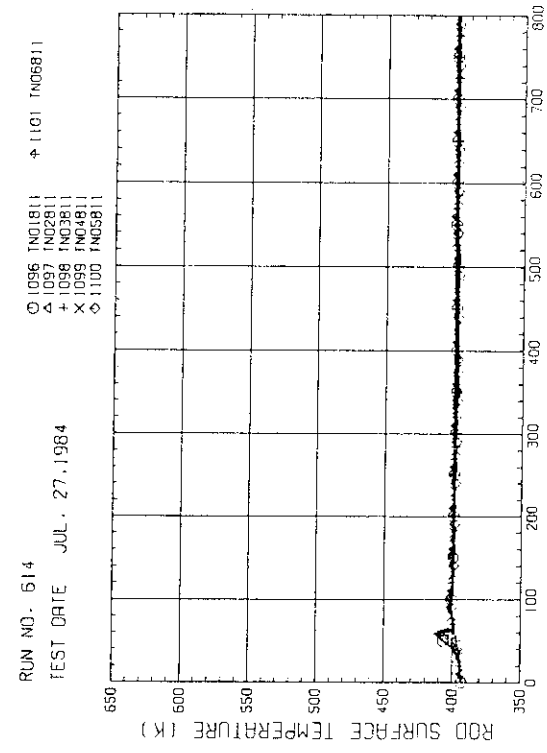

Fig. B-20 NON-HEATED ROD TEMPERATURE (BUNDLE 8-1)

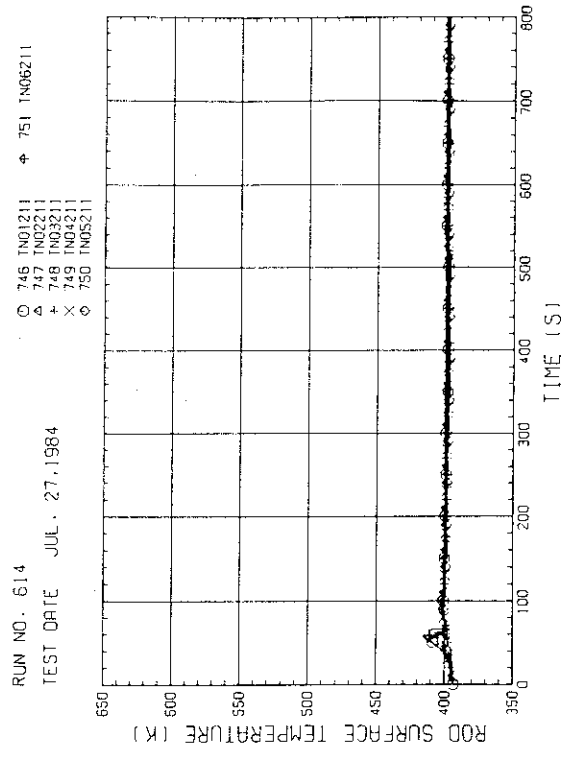

Fig. B-17 NON-HEATED ROD TEMPERATURE (BUNDLE 2-1)

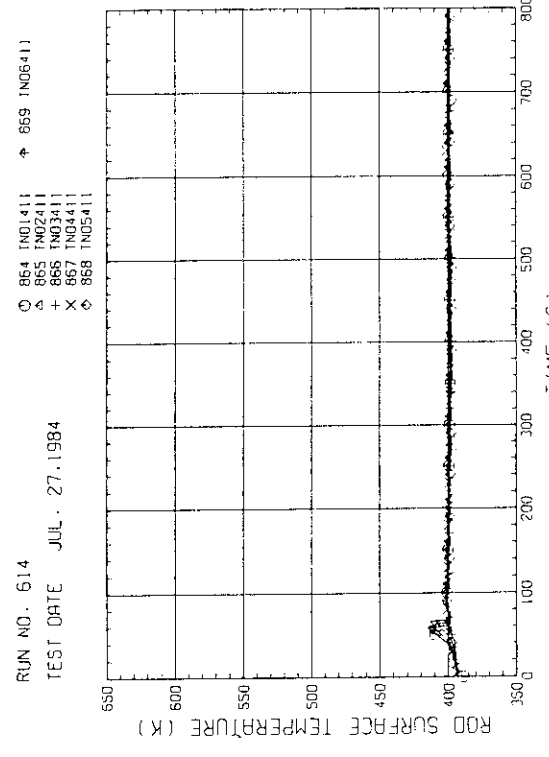

Fig. B-18 NON-HEATED ROD TEMPERATURE (BUNDLE 4-1)

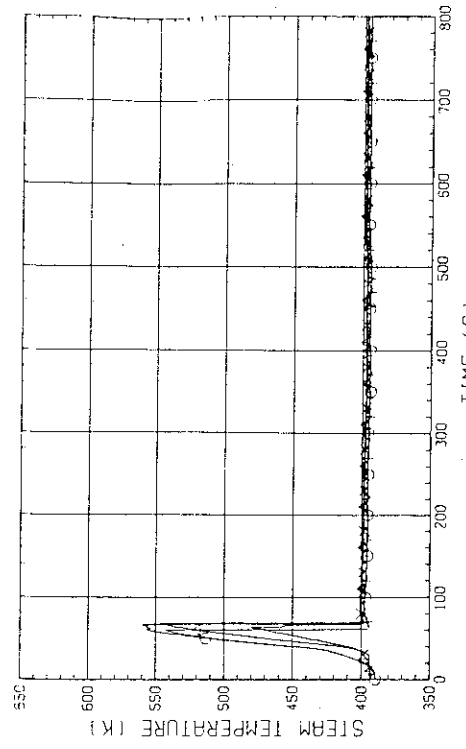

Fig. B-23 STEAM TEMPERATURE IN CORE, BUNDLE 6

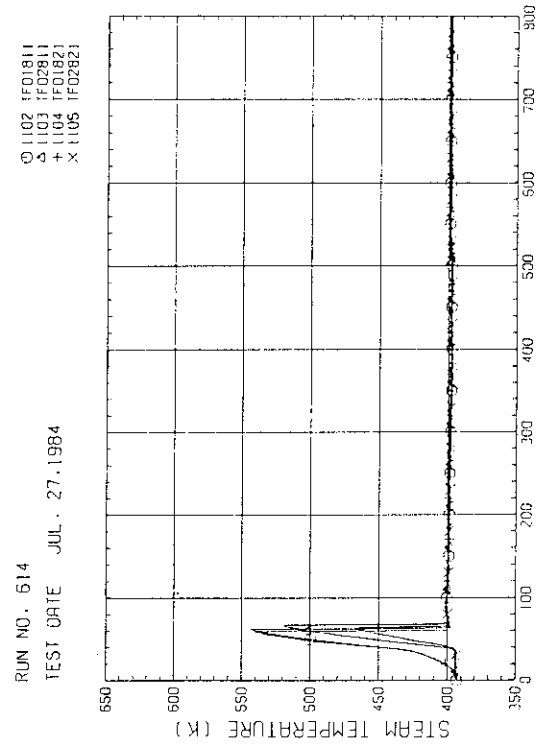

Fig. B-24 STEAM TEMPERATURE IN CORE, BUNDLE 8

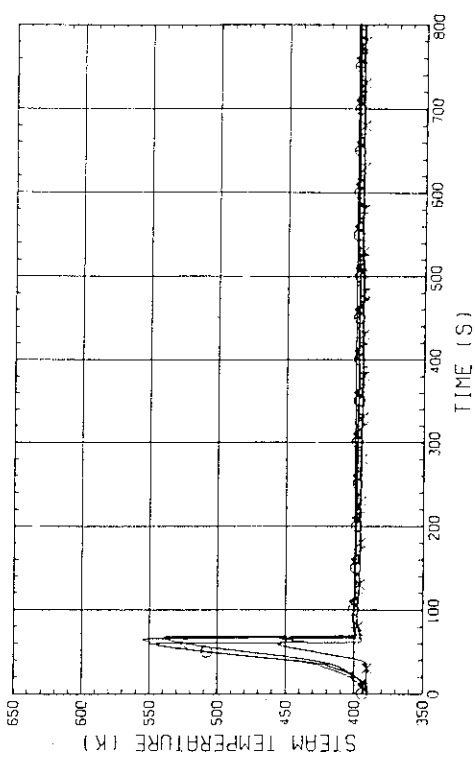

Fig. B-21 STEAM TEMPERATURE IN CORE, BUNDLE 2
(01211-1.735M, 02211-1.875M, 01221-1.38M, 02221-1.915M)

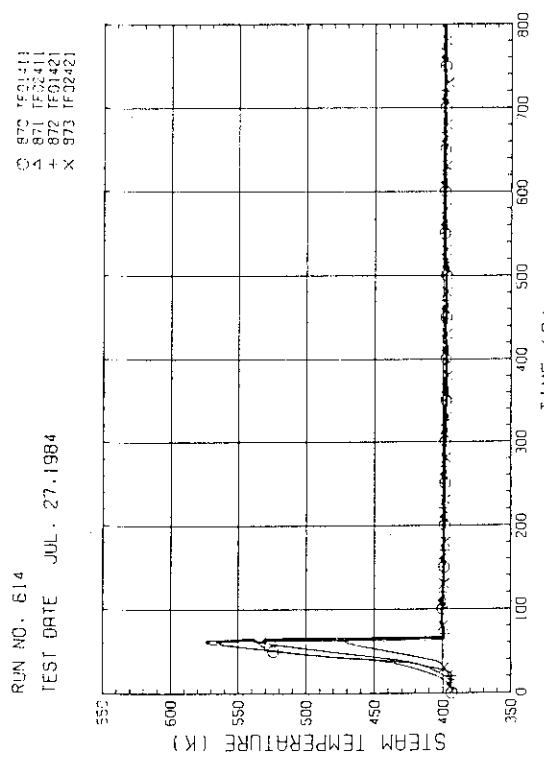

Fig. B-22 STEAM TEMPERATURE IN CORE, BUNDLE 4
(01411-1.735M, 02411-1.875M, 01421-1.38M, 02421-1.915M)

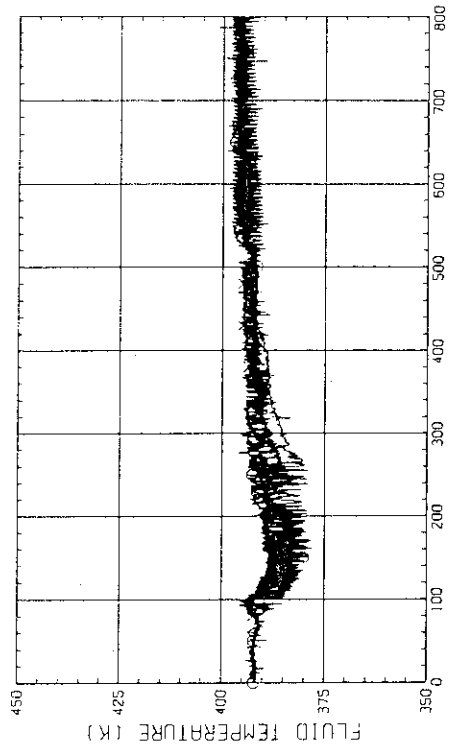

Fig. B-27 FLUID TEMPERATURE AT CORE INLET (BUNDLE 1.2.3.4. 100MM BELOW HEATED PART)

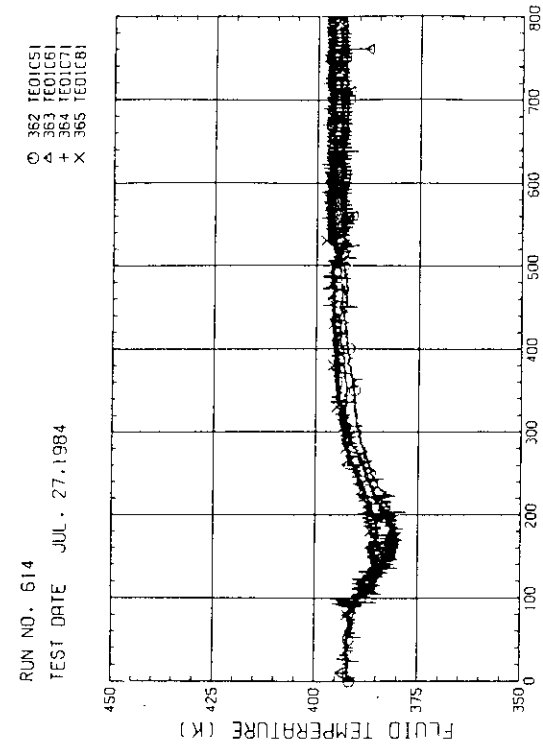

Fig. B-28 FLUID TEMPERATURE AT CORE INLET (BUNDLE 5.6.7.8. 100MM BELOW HEATED PART)

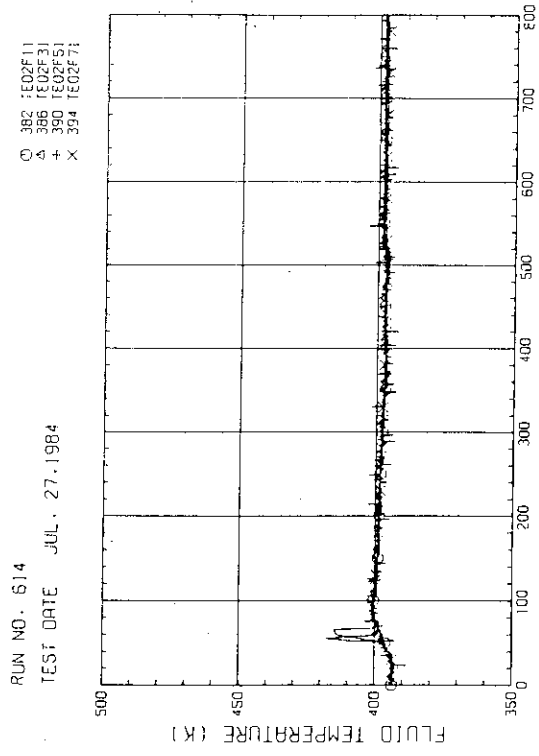

Fig. B-25 FLUID TEMPERATURE JUST ABOVE END BOX TIE PLATE (BUNDLE 1.3.5.7. OPPOSITE SIDE OF COLD LEG. OUTER)

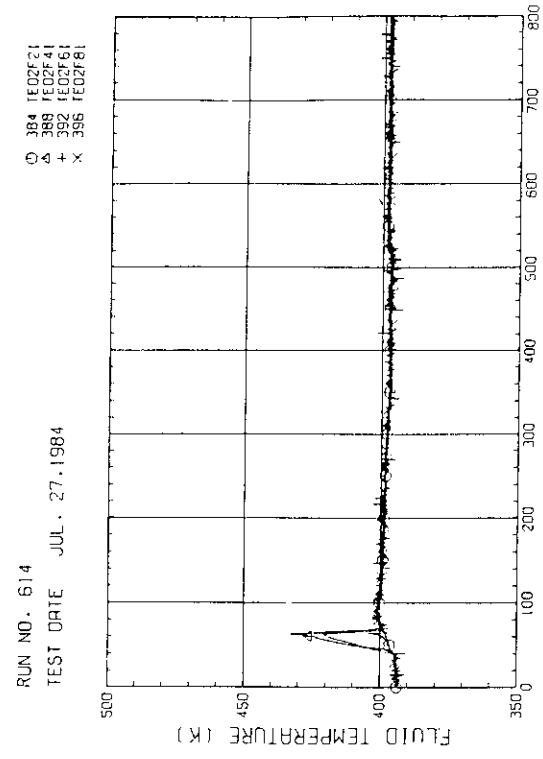

Fig. B-26 FLUID TEMPERATURE JUST ABOVE END BOX TIE PLATE (BUNDLE 2.4.6.8. COLD LEG SIDE. INNER)

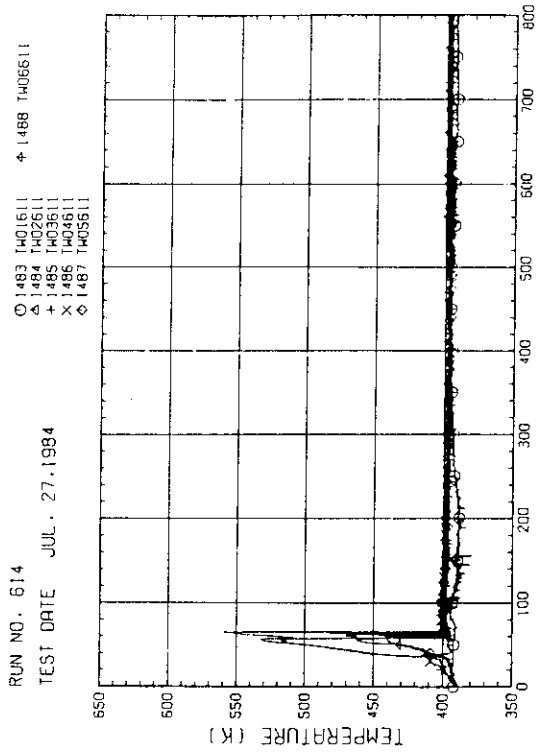

Fig. B-31 TEMPERATURE FOR SPUTTERING DETECTION
BUNDLE 6 . REGION 1 . TYPE 1

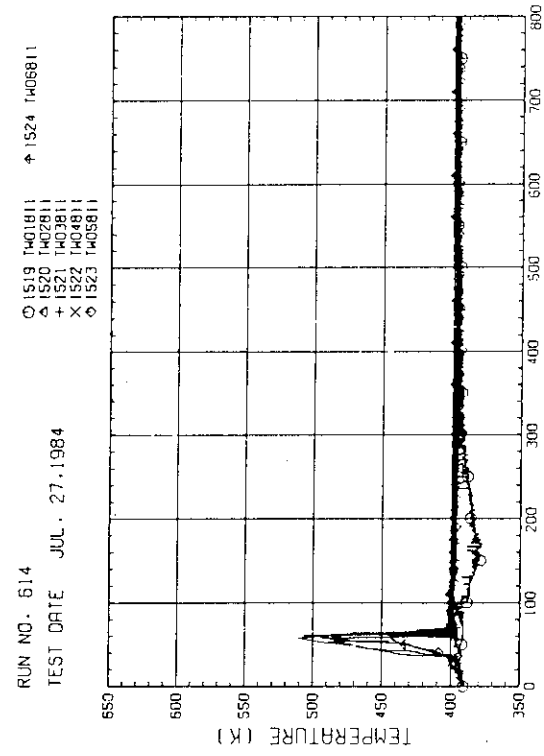

Fig. B-32 TEMPERATURE FOR SPUTTERING DETECTION
BUNDLE 8 . REGION 1 . TYPE 1

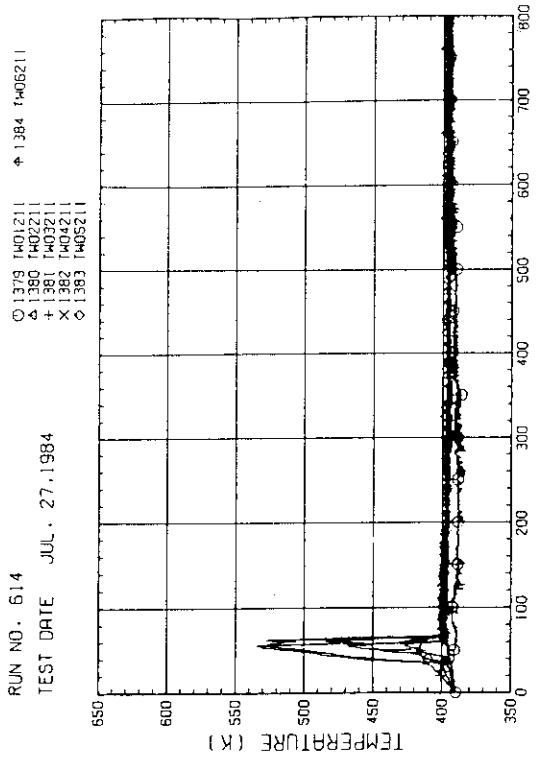

Fig. B-29 TEMPERATURE FOR SPUTTERING DETECTION
BUNDLE 2 . REGION 1 . TYPE 1

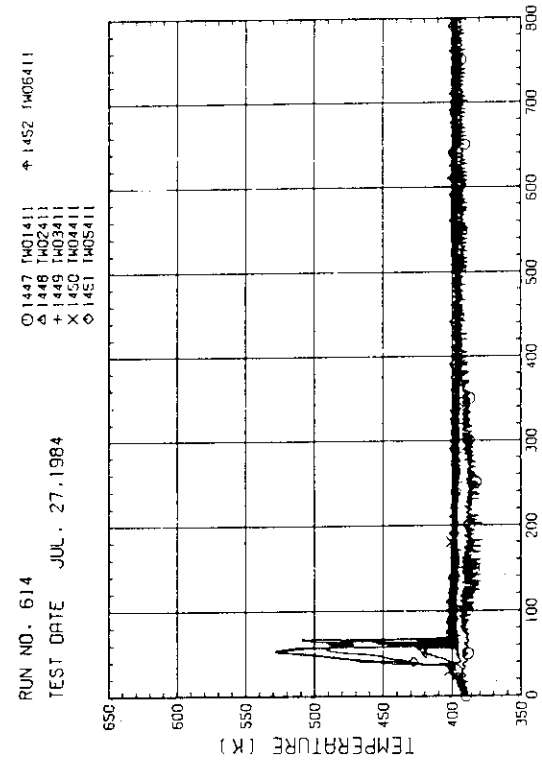

Fig. B-30 TEMPERATURE FOR SPUTTERING DETECTION
BUNDLE 4 . REGION 1 . TYPE 1

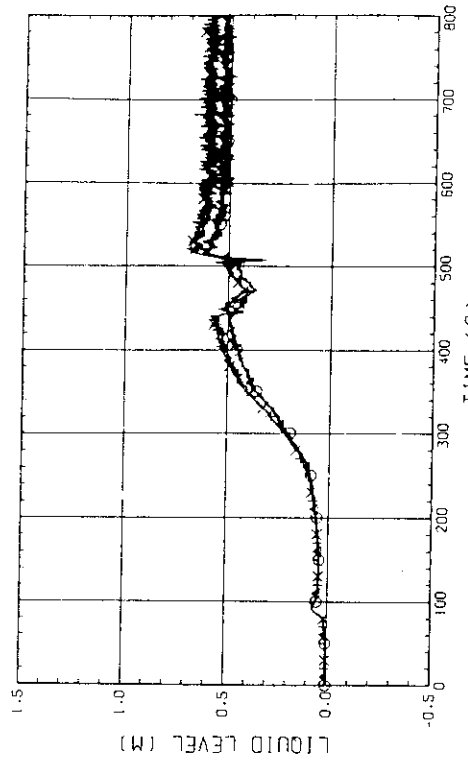

Fig. B-35 LIQUID LEVEL ABOVE UCSP (BUNDLE 1.2.3.4)

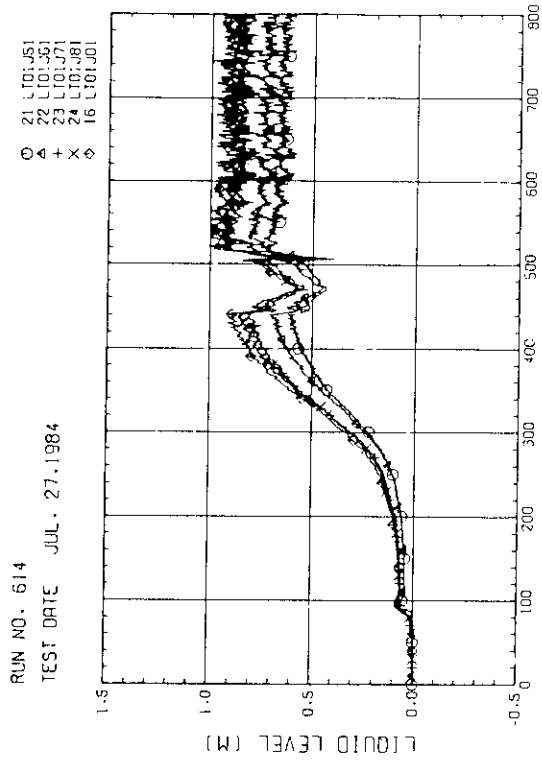

Fig. B-36 LIQUID LEVEL ABOVE UCSP (BUNDLE 5.6.7.8 AND CORE BAFFLE)

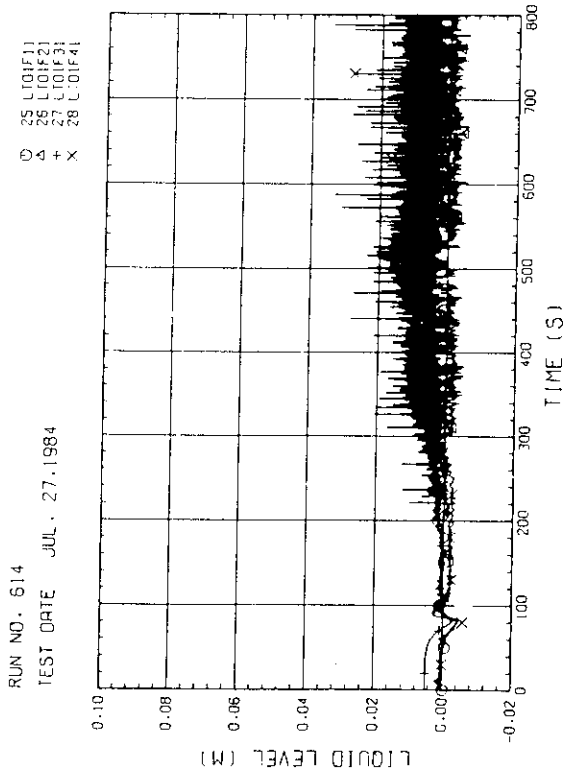

Fig. B-33 LIQUID LEVEL ABOVE END BOX TIE PLATE (BUNDLE 1.2.3.4)

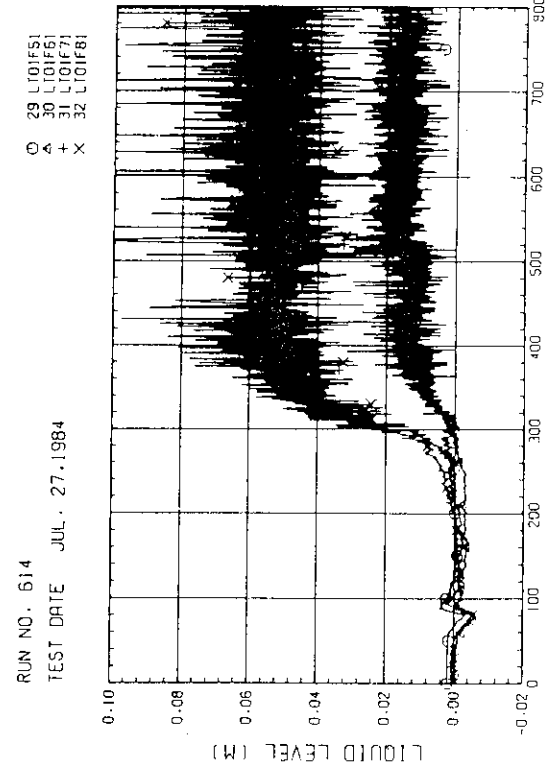

Fig. B-34 LIQUID LEVEL ABOVE END BOX TIE PLATE (BUNDLE 5.6.7.8)

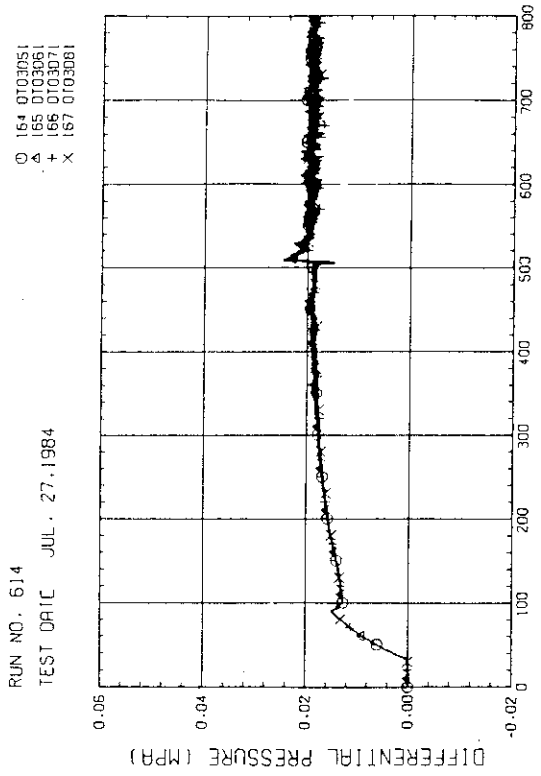

Fig. B-39 DIFFERENTIAL PRESSURE OF CORE FULL HEIGHT (BUNDLE 5.6.7.8)

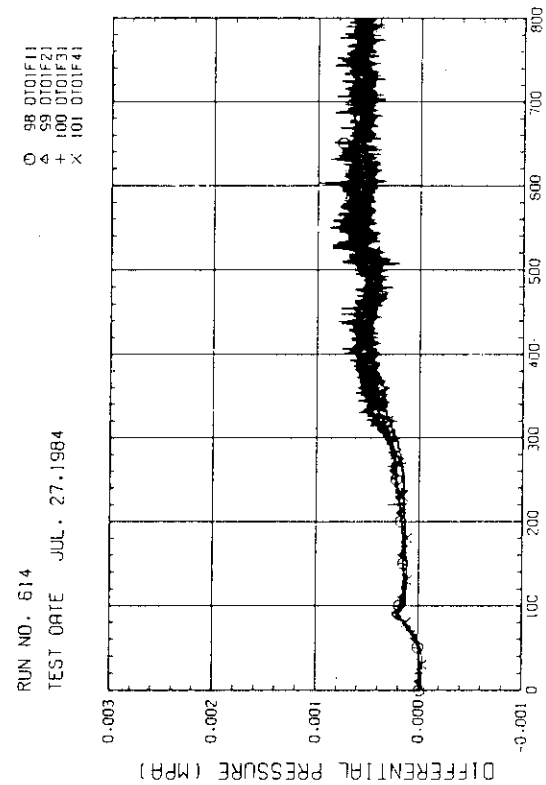

Fig. B-40 DIFFERENTIAL PRESSURE ACROSS END BOX TIE PLATE (BUNDLE 1.2.3.4)

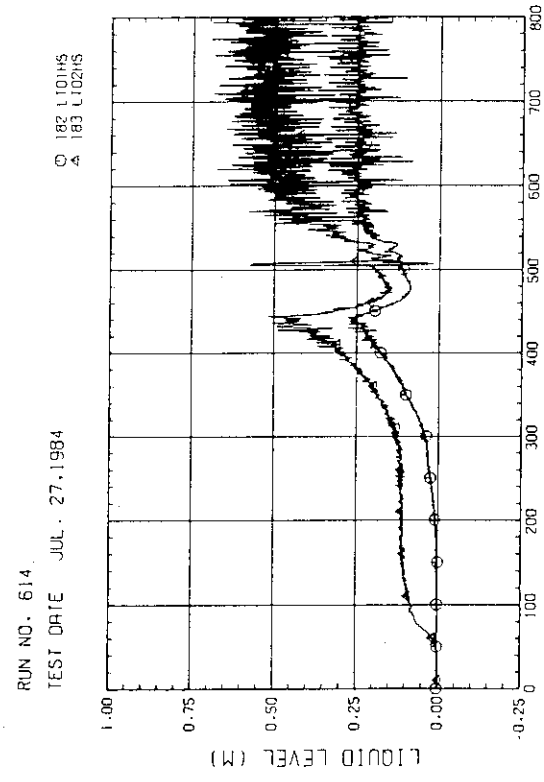

Fig. B-37 LIQUID LEVEL IN HOT LEG (01HS - PV SIDE, 02HS - STEAM/WATER SEPARATOR SIDE)

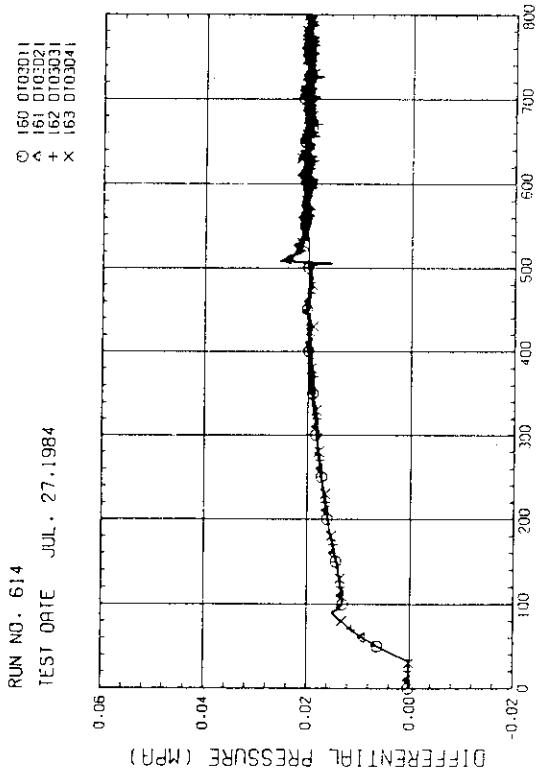

Fig. B-38 DIFFERENTIAL PRESSURE OF CORE FULL HIGHT (BUNDLE 1.2.3.4)

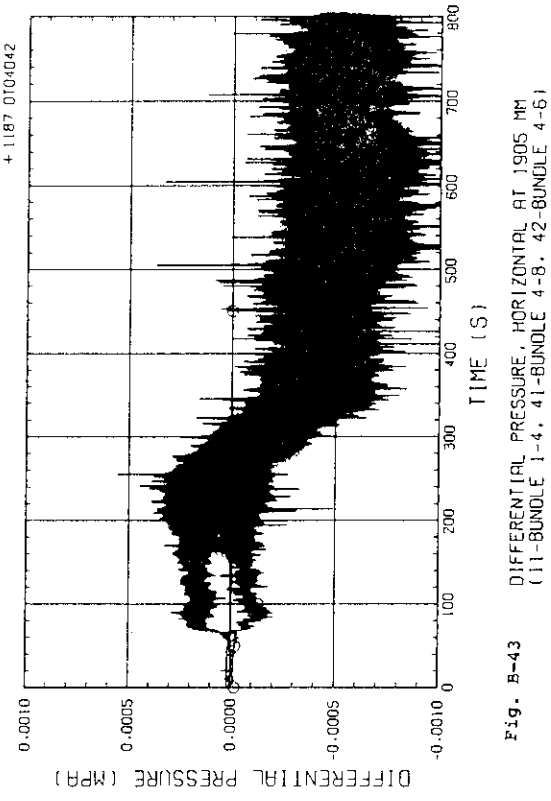

Fig. B-43 DIFFERENTIAL PRESSURE, HORIZONTAL AT 1905 MM (11-BUNDLE 1-4, 41-BUNDLE 4-8, 42-BUNDLE 4-6)

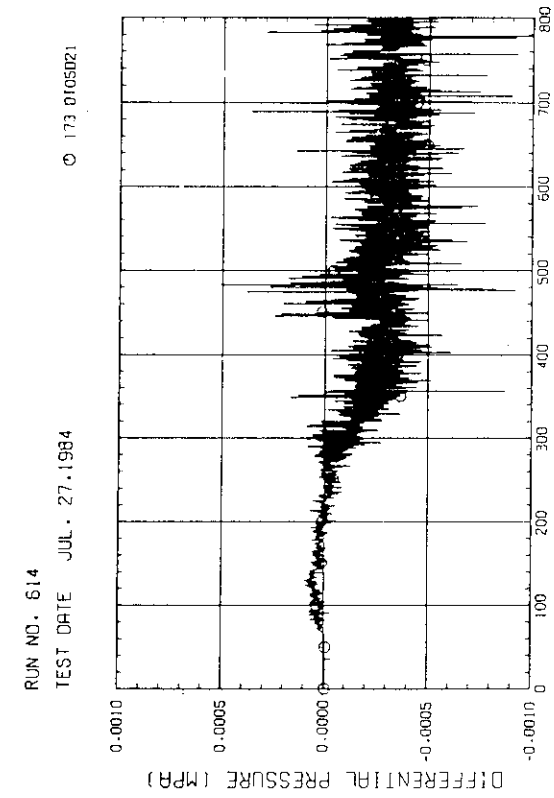

Fig. B-44 DIFFERENTIAL PRESSURE, HORIZONTAL AT 2570 MM (BUNDLE 2-4)

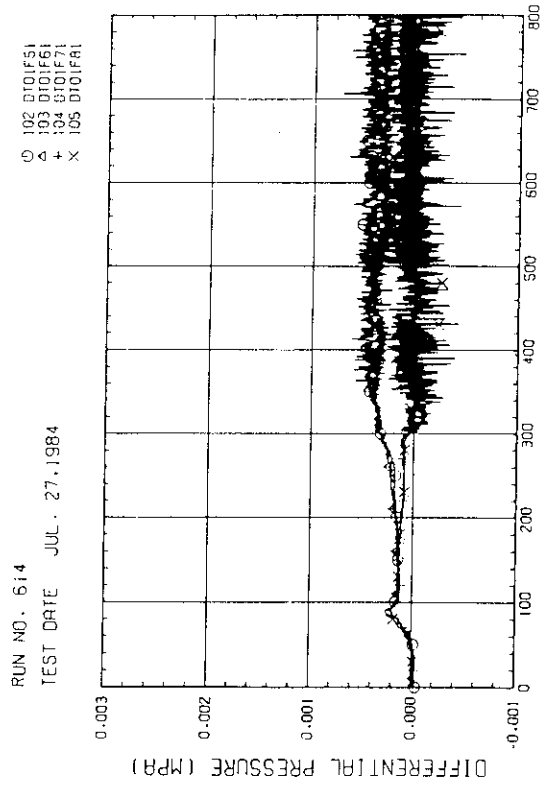

Fig. B-41 DIFFERENTIAL PRESSURE ACROSS END BOX TIE PLATE (BUNDLE 5.6.7.8)

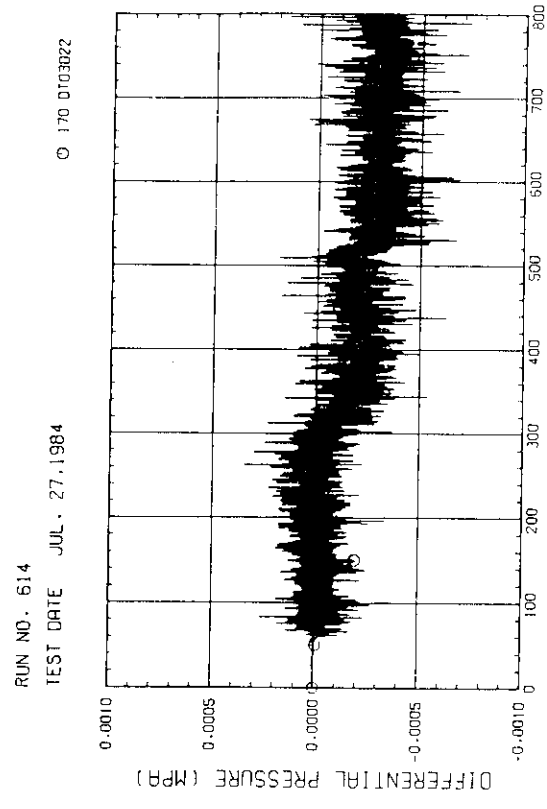

Fig. B-42 DIFFERENTIAL PRESSURE, HORIZONTAL AT 1365 MM (BUNDLE 2-4)

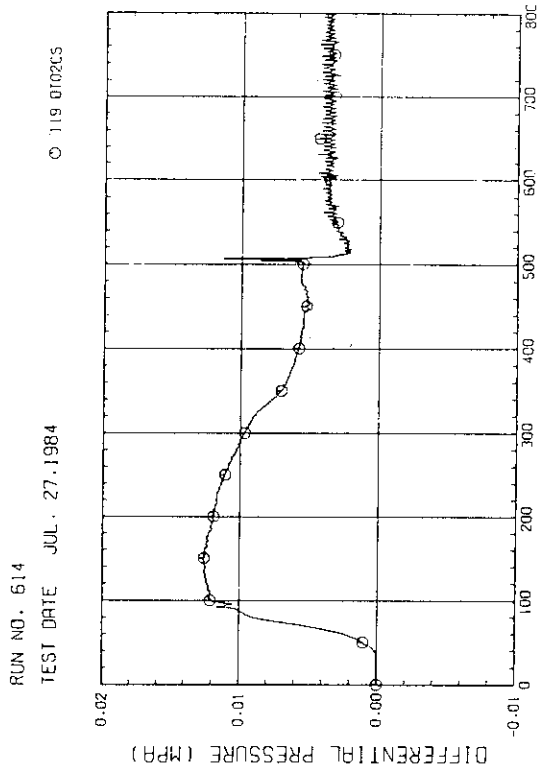

Fig. B-47 DIFFERENTIAL PRESSURE OF INTACT COLD LEG

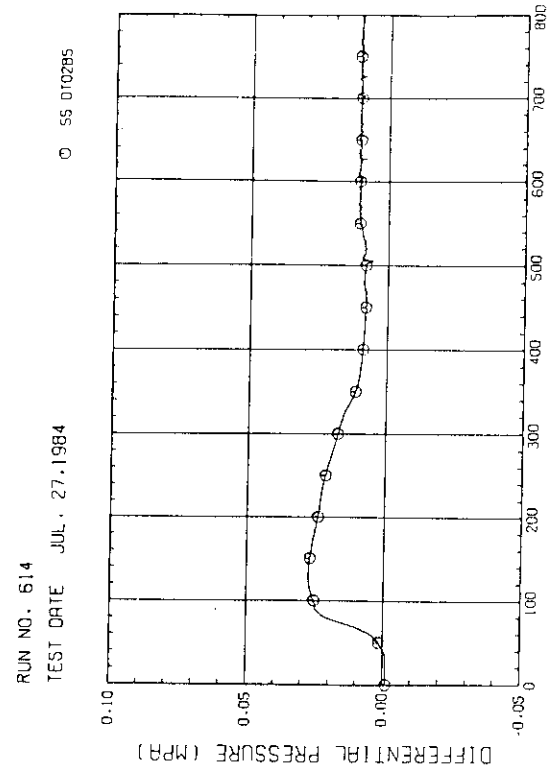

Fig. B-48 DIFFERENTIAL PRESSURE, STEAM/WATER SEPARATOR - CONTAINMENT TANK-II

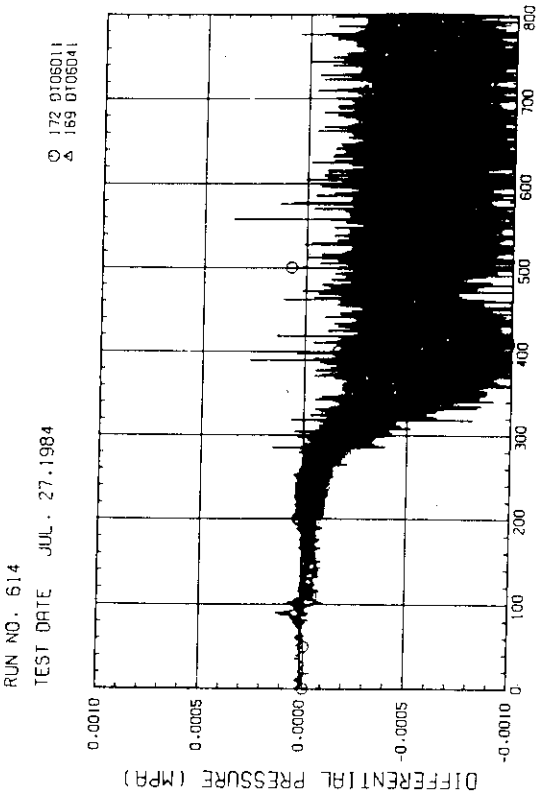

Fig. B-45 DIFFERENTIAL PRESSURE, HORIZONTAL AT 3235 MM (11-BUNDLE 1-4, 41-BUNDLE 4-8)

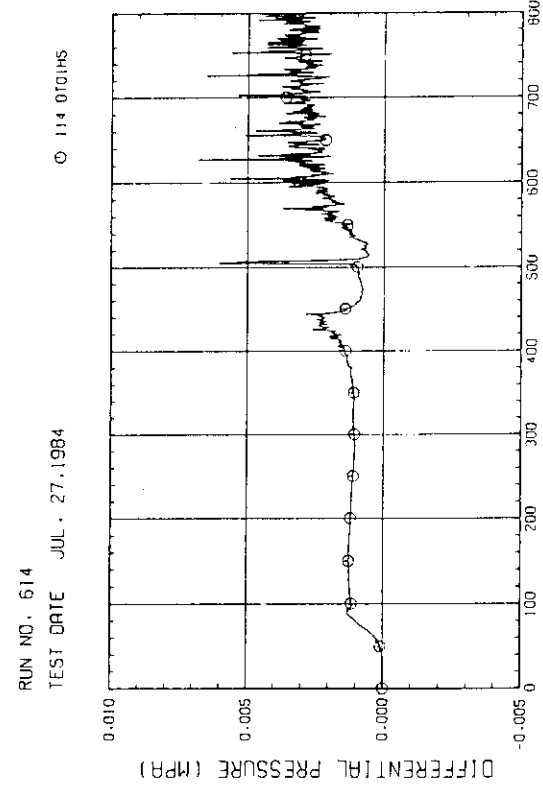

Fig. B-46 DIFFERENTIAL PRESSURE OF HOT LEG, HOT LEG INLET - STEAM/WATER SEPARATOR INLET

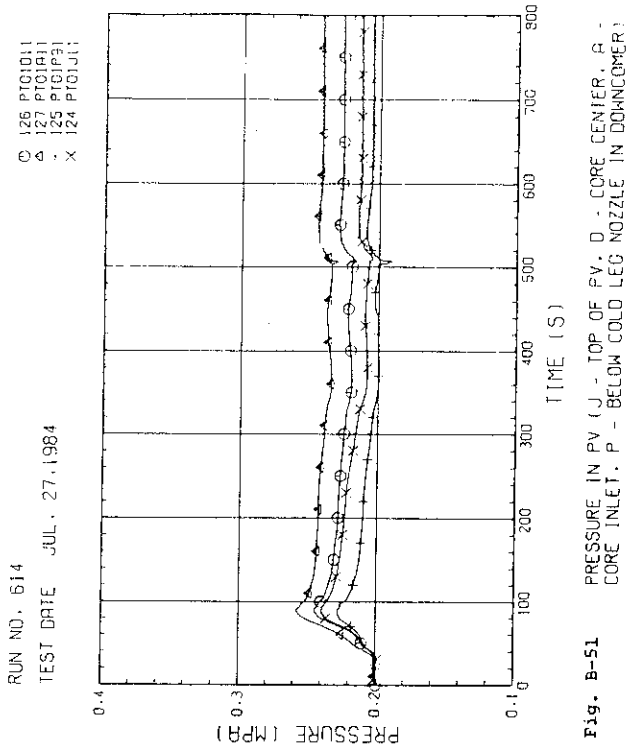

Fig. B-51 PRESSURE IN PV (J - TOP OF PV, D - CORE CENTER, A - CORE INLET, P - BELOW COLD LEG NOZZLE IN DOWNCOMER)

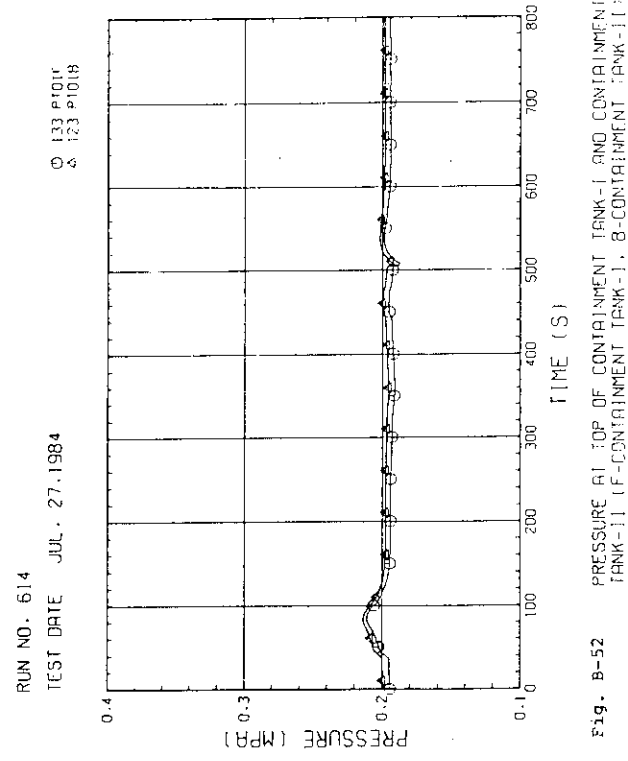

Fig. B-52 PRESSURE AT TOP OF CONTAINMENT TANK-I AND CONTAINMENT TANK-II (F-CONTAINMENT TANK-I, B-CONTAINMENT TANK-II)

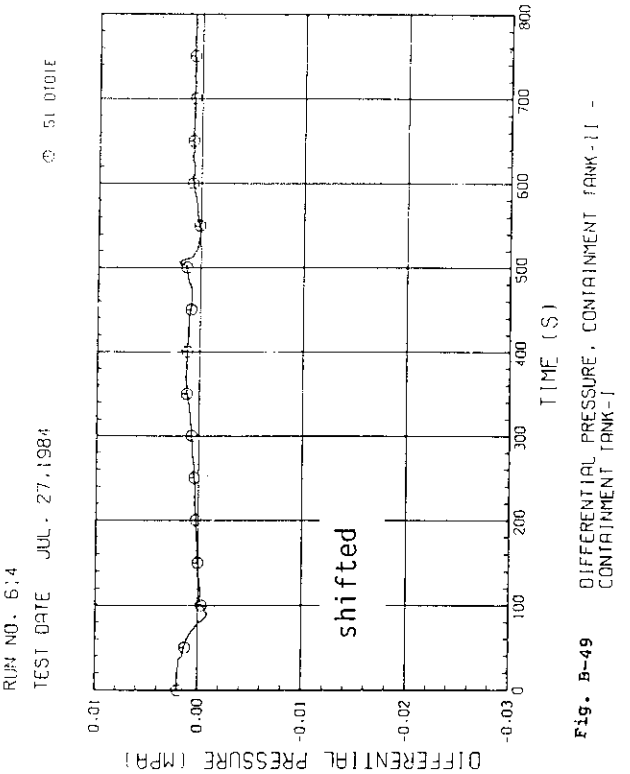

Fig. B-49 DIFFERENTIAL PRESSURE, CONTAINMENT TANK-II - CONTAINMENT TANK-I

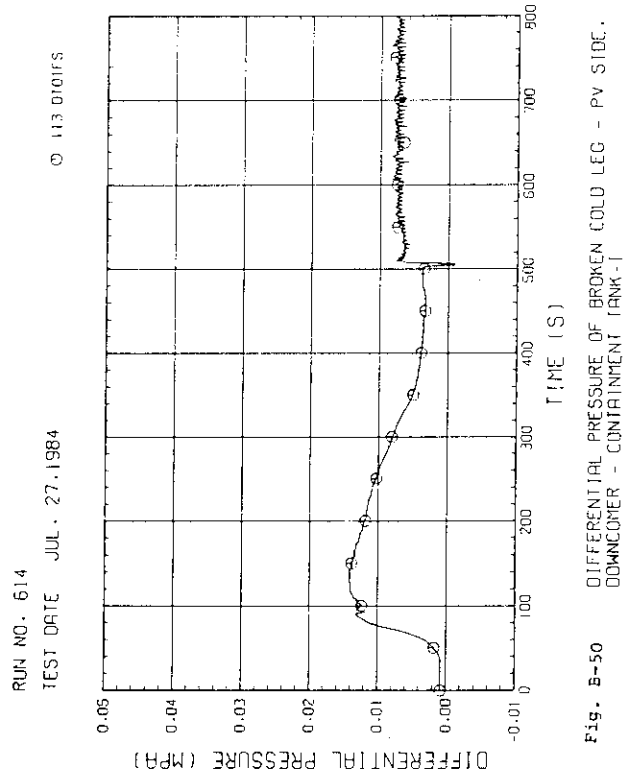

Fig. B-50 DIFFERENTIAL PRESSURE OF BROKEN COLD LEG - PV SIDE, DOWNCOMER - CONTAINMENT TANK-I

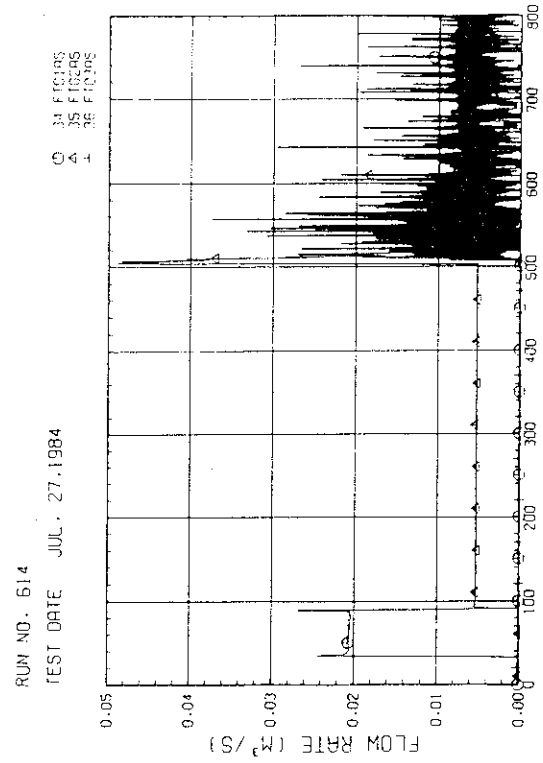

Fig. B-55 FLOW RATE OF ECC WATER (01-LOWER PLENUM, 02-INTACT COLD LEG, 03-BROKEN COLD LEG)

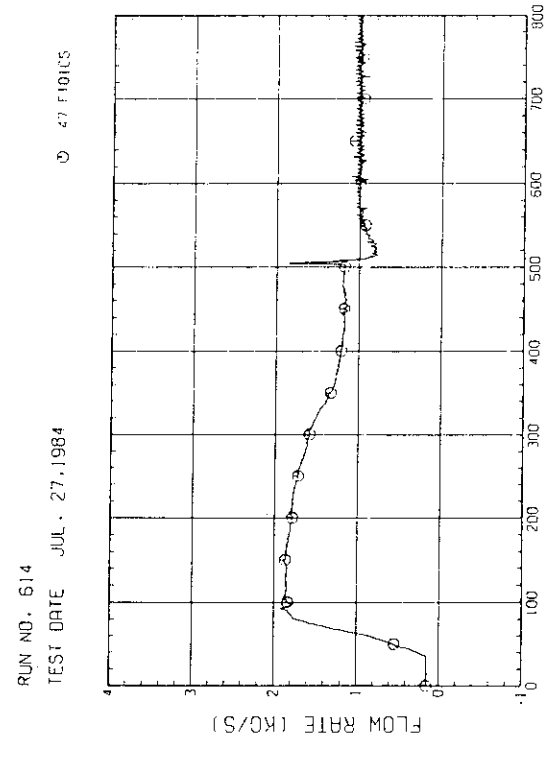

Fig. B-56 MASS FLOW RATE OF INTACT COLD LEG

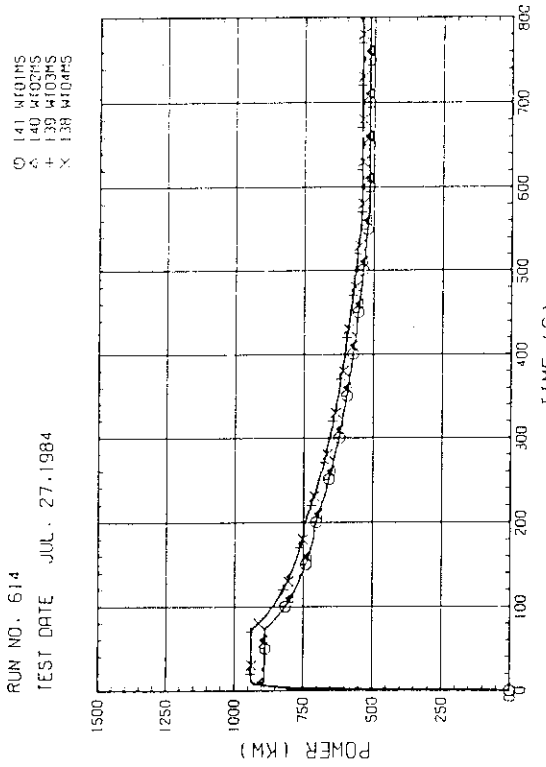

Fig. B-53 BUNDLE POWER (BUNDLE 1.2.3.4)

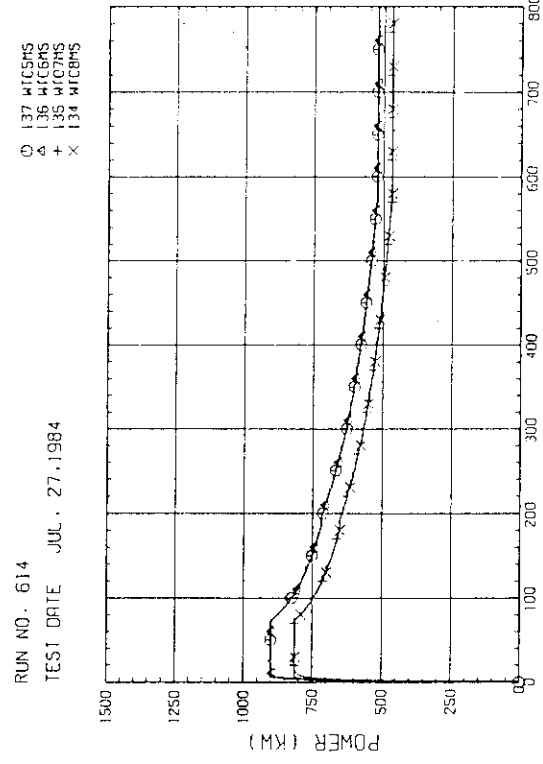

Fig. B-54 BUNDLE POWER (BUNDLE 5.6.7.8)

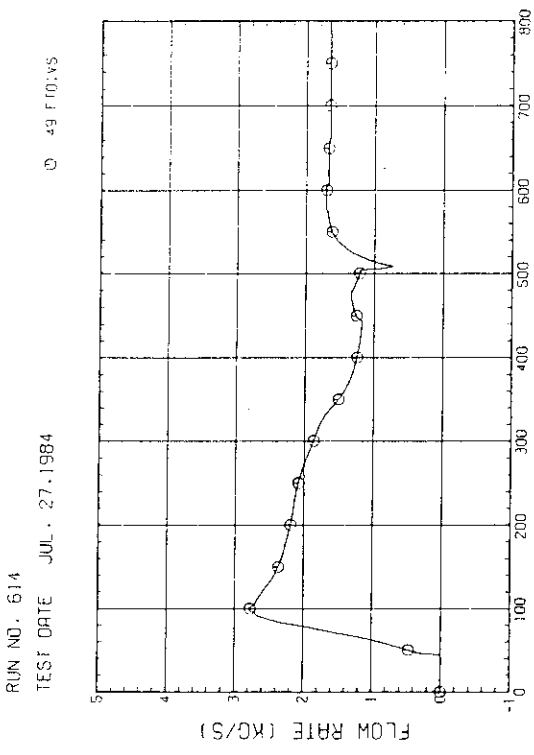

Fig. B-59 STEAM FLOW RATE OF DISCHARGE FROM CONTAINMENT TANK-II

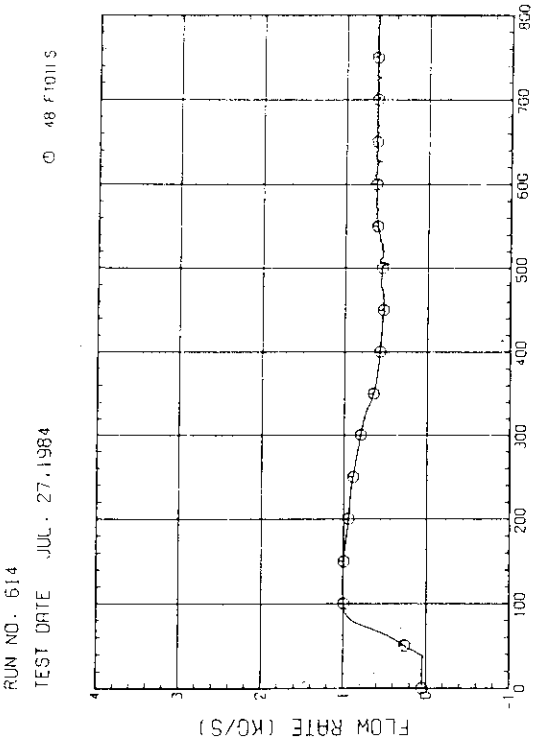

Fig. B-57 MASS FLOW RATE OF BROKEN COLD LEG - STEAM/WATER SEPARATOR SIDE

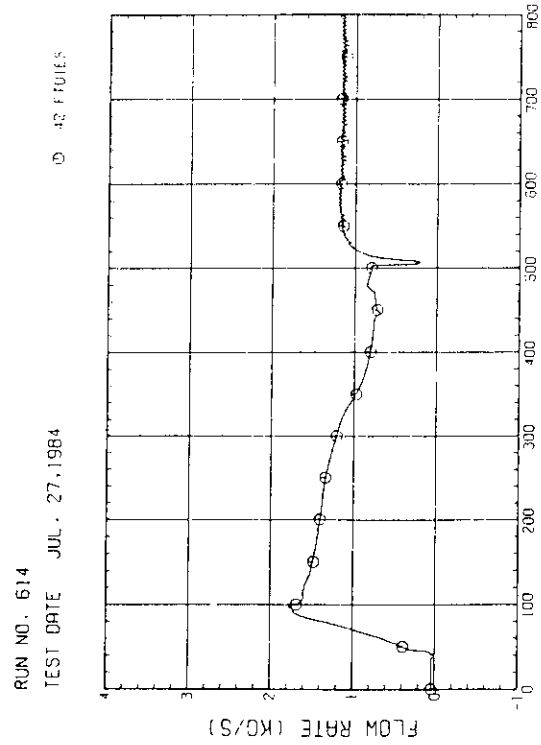

Fig. B-58 MASS FLOW RATE FROM CONTAINMENT TANK-I TO CONTAINMENT TANK-II